Genome-wide profiling of druggable active tumor defense mechanisms to enhance cancer immunotherapy

Rigel J. Kishton[1,2,*,#], Shashank J. Patel[1,2,†,*], Suman K. Vodnala[1,2], Amy E. Decker[3], Yogin Patel[1,2], Madhusudhanan Sukumar[1,2], Tori N. Yamamoto[1,2,4], Zhiya Yu[1,2], Michelle Ji[1,2], Amanda N. Henning[1,2], Devikala Gurusamy[1,2], Douglas C. Palmer[1,2], Winifred Lo[1], Anna Pasetto[1], Parisa Malekzadeh[1], Drew C. Deniger[1], Kris C. Wood[3], Neville E. Sanjana[5,6], Nicholas P. Restifo[1,2,#,§]

[1]Surgery Branch, Center for Cancer Research, National Cancer Institute, Bethesda, MD 20892, USA

[2]Center for Cell-Based Therapy, National Cancer Institute, Bethesda, MD 20892, USA

[3]Department of Pharmacology & Cancer Biology, Duke University School of Medicine, Durham, NC, USA

[4]Immunology Graduate Group, University of Pennsylvania, Philadelphia, PA 19104, USA

[5]New York Genome Center, New York, NY 10013 USA

[6]Department of Biology, New York University, New York, NY 10003, USA

*These authors contributed equally to this work.

†Present address: NextCure Inc., Beltsville, MD 20705, USA

§Present address: Lyell Immunopharma, South San Francisco, CA 94080, USA

#Corresponding authors. NPR: restifon@mail.nih.gov. RJK: kishtonrj@nih.gov.

Summary

All current highly effective anti-tumor immunotherapeutics depend on the activity of T cells, but tumor cells can escape immune recognition by several mechanisms including loss of function in antigen presentation and inflammatory response genes, expression of immunomodulatory proteins and an immunosuppressive tumor microenvironment. In contrast, the comprehensive identification of strategies that sensitize tumor cells to immunotherapy *in vivo* has remained challenging. Here, we combine a two-cell type (2CT) whole-genome CRISPR-Cas9 screen with dynamic transcriptional analysis (DTA) of tumor upon T cell encounter to identify a set of genes that tumor cells express as an active defense against T cell-mediated killing. We then employed small molecule and biologic screens designed to antagonize gene products employed by tumor cells to actively defend against T cell-mediated tumor destruction and found that the inhibition of BIRC2, ITGAV or DNPEP enhanced tumor cell destruction by T cells. Mechanistically, we found that BIRC2 promoted immunotherapy resistance through inhibiting non-canonical NF-κB signaling and limiting inflammatory chemokine production. These findings show the path forward to improving T cell-mediated tumor destruction in the clinic.

Keywords

Cancer immunotherapy, genome-scale CRISPR/Cas9 screen, immunotherapy resistance, immunotherapy sensitization, BIRC2, chemokines, combination therapy

Introduction

Cancer immunotherapies, which harness the body's immune system to attack tumor cells, have driven dramatic improvements in clinical outcomes in patients with certain advanced cancers (Maude et al., 2014; Rosenberg et al., 2011; Topalian et al., 2015). Patients with such cancers can experience significant benefit after being treated with immune checkpoint blockade (Topalian et al., 2012) or with adoptive cell therapy (ACT) of tumor infiltrating lymphocytes (TIL), and chimeric antigen receptor (CAR) or T cell receptor (TCR)-engineered T cells (Rosenberg and Restifo, 2015). However, while much progress has been made, many patients with very common cancers such as most cancers of the breast, colon, pancreas, prostate and brain receive limited or no benefit from existing immunotherapy approaches (Park et al., 2018; Yamamoto et al., 2019). Consequently, strategies to improve the efficacy of cancer immunotherapy are needed to improve patient outcomes.

Multiple factors likely play a role in regulating the efficacy of immunotherapy, including the characteristics of anti-tumor T cells (Kishton et al., 2017; Vodnala et al., 2019), tumor microenvironmental factors including the presence of inhibitory factors such as immunosuppressive cell subsets (Facciabene et al., 2012) or excess potassium (Eil et al., 2016), and a number of tumor intrinsic factors. The loss or mutation of tumor cell genes required for antigen presentation and the response to inflammatory cytokines, such as B_2M (Restifo et al., 1996) and JAK1/2, can profoundly limit the ability of T cells to eliminate tumors (Patel et al., 2017; Zaretsky et al., 2016). Additionally, the activity of various cellular signaling pathways in tumors, including beta-catenin (Wang et al., 2018) and the PI3K signaling pathway (Sharma et al., 2017), have been demonstrated to provide a survival advantage for tumor cells in the

context of immunotherapy. The identification of tumor escape mechanisms may be useful for selecting patients likely to respond to immunotherapy, but have limited utility in the creation of novel strategies for improving therapeutic effects.

A number of approaches have been pursued to optimize the efficacy of cancer immunotherapy, including improving the quality of cell products used in ACT (Gattinoni et al., 2012), altering the tumor microenvironment, and pursuing strategies to combine various pharmacological inhibitors and biologics with immunotherapy treatments as a combination therapy (Robert et al., 2016). Recent efforts to investigate the potential of combining targeted pharmacological inhibitors with immunotherapy have demonstrated potential to improve clinical efficacy (Ribas et al., 2019), indicating such approaches may play an important role in improving the responses of patients to immunotherapy. We sought to systematically sift through strategies and solutions to identify methods for enhancing cell-based immunotherapy on a whole genome scale.

We hypothesized that, as often observed in the context of cancer cells treated with targeted chemotherapies (Singleton et al., 2017), the engagement of anti-tumor T cells with target tumor cells might drive tumor transcription of genes that promote cell survival, mediating resistance to immunotherapy. These genes, comprising a tumor active defense mechanism against immunotherapy, would represent important potential targets for combination therapy. We sought to identify the genetic components of active tumor defense against immunotherapy by combining a genome-scale CRISPR/Cas9 loss of function screen in tumor cells with dynamic transcriptional analysis (DTA) of tumor cells as they interact with antigen-specific T cells. The integration of these cross-platform, multi-omics approaches

allowed us to identify a set of tumor genes, including *BCL2* and *BIRC2,* whose expression was both increased during T cell engagement and required for tumor cell survival in this context. We evaluated the potential for targeting these tumor genes, along with other top hits from the CRISPR screen to improve the efficacy of immunotherapy and uncovered several small molecules and biologics that augmented T cell elimination of tumor cells. Finally, we explored the genetic mechanism through which *BIRC2* acts to limit tumor cell susceptibility to T cell-mediated killing, finding a novel role for *BIRC2* in suppressing tumor cell inflammatory signaling and chemokine production by inhibiting the non-canonical NF-κB signaling pathway. Taken together, these results demonstrate a cross-platform, multi-omics strategy to identify and evaluate clinically relevant tumor targets for use in combinatorial immunotherapy treatment regimens.

Results

A two-cell type (2CT) genome-scale CRIPSR/Cas9 screen optimized to identify tumor genes that promote survival in the context of T cell engagement

To identify active tumor defense genes, we first sought to define tumor genes that are essential for tumor cell survival in the context of tumor antigen-specific T cell engagement. To achieve this, we utilized a two-cell type (2CT) co-culture system in which primary human T cells are transduced with an HLA-A*0201-restricted T cell receptor (TCR) specific for the NY-ESO-1 antigen (NY-ESO-1:157-165 epitope), then co-cultured with NY-ESO-1^{+} Mel624 human melanoma tumor cells (Patel et al., 2017). Our previous study (Patel et al., 2017), in which we sought to identify tumor genes that are essential for effective immunotherapy, utilized an

experimental design in which transduced T cells were cultured with Mel624 melanoma cells at a 0.3 ratio (1:3 E:T) for 12 hours, resulting in a strong T cell selective pressure that eliminated approximately 75% of tumor cells. This experimental design allowed for the identification of tumor genes whose loss promoted cell survival. The goal of our current study was diametrically opposite: Rather than seeking genes involved in tumor escape, we sought to identify genes whose loss *promoted* tumor cell death in the context of T cell engagement. To optimize the 2CT assay for this setting, we reduced the T cell selective pressure by shortening co-culture duration to 6 hours, resulting in the elimination of approximately 25% of tumor cells at a 1:3 E:T ratio **(Figure 1A)**. With these reduced T cell selective pressure conditions established, we transduced Mel624 cells with the GeCKOv2 library **(Figure 1B)** and exposed the transduced tumor cells to ESO T cells at a 1:3 E:T ratio for 6 h. We utilized deep sequencing to profile sgRNA library representation in tumor cells before and after T cell co-culture and, reasoning that sgRNAs targeting genes that promote tumor cell survival would have reduced abundance in surviving tumor cells, ranked all genes by two different scoring metrics: second-most depleted sgRNA **(Figure 1C)** and the RNAi Gene Enrichment Ranking (RIGER) metric **(Figure 1D)**. Top hits identified from the screen included genes such as *TRAF2, BIRC2, ALG11* and *mir1299.* Gene ontology analysis of significantly depleted genes indicated pathway enrichments of death receptor signaling, EIF2 signaling, endoplasmic reticulum stress pathways, and the unfolded protein response **(Figure 1E)**. Demonstrating the reproducibility of this screening method, we found that top genes identified in the 2CT screen including *mir1299, FAM32A, EIF3I, BIRC2* and *BCL2* were also depleted in a replicate screen **(Figure 1F, Table 1)**.

T cell engagement drives tumor cell transcriptional activation of pro-survival pathways

We next utilized dynamic transcriptional analysis (DTA) of the 2CT system to identify tumor genes that are differentially expressed upon T cell engagement with tumor cells. We co-cultured ESO T cells with unmodified Mel624 cells for 0 or 6 h **(Figure 2A)**. ESO T cells and tumor cells were each purified by FACS sorting **(Figure S1A)** and mRNA was extracted and sequenced. As expected, upon encounter with NY-ESO-1 expressing tumor cells, ESO T cells increased the expression of inflammatory cytokines such as *IL2* and *IFNG*, cytolytic molecules including *GZMB*, markers of T cell activation *CD69* and *TNFRSF9* (encoding 4-1BB), transcription factors promoting T cell effector function including *ZEB2,* and pathways supporting anabolic growth. Conversely, tumor-experienced T cells acutely repressed the expression of genes associated with memory and stemness such as *KLF2, TCF7, CD27,* and *LEF1* **(Figure 2B, Figure S1B)**. After co-culture with ESO T cells, Mel624 tumor cells upregulated the expression of genes associated with cellular mediators of inflammation including TNFR and NF-κB pathway signaling. Tumor cells also upregulated the expression of genes that have been associated with resistance to cell death such as *BIRC2, BIRC3, BCL2A1* (**Figure 2C-D)**. We also observed that tumor cells downregulated the expression of genes associated with Notch pathway signaling after T cell engagement (**Figure 2D**). Previous reports have linked the NF-kB signaling pathway with resistance to immunotherapy (Pan et al., 2018). Consistent with this, we found that T cell-experienced tumor cells upregulated a set of NF-κB regulated genes associated with resistance to apoptosis (Dutta et al., 2006), while repressing the expression of the apoptotic effector molecule *BAX* (**Figure 2E)**.

To determine whether the transcriptional and signaling pathway alterations we observed in tumor cells following T cell interaction had functional consequences in regulating tumor cell susceptibility to immunotherapy, we systematically engaged 17 tumor cellular signaling pathways through lentiviral transduction of pathway activating constructs (Martz et al., 2014). Pathway-activated tumor cells were co-cultured with ESO T cells in an arrayed fashion, and the effects of activating each cell signaling pathway on tumor cell survival were measured (**Figure 2F)**. Consistent with previous reports showing NF-kB signaling can promote tumor evasion of immune-mediated destruction (Pan et al., 2018), and with our data indicating upregulation of NF-κB regulated pro-survival genes in tumor cells after ESO T cell engagement, activation of NF-κB signaling or constitutive expression of *BCL2* or *BCL-XL* resulted in tumor cell resistance to T cell-mediated destruction **(Figure 2G, 2H)**. Conversely, constitutive activation of the NOTCH1 signaling cascade sensitized tumor cells to T cell-mediated death **(Figure 2G, 2H)**.

Tumor cells actively express defense mechanisms to avert T cell-mediated destruction

Tumor cell genes that are induced by T cell-encounter and functionally promote tumor cell survival may represent important tumor-intrinsic mechanisms that actively promote immunotherapy resistance. To determine whether such genes could be identified, we focused on genes whose targeting sgRNAs were depleted in both biological replicate CRISPR screens and assessed mRNA expression changes in these tumor genes following T cell encounter. We found 10 CRISPR-depleted genes that had statistically significant increases in mRNA expression after T cell engagement **(Table 2)**, including *SCAF11*, *BIRC2*, *RPAP2*, and *BCL2* **(Figure 3A)**. To validate the functional role of these genes in mediating tumor cell resistance to T cell-induced

apoptosis, we transduced A375 melanoma cells, an additional human melanoma that expresses both HLA-A*0201 and NY-ESO-1 antigen, with Cas9 and three newly-designed sgRNA constructs targeting each candidate gene. We co-cultured these cells with ESO T cells and assessed the impact of gene knockout on tumor cell survival. We considered a candidate gene to be validated if at least two independent gene-targeted sgRNAs resulted in increased tumor cell death upon T cell co-culture. Five of the candidate genes met these criteria, including *BCL2*, *BIRC2*, *LPGAT1*, *SCAF11* and *TOR1AIP1* **(Figure 3B)**. These genes represent strong candidates of actively-induced tumor cell-intrinsic mechanisms of resistance to T cell-mediated killing.

CRISPR-informed drug screen identifies combinatorial immunotherapy targets

To assess the potential utility of targeting active tumor defense mechanisms for combination therapy, we developed a workflow for identifying potential targets for small molecule or biologic inhibition based on these datasets. As an initial step, we considered the five identified and validated tumor active defense genes (**Figure 4A**) along with the top 250 second-most depleted genes from the duplicate CRISPR screens ordered by rank-sum analysis. Genes were first mapped to coded proteins **(Table 3)**, and these proteins were queried for availability of targeted inhibitors using the Drug Gene Interaction Database (DGIDB) (Griffith et al., 2013) **(Table 4)** followed by manual curation. We identified 15 targets for which inhibitors were available, including BIRC2, BCL2, ITGAV and DNPEP **(Table 5)**. When possible, we obtained two independent inhibitors per target to limit drug-specific effects. To assess the impact of inhibitors on T cell elimination of tumor cells, we first performed a high throughput assay in which ESO T cells were co-cultured with A375 melanoma cells in the presence of vehicle or each

inhibitor for 16h **(Figure 4A)**. Assays were performed at two concentrations of each inhibitor and tumor cell viability was measured by colorimetric viability dye. We found that a number of inhibitors were capable of increasing A375 killing compared with ESO T cells alone **(Figure 4B, 4D)**. We reasoned that inhibitors of interest should both significantly increase tumor cell destruction in combination with ESO T cells when compared with ESO T cells alone and should also cause higher tumor cell killing as a combination with ESO T cells compared with inhibitor treatment alone. Our screen revealed several inhibitors that met these criteria, including inhibitors of BIRC2 (birinapant and LCL161), ITGAV (Cilengitide and a monoclonal antibody against ITGAV), DNPEP (CHR2797), BCL2 (Abt199), and ERRα (C29) **(Figure 4C, 4E)**.

Combination treatment increases T cell elimination of melanoma and GI tumor cells

We next tested the effects of these inhibitors in additional 2CT assays in which we assessed the impact of combination therapy on the ability of T cells to eliminate tumors across several tumor antigens and cancer types. To increase the precision of our readouts, we co-cultured TCR transduced T cells with tumor lines expressing target antigens for 16h in the presence or absence of drugs and tumor cell viability was measured at a single cell level using FACS **(Figure 5A)**. Consistent with our initial findings, we found that inhibitors of BIRC2 (birinapant and LCL161), ITGAV (cilengitide and anti-ITGAV) and DNPEP (CHR2797) increased the killing of A375 melanoma cells after co-culturing ESO T cells **(Figure 5B, S2A)**. However, we did not observe increased tumor cell elimination by ESO T cells when BCL2 (Abt199) or ERRα (C29) were inhibited in this assay, suggesting that the observed impacts on cell viability in the high throughput assay could reflect toxicity against anti-tumor T cells. Increases in tumor cell death

in the presence of inhibitors was dependent on the presence of T cells for all validated hits (**Figure S2B)**. Importantly, we also found that, except for α-ITGAV, these drugs increased the killing of a second melanoma line (Mel624 expressing both NY-ESO-1 and MART-1 antigens) after co-culture with both ESO T cells **(Figure 5C)** and T cells transduced with a TCR that confers recognition of MART-1 **(Figure 5D)**.

To determine whether any of the drugs could increase neo-antigen-reactive T cell elimination of epithelial tumor cells, we utilized two independent patient-derived colon cancer cell lines, SB4238 and SB4266. These lines were co-cultured with T cells engineered to express TCRs reactive against mutated proteins expressed by each tumor line. In the case of SB4238, a non-synonymous mutation in NCKAP1 (G1312T, **Figure S2C**) resulted in an D438Y amino acid substitution that was specifically recognized by a TCR identified in patient tumor infiltrating lymphocytes (TILs) **(Figure S2D, S2E)**. A TCR reactive against SB4266 through specific recognition of p53 R248W was previously described (Malekzadeh et al., 2019). We found that TCR-transduced T cells alone were capable of eliminating a modest percentage of SB4266 cells, and this increased in the presence of inhibitors of BIRC2 (birinapant and LCL161), DNPEP (CHR2797), and ITGAV (cilengitide) **(Figure 5E)**. However, only BIRC2 inhibitors birinapant and LCL161 increased neo-antigen reactive T cell elimination of SB4238 tumor cells **(Figure 5F)**.

As BIRC2 inhibition consistently increased T cell elimination of tumor cells irrespective of recognized antigens or cancer types, we next assessed whether the *in vivo* combination treatment of either LCL161 or birinapant along with antigen-specific T cells could increase

tumor control. Indeed, we found that dosing mice bearing established B16 tumors with either LCL161 or birinapant increased the ability of PMEL-transgenic T cells to control tumor growth **(Figure 5G, S2F)** and increased overall survival time **(Figure 5H)**. In summary, the use of a genome-scale CRISPR screen to inform the selection of inhibitors for increasing tumor susceptibility to T cell killing led to the identification of several druggable tumor targets, with BIRC2 displaying the greatest potential across several tumor antigens and histologies.

BIRC2 negatively regulates tumor cell inflammation

As BIRC2 was found to be a component of the active tumor defense against T cell engagement and also could be targeted pharmacologically across a number of settings to increase the efficacy of T cell elimination of multiple tumor cell lines, we sought to further characterize the role and regulation of BIRC2 in tumor cells. Consistent with our observation that T cell engagement increased mRNA expression of *BIRC2* in tumor cells, treatment of A375 or Mel624 melanoma cells with recombinant IFNγ or TNFα (to mimic T cell inflammatory cytokine release) was sufficient to increase the protein expression of BIRC2 **(Figure 6A).** Inhibitors of BIRC2 have been reported to attenuate the cytotoxic effects of TNFα in tumor cells (Vredevoogd et al., 2019), yet genetic studies of BIRC2 function in the context of tumor cell resistance to immunotherapy have not been extensively performed. We utilized CRISPR/Cas9 with newly designed sgRNAs to specifically knock out BIRC2 **(Figure 6B)** and performed mRNA sequencing. BIRC2 knockout cells had increased mRNA expression of pro-inflammatory chemokines and cytokines including *CCL5*, *CSF2*, *CXCL10,* and *CXCL11*, along with increased expression of genes involved in T cell binding and recognition of tumor cells such as *ICAM1* and *HLA-DQA2* **(Figure**

6C). Pathway analysis of genes upregulated in BIRC2 knockout cells revealed enrichment for inflammatory signaling cascades, antigen presentation pathway, the unfolded protein response and NF-κB signaling **(Figure 6D)**. Consistent with the observed changes in mRNA, we found that BIRC2 knockout cells also had increased protein level expression of ICAM1, along with HLA Class I (**Figure 6E)**. We also found increased expression of a number of genes previously associated with response to immune checkpoint blockade (Harlin et al., 2009) in BIRC2 knockout cells **(Figure 6F)**.

BIRC2 had previously been reported to act as a negative regulator of the non-canonical NF-κB signaling cascade (Yang et al., 2016), and Ingenuity Pathway Analysis of transcription factor activation showed increased activation of key non-canonical NF-κB regulators *NFKB2* and *RELB* in addition to *IRF1* in BIRC2 knockout cells **(Figure 6G)**. We found that BIRC2 knockout cells had increased total expression of NFKB2, RELB and IRF1 **(Figure 6H)** and nuclear expression of NFKB2 and RELB was increased **(Figure S3A)** in BIRC2 knockout cells. Importantly, expression of NFKB2 is negatively correlated with the expression of BIRC2 in human melanoma patients **(Figure S3B)** and increased expression of non-canonical NF-κB transcription factor *NFKB2* was associated with increased patient survival, while the expression of canonical NF-κB transcription factor *NFKB1* was associated with decreased survival **(Figure 6I)** in melanoma patients treated with CTLA4 blockade (Van Allen et al., 2015). Additionally, using Tumor Immune Dysfunction and Exclusion (TIDE) computational analysis (Jiang et al., 2018), we determined that combined expression of *NFKB2* and *IRF1* predicts the probability of human

patient response to checkpoint blockade across a number of previously published patient cohorts **(Figure S4A)**.

BIRC2 loss promotes increased T cell migration and recognition of tumor cells

Tumor expression of chemokines including *CCL5* (Dangaj et al., 2019), *CXCL10* (Peng et al., 2015) and the cytokine *CSF2* (Borrello et al., 2009*)* have been linked with the ability of T cells to infiltrate and control tumor growth, and we found that increased mRNA expression of these genes is positively correlated with *NFKB2* expression in human melanoma patients **(Figure S5A-C)**. Consistent with a role for non-canonical NF-κB in promoting inflammatory chemokine production, we found increased abundance of RelB at the *CXCL10* promoter in BIRC2 KO tumor cells **(Figure 7A)**. RelB and NFKB2 were also found to have increased abundance at the promoters of other genes linked with immunotherapy response (Harlin et al., 2009) including *HLA-DMB* **(Figure S5D)**, and *MMP9* **(Figure S5E)** in BIRC2 KO cells.

We found that BIRC2 KO cells secreted significantly higher levels of GM-CSF, CCL5 and CXCL10 proteins **(Figure 7B-D)**. These unexpected findings suggested that BIRC2 might limit tumor production of these critical factors. Consistent with higher levels of these chemokines, genetic knockout of BIRC2 in tumor cells promoted increased migration of ESO T cells across a transwell membrane **(Figure 7E)**. Co-culture of ESO T cells with BIRC2 knockout tumor cells also resulted in increased levels of intracellular IFNγ **(Figure 7F)** and TNFα **(Figure 7G)** in the T cells. We tested the effect of genetic knockout of BIRC2 on tumor susceptibility to ACT *in vivo*. We observed that transducing B16 melanoma cells with BIRC2-targeting sgRNAs along with Cas9

resulted in increased non-canonical NF-κB pathway activity **(Figure S5F)** and increased tumor control after adoptive transfer of syngeneic PMEL TCR transgenic T cells compared with cells transduced with a non-targeting sgRNA **(Figure 7H)**. Finally, *BIRC2* expression in human cancer patients treated with immune checkpoint blockade was also found to correlate with risk of adverse patient outcome (Jiang et al., 2018) **(Figure 7I)**. Together, these data indicate that BIRC2 inhibition may be a potential opportunity to increase the efficacy of immunotherapy-mediated tumor cell killing across multiple cancer types.

Discussion

Tumor immunotherapy has reshaped clinical strategies for the treatment of human cancer and has brought about dramatic improvements in patient outcomes with several types of cancer. In spite of these improvements, most patients still receive minimal or non-durable clinical benefit from immunotherapy treatment strategies (Brahmer et al., 2012). Understanding the mechanisms by which tumor cells resist immunotherapy treatments and developing new therapies to overcome resistance mechanisms and improve the therapeutic efficacy of immunotherapy against cancer is an important focus. Using a two-cell type (2CT) whole-genome CRISPR/Cas9 screen, we have profiled tumor genes that are essential for survival in the face of engagement with tumor-specific T cells. Integrating dynamic transcriptional profiling of the tumor response to T cell engagement with the results of the genome-scale CRISPR screen allowed us to identify tumor genes that are both transcriptionally induced by T cell encounter and function to promote tumor cell survival in this context. Genes implicated in tumor resistance to conventional therapies (Jung et al., 2015; Sartorius and Krammer, 2002), including

BCL2 and *BIRC2,* were among the tumor genes we identified that can negatively regulate tumor cell susceptibility to T cell-mediated destruction. In addition, we identified genes with no previously described role in promoting tumor cell survival, including *TOR1AIP1*, *SCAF11* and *LPGAT1*. The role and regulation of these genes in the context of immunotherapy requires further investigation, but our data suggests that, taken together, these genes represent components of an orchestrated tumor cell defense mechanism that limits the cytotoxic effect of T cells on tumors.

In addition to identifying components of the active tumor defense against T cell engagement at a genome scale, we also assessed the therapeutic potential of targeting these and other top genes identified from the 2CT CRISPR to augment the efficacy of immunotherapy. By interrogating top hits from the screen with a database of druggable proteins, we identified a number of potential tumor targets for combination therapy. We found that the inhibition of several of these targets, including BIRC2, ITGAV and DNPEP, increased tumor antigen-specific T cell-mediated destruction of melanoma cells *in vitro* and BIRC2 inhibition could also augment the *in vitro* destruction of epithelial tumor cells by neo-antigen-specific T cells. Inhibition of BIRC2 during ACT treatment of a murine model of established melanoma demonstrated that two separated BIRC2 inhibitors were capable of increasing T cell control of melanoma growth. The pharmacological inhibition of BIRC2 has been proposed as a potential avenue to increase tumor cell susceptibility to TNFα-mediated toxicity (Vredevoogd et al., 2019). Taken together, these data suggest that BIRC2 inhibitors may increase the effects of cancer immunotherapy in

human patients. This could be especially beneficial in tumor histologies for which current immunotherapy treatment efficacy is low.

Although a number of functional genomics studies have identified BIRC2 as a negative regulator of susceptibility to immunotherapy (Manguso et al., 2017; Pan et al., 2018; Vredevoogd et al., 2019), mechanistic insight into the role of BIRC2 in promoting tumor cell survival in this context have remained limited. While BIRC2 and other related proteins are often thought to inhibit cellular apoptosis through inhibiting the pro-apoptotic activities of caspases, additional functions have been characterized (Dubrez-Daloz et al., 2008). Further, BIRC2 has been reported to bind, but not inhibit the function of caspases (Eckelman and Salvesen, 2006), suggesting that direct inhibition of cellular apoptosis may not account for the effects of BIRC2 on tumor susceptibility to immunotherapy. Consistent with previous reports in the setting of B cell malignancies (Yang et al., 2016), we found that BIRC2 acts as an important negative regulator of the non-canonical NF-κB signaling cascade. Activation of non-canonical NF-κB signaling by genetic deletion of *BIRC2* promoted increased tumor cell destruction by upregulating tumor cell antigen presentation pathways and the production of pro-inflammatory chemokines that have been linked with clinical responses to immunotherapy (Dangaj et al., 2019; Harlin et al., 2009; Peng et al., 2015). It is notable that the expression of non-canonical NF-κB transcription factor *NFKB2* was positively correlated with survival in patients treated with CTLA blockade (Van Allen et al., 2015) and that *NFKB2* and *IRF1* expression could predict responses across several clinical cohorts of human immunotherapy patients. Further work to study the direct role of the non-canonical NF-κB signaling pathway in regulating the efficacy of

immunotherapy will be necessary to establish a role for the pathway in regulating tumor susceptibility apart from BIRC2-mediated effects.

Overall, our work here describes the use of genome-scale functional genomics to rapidly identify targets for combination therapies to increase the efficacy of cancer immunotherapy. Combining functional genomics studies in a two-cell type setting with transcriptional dynamics studies can also be utilized to identify active, acute regulators of resistance and susceptibility to selective pressures. As recent works have demonstrated the possibility of conducting genome-scale functional genomics studies in primary T cells (Shifrut et al., 2018), similar approaches might be utilized to identify T cell-intrinsic negative regulators of anti-tumor effects for targeted inhibition to improve immunotherapy. Integrating functional genomics data from both tumor and T cells settings may help to optimize new immunotherapy strategies to promote increased therapeutic effects and improved patient outcomes.

Acknowledgments

The authors of this article were supported by the Center for Cell-Based Therapy, NCI, NIH (Bethesda, MD)), NIH Center for Regenerative Medicine, the Milstein Family Foundation, and the Intramural Research Program of the NCI (ZIA BC010763). We would like to thank Erina He for illustrations used in the manuscript. The authors would like to thank members of the Restifo, Rosenberg and Yang labs for helpful discussions and suggestions. N.E.S. is supported by NYU and NYGC startup funds, NIH/NHGRI (R00HG008171, DP2HG010099), NIH/NCI

(R01CA218668), DARPA (D18AP00053), the Sidney Kimmel Foundation, the Melanoma Research Alliance, and the Brain and Behavior Foundation.

Author contributions

R.J.K. and S.J.P. and N.P.R. designed the study and wrote the manuscript. R.J.K., S.J.P., S.K.V., A.E.D., Y.P., M.S., T.N.Y., Z.Y., M.J., W.L., A.P., P.M., D.D.D., A.N.H., N.E.S. performed experiments or provided reagents. K.C.W. and N.E.S. provided reagents and expertise.

Declaration of Interests

N.P.R. holds equity in and is employed by Lyell Immunopharma, South San Francisco, USA.

N.E.S. is a scientific advisor for Vertex.

Figure titles and legends

Figure 1. A genome-scale 2CT assay optimized for identifying tumor genes promoting resistance to T cell-mediated death. (A) Mel624 melanoma cells were co-cultured with ESO T cells at a 1:3 E:T ratio for 6 or 12 hr and tumor cell survival was measured by flow cytometry. **(B)** Experimental design of genome-scale CRISPR/Cas9 2CT screen in which Mel624 cells were transduced with the GECKOv2 library and cultured with ESO T cells for 6 hr. sgRNA representation was measured in control and ESO T cell treated tumor cells. Depletion of sgRNA representation in ESO T cell treated tumor cells was compared with control treated cells and depicted as **(C)** a scatterplot of the normalized enrichment of the most-depleted sgRNA vs. the second-most depleted sgRNA for all genes after ESO T cell treatment (top 100 most depleted genes depicted in enlarged region) or **(D)** RIGER analysis was performed to identify top depleted genes. **(E)** Top 250 genes for which sgRNAs were significantly ($P < 0.05$) depleted by RIGER ranking were analyzed by Ingenuity Pathway Analysis (IPA) and enriched pathways were determined. **(F)** Second-most depleted sgRNAs for genes treated with ESO T cells were compared in biological replicate screens. Data is representative of two biological replicate experiments with four technical replicates in each condition **(A)** or depicts data from one **(C-E)** or two **(F)** genome-scale CRISPR screens.

Figure 2. Dynamic transcriptional profiling of 2CT interaction reveals tumor transcriptional response to T cell engagement. (A) Experimental design of transcriptional profiling of dynamics of ESO T cell interaction with Mel624 tumor cells. Cells were co-cultured at a 1:3 E:T ratio for 0 or 6 hr and each cell population was sorted by FACS. mRNA expression levels were quantified by RNA sequencing. **(B)** Volcano plot representing differentially expressed genes analyzed by RNA-seq of CD3+mTCRb+ T cells that were co-cultured with Mel624 cells for 0 or 6 hr. Abundance is represented as relative fold change (*x* axis) versus significance (*y* axis). **(C)** Volcano plot representing differentially expressed genes analyzed by RNA-seq of Mel624 cells that were co-cultured with ESO T cells for 0 or 6 hr. Abundance is represented as relative fold change (*x* axis) versus significance (*y* axis). **(D)** Ingenuity Pathway Analysis (IPA) of Mel624 genes that were significantly upregulated or downregulated upon ESO T cell co-culture. **(E)** Heatmap of NF-κB regulated apoptosis gene expression in Mel624 cells following a 0 or 6 hr co-culture with ESO T cells. **(F)** Experimental design of tumor pathway activation assay. A375 melanoma cells were transduced via lentivirus with cDNA ORFs encoding cellular signaling pathway activating constructs. Transduced cells were cultured with ESO T cells in an arrayed fashion, and the impact of pathway activation on susceptibility to T cell-mediated killing was assessed. **(G)** Percent change in tumor cell death (compared with control construct) for each pathway-activated cell line. Relative percent change in tumor cell death is plotted (*x* axis) versus significance (*y* axis). **(H)** Percent change in tumor cell death in replicate pathway activation screens. Data is pooled from three independent experiments **(B-E)**, is representative of 2 independent experiments with four technical replicates per group **(G)** or depicts the results of 2 independent experiments **(H)**.

Figure 3. Identification of T cell-induced tumor-intrinsic genes which act to promote survival. **(A)** Volcano plot representing differentially expressed tumor genes that were identified as being significantly depleted from duplicate CRISPR 2CT screens by RIGER analysis (n=42 genes). Expression of genes was analyzed by RNA-seq as in Figure 2 with abundance represented as relative fold change (*x* axis) versus significance (*y* axis). Ten genes which met CRISPR screen depletion criteria were significantly induced by T cell engagement (red dots; *P* value < 0.05, fold change > 1.3. **(B)** The effect of gene knockout on tumor susceptibility to killing by T cells was measured by flow cytometry. Statistically significant sgRNAs for individual genes are indicated by red dots, as they resulted in a significant increase in tumor killing by T cells relative to non-targeting sgRNA ($p < 0.05$). A gene was considered validated (* at top) if two or more sgRNAs were statistically significant. Data is pooled from three independent experiments **(A)** or is representative of three independent experiments **(B)**. *P* values calculated for negatively enriched gene-targeting sgRNAs compared to control sgRNA by two tailed Student's *t* test.

Figure 4. Inhibitors of CRISPR screen-identified genes sensitizes tumor cells to T cell-mediated killing. **(A)** Workflow utilized to identify and screen inhibitors for capacity to increase T cell-mediated destruction of tumor cells. Top 250 hits from CRISPR screen were filtered to identify targets with available inhibitors. A375 melanoma cells were co-cultured with ESO T cells at a 1:2 E:T ratio for 16hr in the presence or absence of inhibitors. Co-cultures washed and tumor cell viability was measured with WST1 viability reagent. The impact of inhibitors on ESO T cell killing of A375 cells was measured at low (500 nM except for α-ITGAV at 250 ng/mL and Fomepizole and Dalfampridine at 500 μM) and high (5 μM except for α-ITGAV at 2.5 μg/mL and Fomepizole and Dalfampridine at 5 mM) concentrations **(B, D)**. **(C,E)** Plot of *p* values (significance threshold $P < 0.05$, dotted line) between tumor elimination by the combination inhibitor and ESO T cell treatment versus ESO T cells alone (*x* axis) and tumor elimination by the combination treatment versus inhibitor alone (*y* axis). Data is representative of three independent experiments with four technical replicates per sample **(B-E)**. *P* values calculated by two tailed Student's *t* test.

Figure 5. Inhibitors sensitize tumor cells to T cell-mediated killing irrespective of antigen target. **(A)** Depiction of experimental design. Tumor cells were co-cultured with T cells at an E:T ratio of 1:2 for 16 hr in the presence or absence of inhibitors and tumor cell viability was measured by flow cytometry. **(B)** A375 melanoma cells were co-cultured with ESO T cells along with inhibitors at 5μM except for α-ITGAV at 2.5 μg/mL, and tumor cell elimination was measured by flow cytometry. **(C)** Mel624 melanoma cells were co-cultured with ESO T cells along with inhibitors at 5μM except for α-ITGAV at 2.5 μg/mL, and tumor cell elimination was measured by flow cytometry. **(D)** Mel624 melanoma cells were co-cultured with MART-1 T cells along with inhibitors at 5μM except for α-ITGAV at 2.5 μg/mL, and tumor cell elimination was measured by flow cytometry. **(E)** Colon cancer cell line SB4266 was co-cultured with T cells transduced with a TCR reactive against p53 R248W mutation along with inhibitors at 5μM. Tumor cell death was measured by flow cytometry. **(F)** Colon cancer cell line SB4238 was co-cultured with T cells transduced with a TCR reactive against NCKAP1 D438Y along with inhibitors at 5μM. Tumor cell elimination was measured by flow cytometry. **(G, H)** Subcutaneous tumor growth in mice receiving ACT of PMEL1 T cells along with vehicle or

LCL161 (30 mg drug/kg body weight). Mice were treated with LCL161 via IP injection every 48hr beginning 24hr after PMEL1 T cell infusion for a total of 5 doses. Tumor area **(G)** and mouse survival **(H)** are shown. Data are representative of four **(B-C)**, three **(D, G-H)** or two **(E-F)** independent experiments with four technical replicates per groups **(B-F)** or 10 mice per group **(G-H)**. * $P < 0.05$, ** $P < 0.01$. *P* values for *in vitro* assays **(B-F)** calculated by one-way ANOVA with multiple comparisons corrected with Dunnett adjustment. *P* values for *in vivo* assays **(G-H)** calculated by Wilcoxon rank sum test **(G)** and or log-rank test **(H)**. Inhibitors of the same targets which were found to significantly increase T cell killing of tumor are indicated in the same color. BIRC2 (Blue bars), DNPEP (Red Bars), ITGAV (Green bars).

Figure 6. BIRC2 negatively regulates tumor inflammation and non-canonical NF-κB signaling. **(A)** A375 (left panel) or Mel624 (right panel) melanoma cells were treated with IFNγ (100 ng/mL) or TNFα (100 ng/mL) for 8hr and western blot analysis was performed. **(B)** A375 cells were transduced with Cas9 and non-targeting (NT sgRNA) or BIRC2 targeted sgRNAs and western blot analysis was performed. **(C)** Volcano plot representing differentially expressed genes in A375 cells transduced with Cas9 and BIRC2 targeting sgRNA versus NT sgRNA. Expression of genes was analyzed by RNA-seq as in Figure 2 with abundance represented as relative fold change (*x* axis) versus significance (*y* axis). **(D)** Ingenuity pathway analysis of genes significantly upregulated in BIRC2 KO A375 cells. **(E)** A375 cells were transduced with Cas9 and NT sgRNA or BIRC2 targeted sgRNAs and western blot analysis was performed. **(F)** Heatmap quantifying mRNA expression of genes reported to be differentially expressed in patients responding to checkpoint blockade therapy in melanoma (Harlin *et al*., 2009) in A375 cells transduced with Cas9 and NT sgRNA or BIRC2 targeting sgRNA. **(G)** Volcano plot representing transcription factor activation scores in mRNA expression profiles of BIRC2 KO A375 cells. Transcription factor activation was analyzed by IPA with increased transcription factor activity represented as positive *z* scores (*x* axis) and increased mRNA expression of transcription factor represented as positive fold change (*y* axis). **(H)** A375 cells were transduced with Cas9 and NT sgRNA or BIRC2 targeted sgRNAs and western blot analysis was performed. **(I)** Analysis of reported progression free survival of patients treated with CTLA4 blockade (Van Allen *et al*., 2015) based on mRNA expression of NFKB1 or NFKB2. Patients were stratified into groups based on whether they were above or below median mRNA expression for each gene (NFKB1=16.82, *NFKB2*=8.62). Data is representative of three independent experiments **(A, E, H)**, two independent experiment **(B)**, is pooled from a single experiment with three biological replicates per group **(C-D, F-G)** or represents analysis of 21 patients in each group **(I)**. *P* values calculated by log-rank test.

Figure 7. Genetic loss of BIRC2 increases tumor production of inflammatory chemokines and promotes T cell migration. (A) ChIP-seq analysis of RELB abundance at *CXCL10* locus in A375 cells transduced with Cas9 and NT sgRNA or BIRC2 targeting sgRNA. **(B-E)** A375 cells transduced with Cas9 and NT sgRNA or BIRC2 targeting sgRNA were assayed for production of **(B)** GM-CSF, **(C)** CCL5/RANTES, **(D)** CXCL10 and **(E)** ability to induce migration of ESO T cells across a transwell membrane. **(F-G)** Intracellular cytokine production of ESO T cells that were co-cultured with A375 cells transduced with Cas9 and NT sgRNA or BIRC2 targeting sgRNAs for 5 hr in the presence of brefeldin and monensin. **(H)** Growth curve of subcutaneous B16 melanoma

tumors that were modified with Cas9 and NT sgRNA or BIRC2 targeting sgRNA. Mice were treated with PMEL1 T cells and tumor area was measured over time. **(I)** Heatmap displaying normalized *Z* scores from Cox-PH regression analysis of BIRC2 expression in published human immunotherapy datasets (Jiang et al., 2018). Data is representative of two independent experiments **(A-D),** three independent experiments **(E-G)**, three independent experiments with at least 8 mice per group **(H)**. **P* < 0.05. *P* values calculated by two tailed Student's *t* test.

Table 1: Tumor genes identified as significantly depleted after genome 2CT screens

Screen 1				**Screen 2**		
gene_id	riger	sigLabelSwitchFDR		gene_id	riger	sigLabelSwitchFDR
hsa-mir-1299	101.5	0.00000		AHSG	197	0.00000
ALG11	319.75	0.00001		CHCHD10	237	0.00000
BIRC2	327.75	0.00001		CBLL1	260.25	0.00000
FAM32A	342	0.00001		KRTAP19-7	362.75	0.00001
KIF3C	404.5	0.00001		PRSS16	424.25	0.00001
LAPTM4A	442.75	0.00002		GOLGA7B	455	0.00001
KRTAP3-2	490.5	0.00002		FAM32A	480.25	0.00001
ARSK	498.25	0.00002		ARSD	489.75	0.00001
HHLA3	532.25	0.00002		hsa-mir-1299	490.5	0.00001
LOC730183	543.5	0.00002		PGM3	493.5	0.00001
LRR1	617.5	0.00002		APOBEC1	509.5	0.00001
MED26	635.25	0.00002		SFR1	563.75	0.00002
hsa-mir-197	654.5	0.00002		ENO4	662	0.00004
TRAF2	703.25	0.00002		SLC6A18	664.75	0.00004
EIF3I	720.5	0.00002		CXADR	685	0.00004
RBM14	730.25	0.00003		ZFYVE28	689.25	0.00004
hsa-mir-181b-2	782	0.00004		DNAJC16	694.25	0.00004
VPS13D	800.5	0.00004		SPDYA	701.25	0.00004
SCRT1	825.5	0.00004		hsa-mir-4435-1	764.75	0.00004
HES4	830.25	0.00004		ARL2BP	765.75	0.00004
DPEP2	864.75	0.00005		HLCS	769.25	0.00004
MUC7	883.5	0.00005		CCDC62	780.5	0.00004
ASPH	894	0.00006		RAD21	799.5	0.00004
EMC2	907.5	0.00006		hsa-mir-30d	834.5	0.00005
OSTM1	939.75	0.00006		CASKIN2	835.5	0.00005
ZNF124	942.25	0.00006		EMID1	893.25	0.00006
DCUN1D1	960.75	0.00007		TWIST2	905	0.00006
TCEAL7	987	0.00007		SMC5	905.5	0.00006
RRM1	989.75	0.00007		ECM1	944.25	0.00006
SLC26A9	994.5	0.00007		APPL1	958.75	0.00007
TCEB3CL	997.75	0.00007		COL11A1	966	0.00007
ZNF136	1038	0.00008		MRPS24	992.75	0.00007
TMOD4	1038.5	0.00008		THEMIS2	998.75	0.00007
PACRG	1049.75	0.00008		FOSL2	1006.75	0.00008
RALGAPA2	1078.75	0.00008		PUS10	1012.5	0.00008
CLDND1	1095.25	0.00008		GPR12	1037.5	0.00008

PROL1	1099.25	0.00008		SCAF11	1046.25	0.00009
TDO2	1133	0.00010		ISCU	1049.5	0.00009
MT1B	1171.25	0.00010		EIF3I	1052.25	0.00009
COG3	1177.5	0.00011		POLR2B	1069	0.00009
CHMP7	1200	0.00012		ACSL1	1071.75	0.00009
TMX4	1202	0.00012		ZNF232	1080.5	0.00009
GIMD1	1202.75	0.00012		KAT5	1105	0.00009
METTL14	1241.75	0.00012		ZGPAT	1114.25	0.00009
ORC1	1257	0.00013		ZBBX	1123.5	0.00009
CWC27	1264.25	0.00013		RLN3	1123.75	0.00009
DPAGT1	1275	0.00013		PPCS	1129.5	0.00010
GPS2	1276.75	0.00013		TMIGD1	1132	0.00010
SCEL	1278.25	0.00013		RPL6	1153.75	0.00010
ARMC3	1279.5	0.00013		ST8SIA6	1161	0.00010
RBM10	1294.5	0.00013		UBE2N	1177.25	0.00011
hsa-mir-6775	1354.75	0.00016		hsa-mir-597	1196.25	0.00011
RNF31	1355.75	0.00016		MUT	1200	0.00012
SCD5	1356	0.00016		MPG	1200.75	0.00012
MPL	1376.75	0.00016		AHSA1	1249.25	0.00012
NHSL1	1383	0.00016		TOR1AIP1	1279.5	0.00013
CNGB1	1424.5	0.00017		hsa-mir-3652	1289	0.00013
C22orf26	1425	0.00017		SNAP25	1295.5	0.00014
CLEC16A	1448.25	0.00018		ITSN2	1356.25	0.00016
hsa-mir-1207	1453	0.00018		CCR8	1391.5	0.00016
NLRC5	1456.25	0.00018		PIF1	1441	0.00017
DDX21	1460.5	0.00018		TAS2R14	1451.5	0.00017
FBXW7	1475	0.00018		OR2D3	1466.5	0.00018
MOBP	1507.25	0.00019		STK11IP	1472.25	0.00018
SART3	1513	0.00019		DHX35	1473	0.00018
NKX1-2	1536.75	0.00019		SHOC2	1545	0.00020
RPL23	1540.25	0.00019		FIGLA	1589	0.00022
YTHDF2	1591.5	0.00021		CRCP	1605	0.00022
hsa-mir-615	1592.25	0.00021		CYB5R3	1613.75	0.00023
PRAMEF20	1604.25	0.00022		CAT	1633.75	0.00023
IL3	1604.75	0.00022		ATG13	1650.25	0.00024
GABRR2	1620.75	0.00022		PHAX	1673	0.00024
OR5H14	1623	0.00022		GUF1	1685.25	0.00024
CHST10	1632.25	0.00023		NDUFS8	1714.75	0.00025
RPL13	1638.75	0.00023		NAPSA	1737.5	0.00026

HIST2H2BE	1643.75	0.00023		MX2	1744.75	0.00026
THOP1	1649.25	0.00023		PRTG	1750.25	0.00026
DGAT2L6	1669.5	0.00024		OARD1	1754	0.00026
KRTAP19-6	1697	0.00024		BTG3	1767.25	0.00026
SUPT5H	1704	0.00024		CHST3	1799.5	0.00028
NLRP8	1706.25	0.00024		PPIA	1847.75	0.00029
OR4C11	1707	0.00024		SH2B3	1853	0.00029
SLC25A24	1716.75	0.00024		HIF3A	1860.25	0.00029
VPS29	1720.5	0.00024		ATL2	1862	0.00029
TMEM47	1734	0.00025		IL9	1871.25	0.00029
LRRC4	1752.75	0.00025		DESI2	1886.5	0.00030
ZNF227	1783.25	0.00026		CDC20	1886.75	0.00030
FBXO36	1809.75	0.00028		ATG16L2	1887.5	0.00030
GJC2	1815.5	0.00028		BTBD2	1890.25	0.00030
GPD1L	1816	0.00028		KIF21A	1900.75	0.00031
ZPLD1	1823	0.00028		NEURL2	1911.5	0.00031
P4HA2	1825.25	0.00028		SLC44A1	1925	0.00031
hsa-mir-4442	1852.5	0.00030		MRPL34	1993.5	0.00033
ROS1	1873.25	0.00031		TMED2	2018	0.00034
TTC30A	1881.5	0.00031		PDK3	2062.25	0.00036
POLRMT	1887.75	0.00031		FMNL3	2076	0.00037
RBL2	1891.25	0.00031		OXCT1	2084	0.00037
SEH1L	1909.25	0.00032		C8orf42	2101.25	0.00038
DDX59	1914.75	0.00032		PCCB	2124.25	0.00039
SERTAD2	1929.75	0.00032		SPATA31A6	2126.25	0.00039
ABI3BP	1930.75	0.00032		NRCAM	2135.5	0.00039
DPT	1978	0.00034		hsa-mir-519c	2152.5	0.00040
GRHPR	2012	0.00035		GAR1	2155.75	0.00040
KRTAP4-9	2017	0.00035		TMEM91	2179.25	0.00041
LCN2	2017.75	0.00035		RBL2	2188	0.00042
MEX3B	2029.25	0.00035		HPS6	2228.75	0.00043
RLTPR	2030	0.00035		EGR2	2232.25	0.00044
POLR3H	2037.5	0.00035		CCNB1IP1	2233	0.00044
RAD17	2048.5	0.00036		SAA2	2237	0.00044
CCDC125	2081.75	0.00037		hsa-mir-3687	2256	0.00044
UQCR11	2095.75	0.00037		ITGA7	2289	0.00046
LCE2C	2111.5	0.00038		DSTN	2294.75	0.00046
hsa-mir-3180-3	2158.75	0.00041		ENY2	2308	0.00046
FAM3B	2161.25	0.00041		PIP5KL1	2314.25	0.00046

DNMT3B	2187.75	0.00042		VAMP8	2330.5	0.00047
RPS25	2218	0.00043		KIF3A	2340	0.00047
TRIM43B	2234.5	0.00044		ISX	2344.5	0.00047
IFIT1	2236.5	0.00044		GNL3L	2344.5	0.00047
PPP1R3F	2250.5	0.00045		RASSF8	2367.5	0.00048
SNRPD3	2270.75	0.00045		FMO4	2399.75	0.00050
hsa-mir-6726	2315	0.00046		SYCE1	2414.25	0.00050
hsa-mir-147a	2321	0.00046		IL17D	2421	0.00050
TCEAL6	2325.25	0.00046		CINP	2423.5	0.00050
STRAP	2334.75	0.00046		PRPF3	2483.5	0.00053
DIDO1	2397	0.00049		FBXL13	2484	0.00053
EIF4G1	2413.5	0.00050		EIF2A	2484.5	0.00053
C2orf49	2413.75	0.00050		ATP8B4	2501	0.00053
SPRR1B	2420.25	0.00050		ALG11	2518.5	0.00054
TRAF3IP3	2462.25	0.00053		DDIT4L	2525.5	0.00055
C22orf23	2466	0.00053		GATA2	2529.75	0.00055
TMEM184A	2493	0.00053		IGSF9	2535	0.00056
CDC123	2508.75	0.00053		hsa-mir-146b	2553.5	0.00056
B3GNT8	2523.25	0.00054		DPY19L4	2613.5	0.00059
SLC6A6	2547.75	0.00055		C15orf61	2640.25	0.00059
ADM5	2548	0.00055		CDCA8	2681.75	0.00061
TRA2B	2565.25	0.00056		DDX46	2689.25	0.00062
ATF4	2577.75	0.00057		ZNF469	2705	0.00063
SLC7A9	2590.75	0.00058		OR52E2	2712	0.00063
hsa-mir-1289-1	2594.5	0.00058		NPAS2	2718.5	0.00064
CYB5R3	2601.5	0.00058		P2RX4	2724.75	0.00064
hsa-mir-4539	2623.5	0.00059		NFKBIL1	2780	0.00067
SLC5A7	2652.75	0.00061		TLCD2	2836.75	0.00072
RIOK1	2687.75	0.00064		LILRA4	2848	0.00072
CCDC58	2705.75	0.00065		SRSF2	2902.5	0.00075
hsa-mir-4456	2714.75	0.00066		MYH4	2909.75	0.00076
FKBP6	2740.75	0.00068		KAL1	2955.75	0.00078
COLEC11	2742	0.00068		ABHD3	2970	0.00079
C9orf85	2752.75	0.00069		PGD	2970.25	0.00079
SUMO1	2791	0.00070		RELB	3007.5	0.00081
RAB17	2811.5	0.00071		PCNA	3011.75	0.00081
SNRPF	2815.25	0.00071		RALB	3021.25	0.00082
PLK2	2840.5	0.00073		COL5A1	3035.5	0.00082
EML3	2841.75	0.00073		HAL	3037.25	0.00083

LPPR5	2845.25	0.00073		hsa-mir-4538	3042.25	0.00083
RPAP2	2847.5	0.00073		OR1L8	3050.5	0.00083
SLC9C2	2862.5	0.00074		NonTargetingControlGuideForHuman_0561	3078.25	0.00086
CDC45	2877.5	0.00074		HDDC2	3099.5	0.00087
hsa-mir-6868	2935	0.00076		hsa-mir-8060	3129.25	0.00088
SFPQ	2936.5	0.00076		IL6	3130	0.00089
SLC5A9	2939.75	0.00076		PNMA3	3161.25	0.00090
CHST13	2940.5	0.00076		LOC100507462	3239.25	0.00095
VAV1	2996.25	0.00078		BIRC2	3240.25	0.00095
hsa-mir-208a	3002.25	0.00078		hsa-mir-1825	3241.25	0.00095
ENY2	3013.75	0.00079		LRRFIP2	3243.75	0.00095
GALR3	3025	0.00079		SBNO1	3288	0.00098
MTA1	3028.25	0.00080		KCNG2	3312	0.00100
DDX1	3049.75	0.00081		MYO1E	3312.5	0.00100
hsa-mir-4651	3050.25	0.00081		RQCD1	3319.25	0.00101
TYW5	3051.25	0.00081		MADD	3359.75	0.00104
BAP1	3068.25	0.00082		KRTAP5-11	3373.25	0.00104
ATP6V1C1	3100.75	0.00082		CAV1	3386.75	0.00106
ALDH2	3119.75	0.00083		CCNA2	3397.75	0.00107
hsa-mir-3129	3124.5	0.00083		REG1B	3415.75	0.00108
RRH	3137.25	0.00085		IL1R1	3469.5	0.00111
CHRM3	3142.25	0.00085		PDCL2	3473.5	0.00111
SF1	3183.25	0.00087		OR1L6	3501.5	0.00113
OCEL1	3211.75	0.00089		RPS26	3502.5	0.00113
FFAR3	3216.5	0.00089		hsa-mir-4697	3526.75	0.00114
ACTC1	3216.5	0.00089		WIBG	3561	0.00117
PPFIBP1	3246.25	0.00090		PSTK	3562.75	0.00117
hsa-mir-6794	3262.25	0.00091		TMED10	3564	0.00117
MTMR14	3265.5	0.00091		CEBPG	3593.25	0.00119
INSL4	3293.5	0.00093		DEGS2	3611.25	0.00119
CHRNA3	3298.75	0.00094		C12orf56	3620.5	0.00120
hsa-mir-663b	3299.25	0.00094		DLD	3685	0.00124
WARS2	3313.25	0.00094		TDGF1	3693.25	0.00124
ATAD5	3325.75	0.00095		PIH1D3	3701	0.00124
hsa-mir-5787	3331.5	0.00095		BUD31	3721.5	0.00126
PSMC5	3336	0.00096		TRPV6	3721.5	0.00126
LOC100507462	3336.25	0.00096		SPC25	3724.25	0.00126
PRPF40A	3356.5	0.00096		DNAJB8	3769	0.00128
SLC2A8	3361.25	0.00097		NonTargetingControlGuideForHuman_0852	3828.25	0.00132

MRPL44	3365.25	0.00097		NonTargetingControlGuideForHuman_0766	3832	0.00132
RPF1	3366.25	0.00097		KLHL31	3832.25	0.00132
TTF2	3392.5	0.00099		hsa-mir-1289-1	3835	0.00133
GLYAT	3408.75	0.00099		PSD4	3837.5	0.00133
ZNF69	3437	0.00102		CUL4A	3874.25	0.00135
BYSL	3442.5	0.00103		LCK	3878	0.00136
KAL1	3448.25	0.00103		RLN1	3901.25	0.00138
hsa-mir-3143	3456.75	0.00103		CSPG5	3931.5	0.00139
PGS1	3471.5	0.00105		KRTAP5-10	3932.5	0.00140
WBP2	3486.75	0.00106		hsa-mir-1251	3994	0.00144
ZNF480	3494	0.00106		ARHGEF11	4001.25	0.00144
PHYH	3549.5	0.00109		ZMYND15	4046.5	0.00148
COX5B	3552	0.00109		AZI1	4049	0.00148
PTMS	3554.5	0.00109		PTPRCAP	4089	0.00152
EEF1B2	3558	0.00110		CCDC172	4108.25	0.00153
MXD4	3580.5	0.00110		ZNF778	4117.75	0.00154
HOXB8	3593.5	0.00111		LAMTOR3	4157	0.00158
TMEM144	3609.75	0.00112		2-Mar	4158.5	0.00158
SOX18	3612	0.00112		ISCA2	4167.5	0.00160
RBM14-RBM4	3649.75	0.00114		POGLUT1	4169	0.00160
hsa-mir-485	3674.75	0.00117		WBP11	4171	0.00160
BRICD5	3702.25	0.00119		SYDE2	4239.75	0.00166
PPP1R27	3747.75	0.00122		PDP1	4293.75	0.00170
hsa-mir-6880	3803.25	0.00125		PGR	4309.75	0.00171
KRTAP4-6	3812.5	0.00126		LOC440563	4314.5	0.00172
hsa-mir-4425	3813	0.00126		CHGA	4316.25	0.00172
AKIRIN1	3841.75	0.00127		ANKRD42	4331.25	0.00173
FAM114A2	3845.5	0.00127		SHARPIN	4346.75	0.00174
IL36RN	3861	0.00128		SRGAP2	4355.5	0.00174
PRPF3	3902.25	0.00132		TMEM37	4364.75	0.00175
hsa-mir-548w	3941.75	0.00135		RPL12	4374	0.00176
THAP5	3951.5	0.00136		ELTD1	4390.25	0.00176
DPM2	3955.5	0.00136		MT3	4394.25	0.00176
CDR2L	3964.25	0.00136		GART	4396.5	0.00177
WDR45B	4002.5	0.00137		TRIM37	4405.5	0.00177
LYRM1	4044.5	0.00140		KRTAP5-1	4411.5	0.00178
PTPLAD1	4053.5	0.00140		SNX1	4428.5	0.00180
NLRC4	4055.75	0.00140		USP8	4429.75	0.00181
OTOR	4095.25	0.00143		KITLG	4443.25	0.00181

DYDC1	4109.75	0.00145		FAM216A	4447.75	0.00182
BARHL2	4139.25	0.00147		CDH7	4468.25	0.00183
hsa-mir-3197	4151.5	0.00148		EPB41	4487.25	0.00185
PARP10	4173	0.00149		TOM1L1	4487.75	0.00185
TNFRSF10B	4226.5	0.00156		PIP5K1A	4506.25	0.00187
WFDC6	4236	0.00156		FOLR1	4523.75	0.00188
FAM126A	4238.5	0.00157		MRPL45	4524.75	0.00189
TAF4	4252.75	0.00158		UQCRFS1	4551.25	0.00192
TMIGD1	4256	0.00158		RPLP0	4567.25	0.00193
hsa-mir-19a	4283.25	0.00159		ADAMTS4	4570.75	0.00193
LIN7A	4283.5	0.00159		PDCD11	4659.5	0.00200
POLR3F	4311.5	0.00163		COPE	4700.5	0.00202
RNPS1	4325.75	0.00164		FAM50A	4719.5	0.00203
STUB1	4333.25	0.00165		DDX51	4785	0.00210
CST4	4351.5	0.00167		FOXD4L5	4811.75	0.00214
BCL2	4373	0.00168		NAALAD2	4818.25	0.00215
POLD2	4428.5	0.00172		RPAP2	4818.75	0.00215
PUS7	4470.75	0.00176		TAC1	4843.25	0.00217
OR2B11	4497	0.00177		DAOA	4852.75	0.00218
COL7A1	4497.25	0.00177		hsa-mir-2276	4871.5	0.00219
CCDC151	4498.75	0.00177		C14orf119	4877.25	0.00220
HMGB4	4565.75	0.00182		NME8	4883.5	0.00221
TOP1	4568.5	0.00182		TBCD	4890.75	0.00221
UBE2I	4579.5	0.00183		DLGAP4	4962	0.00229
ABCG8	4616.25	0.00185		hsa-mir-3185	4990.75	0.00231
SLA2	4661.5	0.00189		ZNF350	5005.75	0.00232
TREML1	4665.5	0.00190		PRRG1	5008.25	0.00232
CHMP4B	4666.5	0.00190		MAGEA3	5032	0.00233
MAT2A	4670	0.00190		MAL	5051.75	0.00235
ZBTB41	4678.75	0.00190		KISS1R	5101.75	0.00239
CASP6	4683.5	0.00191		MGA	5164.5	0.00244
METTL2B	4721.75	0.00195		CELSR2	5180.25	0.00246
RHO	4734.5	0.00196		ERO1L	5184.75	0.00246
HOXC8	4744.25	0.00196		BCL2	5231.25	0.00250
hsa-mir-320c-1	4750	0.00197		RPH3AL	5243	0.00250
RPS16	4755	0.00197		TXNDC16	5261	0.00252
WSB2	4760.5	0.00198		SMIM8	5297	0.00256
CINP	4770.75	0.00198		hsa-mir-101-1	5315.5	0.00258
SLC16A3	4771.5	0.00198		BRPF1	5317	0.00258

MS4A14	4801.25	0.00200		ICA1L	5325.75	0.00259
C1orf194	4818.5	0.00201		PRKRIP1	5331.5	0.00260
CCDC93	4898.5	0.00207		hsa-mir-4690	5346	0.00262
OR5H6	4912.5	0.00208		ROBO4	5349.25	0.00262
STXBP4	4940	0.00210		FOCAD	5426	0.00267
CWF19L2	4942	0.00210		DSG3	5446	0.00269
PHF8	4944	0.00210		CC2D1A	5450.5	0.00270
DDHD2	4951.25	0.00211		ZNF134	5455.25	0.00271
ZNF665	4955.5	0.00212		ATP11B	5460.75	0.00272
MYRIP	4958.25	0.00212		TMEM238	5515	0.00277
ATP6V0C	4971.25	0.00213		MARCKSL1	5533.25	0.00277
MNS1	4990.5	0.00214		WNT7A	5538.25	0.00278
GATAD2A	4994.75	0.00214		ZNF98	5589.5	0.00283
C1orf111	5005.75	0.00216		HAX1	5599.25	0.00285
hsa-mir-6777	5024.75	0.00217		PRKX	5607.25	0.00285
PNMAL1	5095	0.00223		SNX14	5691.75	0.00295
OR1N2	5100	0.00224		ZNF607	5719.75	0.00298
IL12A	5131	0.00226		FAHD1	5781.5	0.00306
KRT24	5163.5	0.00228		ZNF575	5787.5	0.00306
CSF1	5193.75	0.00231		CFP	5852.75	0.00312
SMIM15	5199.25	0.00231		ARHGAP40	5876.25	0.00314
RNF135	5200.5	0.00231		TSPYL6	5884.5	0.00314
hsa-mir-142	5234.5	0.00234		INSIG2	5924	0.00317
C19orf67	5252.75	0.00235		EFNB1	5935.5	0.00318
NDNL2	5254.5	0.00235		CCSAP	5977	0.00323
PAK1IP1	5258.5	0.00235		PKP4	5998.5	0.00325
RPL7	5262.25	0.00236		CNGA1	6005.75	0.00326
GAGE10	5285.5	0.00237		RAG2	6087.75	0.00334
IDE	5287.75	0.00237		KCNJ9	6121.5	0.00337
CCDC101	5310.25	0.00240		C9orf153	6127	0.00338
TUBA3D	5315.5	0.00240		EAF2	6142	0.00339
DOK6	5356.25	0.00244		AUH	6165.5	0.00343
SPAST	5369.25	0.00245		SLFN5	6166.25	0.00343
ZNF175	5375.25	0.00245		RNF130	6192.5	0.00346
OR5M1	5415.25	0.00249		FIZ1	6204	0.00348
MYOCD	5450.5	0.00254		HSCB	6212.75	0.00349
CETN2	5521	0.00260		SLC34A3	6227.5	0.00350
NME6	5521.5	0.00260		EOGT	6228.5	0.00351
BUB1	5540.75	0.00261		LDHA	6251	0.00352

hsa-mir-3923	5555	0.00263		ZC3H12C	6257	0.00353
FASN	5593.25	0.00265		AKIRIN1	6262	0.00354
PITHD1	5595	0.00265		IWS1	6288	0.00357
RPS19	5622.25	0.00266		TRAF5	6356	0.00366
SYNGR3	5687.25	0.00272		TMEM17	6371.5	0.00367
hsa-mir-4421	5749.75	0.00278		ARFIP2	6400.5	0.00370
PPAPDC1A	5762.75	0.00280		TOMM7	6401.5	0.00370
LRMP	5770.25	0.00281		hsa-mir-3689d-2	6415.25	0.00372
ECI1	5785.75	0.00282		PLEKHF1	6504.5	0.00382
TCFL5	5790.25	0.00282		SENP5	6525	0.00384
ECHDC3	5811.75	0.00285		MANSC1	6545	0.00386
HCRTR1	5812.75	0.00285		SERTAD2	6550.75	0.00387
IST1	5838	0.00289		MEX3D	6564	0.00388
hsa-mir-6820	5860.5	0.00291		CCDC42B	6579.75	0.00389
hsa-mir-4448	5884	0.00294		FAM104A	6580	0.00389
TAF10	5896.5	0.00295		POMP	6623.75	0.00395
ATP5H	5975.75	0.00303		LPGAT1	6642	0.00397
SLC27A5	5982.25	0.00304		SLC12A1	6649.5	0.00397
TCP11X2	6038.75	0.00309		hsa-mir-6749	6670.75	0.00399
SOX10	6047.75	0.00310		TBPL2	6676.75	0.00401
SAC3D1	6055.75	0.00310		SC5D	6690.5	0.00402
TWF1	6063	0.00310		NGEF	6695.5	0.00403
DNAJC1	6099	0.00313		MED22	6701.5	0.00404
CAPN13	6116.5	0.00315		MIDN	6701.5	0.00404
AKAP1	6151.75	0.00320		MPZL1	6706.25	0.00404
CTGF	6206.5	0.00326		WDR60	6738	0.00408
SAP30BP	6221.5	0.00328		FBXL15	6757.75	0.00409
LBX1	6244.5	0.00329		VRK3	6780	0.00413
SYBU	6272.75	0.00332		ITGA10	6786.5	0.00413
LALBA	6309	0.00337		MIER1	6806	0.00416
NCAPH2	6311.75	0.00338		DBI	6812.75	0.00417
PBX1	6315.75	0.00339		COG8	6826	0.00419
HMGB1	6361	0.00344		OR13H1	6840	0.00419
hsa-mir-1249	6398	0.00350		hsa-mir-5687	6869.5	0.00424
hsa-mir-3173	6438.75	0.00353		RPL22L1	6886.5	0.00426
GIPC2	6450	0.00354		KCNIP1	6887.75	0.00426
TRIML1	6466.25	0.00357		COPA	6897.75	0.00428
YIPF6	6476.5	0.00358		ZNF549	6916.75	0.00430
C9orf3	6513	0.00361		NKX2-2	7036	0.00448

hsa-mir-215	6532.75	0.00364		WDR45B	7064.25	0.00450
ATPAF1	6537.5	0.00365		CYP4F2	7078.25	0.00453
hsa-mir-5591	6585.25	0.00371		hsa-mir-6165	7106.75	0.00456
hsa-mir-4443	6595.25	0.00372		BSCL2	7107.25	0.00456
ACADSB	6607.5	0.00373		SLC25A25	7179.75	0.00464
C11orf48	6650.75	0.00379		LARP6	7231.75	0.00471
C11orf71	6699.25	0.00383		CTNND2	7241.25	0.00473
hsa-mir-583	6735.75	0.00386		CAV2	7244.5	0.00473
BAG3	6743	0.00387		PIGM	7273.75	0.00475
hsa-mir-661	6754.5	0.00388		ESD	7284.25	0.00477
TPM4	6768.75	0.00389		JAM2	7310.5	0.00479
TMPRSS11D	6801	0.00394		MECOM	7321.25	0.00481
C1orf185	6806.25	0.00394		GRIA2	7335.75	0.00482
hsa-mir-6743	6824	0.00396		FAM63B	7339.75	0.00482
C16orf70	6841	0.00400		WDR18	7346.75	0.00483
ZNF24	6843.25	0.00400		SRSF10	7362.75	0.00485
ARHGAP24	6850.25	0.00400		BIK	7364.75	0.00486
HECW1	6869.75	0.00402		CAPN12	7384.75	0.00489
SLC39A12	6894.75	0.00405		WDR44	7405.5	0.00492
OSBPL3	6949	0.00411		C11orf54	7444.5	0.00496
hsa-mir-3163	6961.75	0.00413		FARSB	7446	0.00496
PIGX	6969.25	0.00414		hsa-mir-4419a	7473	0.00501
ERCC4	6982.75	0.00416		SEMA7A	7488.75	0.00502
PITPNM1	7029.25	0.00421		ZNF416	7600.5	0.00520
MILR1	7114	0.00433		WNT6	7607.75	0.00520
AAK1	7194	0.00442		NonTargetingControlGuideForHuman_0811	7615.75	0.00522
PRSS55	7202	0.00444		ELOVL4	7634.75	0.00525
MBP	7217	0.00446		MEIG1	7648.75	0.00527
TEX37	7221.75	0.00446		OLA1	7678.75	0.00529
LARS2	7242.75	0.00447		HSBP1L1	7695	0.00531
LYSMD4	7270.5	0.00449		ZMAT3	7709.25	0.00532
NonTargetingControlGuideForHuman_0625	7285.25	0.00451		ATRNL1	7734.5	0.00536
BIRC6	7287.5	0.00451		FAM3B	7768.5	0.00540
hsa-mir-378d-1	7300.75	0.00453		CLEC2B	7777.75	0.00541
F10	7317.25	0.00455		CCL4L2	7781.75	0.00542
SPATA31A6	7334	0.00457		SFTA3	7789.5	0.00544
FXYD2	7335	0.00457		ANXA1	7845	0.00550
hsa-mir-744	7353.25	0.00460		PLK5	7871	0.00553
EGR2	7373.25	0.00462		ARPP19	7877.75	0.00554

FRS2	7430.25	0.00470		ZNF556	7888.25	0.00555
ZNF556	7474	0.00476		CHMP2B	7932.5	0.00561
CLMN	7507	0.00481		ARHGAP20	7952.5	0.00564
KLHL36	7512	0.00482		KBTBD13	8036	0.00577
OR2F2	7551.25	0.00489		CREB3L2	8058.5	0.00581
NAA25	7614	0.00498		ZNF654	8067	0.00582
GRK7	7624.5	0.00500		SPACA1	8085	0.00584
DOCK1	7626.5	0.00500		CXXC1	8101.75	0.00587
USP37	7635.75	0.00500		ZNF322	8121.5	0.00590
ZNF329	7637.5	0.00501		SKA3	8184.5	0.00599
LDHB	7638.25	0.00501		FSD1	8239.75	0.00605
ARL4A	7680.75	0.00506		TSG101	8264.5	0.00608
DVL2	7756.75	0.00516		hsa-mir-346	8269.25	0.00608
HMX1	7762.75	0.00517		SLC44A5	8294	0.00613
RNF186	7781.25	0.00520		SERHL2	8295	0.00613
hsa-mir-6845	7802.75	0.00523		DUS3L	8301.75	0.00613
NPPB	7803.75	0.00524		HOXA11	8362.5	0.00621
NonTargetingControlGuideForHuman_0582	7827.25	0.00526		PCMT1	8368.75	0.00622
ADAM33	7846.25	0.00528		PTER	8397.5	0.00626
SETD9	7857.25	0.00529		XRCC2	8462.25	0.00639
YPEL1	7864.25	0.00531		MOSPD2	8493.25	0.00642
COPS8	7924.75	0.00538		SI	8494.75	0.00642
DYDC2	7957	0.00540		WIZ	8511.5	0.00644
RNF13	8064.5	0.00556		CISD3	8549.75	0.00649
SLC25A25	8076.25	0.00558		DEFB125	8567.5	0.00651
OTUD6A	8087	0.00560		TMEM185B	8571.5	0.00651
ITGAV	8093	0.00560		SLC23A3	8603.25	0.00655
CNTFR	8126	0.00564		TDG	8653	0.00661
SNRPD2	8135	0.00566		TSGA13	8655	0.00661
NPS	8148.5	0.00568		NDUFA3	8679.25	0.00664
LAMTOR1	8189.5	0.00575		PRCP	8751.25	0.00675
CD200R1L	8203.5	0.00576		ZDHHC16	8774	0.00679
XPO4	8223.5	0.00578		AKTIP	8792.75	0.00681
AXIN1	8229.75	0.00580		SLC30A3	8840.25	0.00690
PLA2G7	8273.75	0.00586		FSIP2	8859	0.00692
RPP40	8311.5	0.00592		SP6	8909.5	0.00700
KRTAP5-7	8392.25	0.00604		SRSF3	8910.25	0.00700
CD160	8425.5	0.00608		CDC37	8921.75	0.00701
SRPX2	8480	0.00616		HGD	8922	0.00701

ZNF586	8492	0.00617		SLC7A6OS	8946	0.00706
HTATIP2	8501	0.00620		WFDC12	9044.75	0.00721
SLC25A38	8548.25	0.00627		GPRC5B	9050.75	0.00722
CCDC66	8565.25	0.00630		ECM2	9091.75	0.00729
TSR2	8594.25	0.00633		IL1R2	9118.75	0.00733
ASGR1	8604.25	0.00634		FEN1	9131.25	0.00733
MDN1	8667.25	0.00644		BAG5	9217	0.00745
POLR3C	8685	0.00644		MSANTD1	9222.5	0.00745
GPHB5	8697.25	0.00646		GTF2H1	9223.25	0.00745
TSPYL2	8714	0.00647		hsa-mir-4292	9233.75	0.00747
PPA2	8740	0.00651		RWDD2B	9247.5	0.00750
NonTargetingControlGuideForHuman_0258	8741.5	0.00651		SLC25A28	9271.75	0.00754
RNF5	8759.75	0.00654		MAPK13	9278.25	0.00755
OR10J5	8809.5	0.00663		hsa-mir-2861	9335.75	0.00764
hsa-mir-4697	8810.25	0.00663		APAF1	9339.75	0.00765
TRAPPC2L	8843.5	0.00670		OR2A14	9339.75	0.00765
SPATS2	8851.5	0.00670		BOD1	9341	0.00765
EPRS	8874.75	0.00672		GLI1	9401	0.00774
CTSK	8886.5	0.00674		KRTAP5-3	9401.5	0.00774
ISCU	8926.25	0.00680		FKBPL	9403.5	0.00775
SLC30A6	8941.25	0.00681		TMEM57	9428.25	0.00778
SEMA3E	8986.5	0.00688		NPAT	9437.5	0.00780
GUCY1A3	9024.75	0.00695		NEK8	9494.25	0.00789
NonTargetingControlGuideForHuman_0042	9069.5	0.00703		TROAP	9505.75	0.00791
hsa-mir-4755	9184.25	0.00722		RPS16	9529.5	0.00794
OR52H1	9206	0.00727		NUDT8	9556	0.00799
FAM206A	9206.5	0.00727		CD300LD	9559	0.00799
APCDD1	9233.25	0.00732		C10orf99	9561.5	0.00800
hsa-mir-3915	9233.5	0.00732		TXLNB	9576	0.00803
DNAJB5	9313.75	0.00744		TUBB4B	9588.25	0.00805
HENMT1	9345.75	0.00749		CRYBA4	9646.75	0.00816
NUDC	9406.5	0.00759		GIMAP2	9703	0.00824
CHMP6	9427.25	0.00762		OR10J3	9765.5	0.00834
MTMR6	9429	0.00763		CLDN2	9773.25	0.00835
TACC1	9499.75	0.00772		SEBOX	9781	0.00837
KARS	9516	0.00774		MTRNR2L2	9809.25	0.00843
FTSJD1	9522.25	0.00775		C1orf86	9861.5	0.00853
MEGF10	9523	0.00775		RNF180	9883.25	0.00856
IGLON5	9556.5	0.00781		KIAA1429	9886.25	0.00856

ATP6V0A1	9624.25	0.00790		NUP85	9913.5	0.00860
hsa-mir-5586	9640.75	0.00794		hsa-mir-1285-2	9915.75	0.00860
MTRR	9743.5	0.00810		USP25	9940.5	0.00865
PLEKHM3	9757.75	0.00811		CCDC88A	9941.5	0.00865
TAS2R40	9764.25	0.00813		TBCA	9942.25	0.00865
CDK12	9773.25	0.00815		DNAJB6	10016	0.00881
PPME1	9839	0.00828		CUL3	10043.75	0.00886
GATAD2B	9852.75	0.00830		ACTR10	10070.25	0.00889
OTUD7B	9864.25	0.00832		NonTargetingControlGuideForHuman_0491	10094	0.00893
PPARD	9867.25	0.00832		MTIF3	10096.75	0.00893
EFCAB6	9869	0.00832		HDHD2	10115.75	0.00895
TMEM127	9875.25	0.00834		LMAN1	10121	0.00896
ANAPC16	9888.25	0.00836		CHUK	10188	0.00908
KRTAP9-9	9935.5	0.00847		DDO	10205	0.00912
PSMG1	9940.5	0.00848		ZNF726	10229	0.00917
ARRDC1	9993.75	0.00858		SERPINB13	10256	0.00922
hsa-mir-381	10037.75	0.00866		MYH14	10355.5	0.00941
hsa-mir-501	10044.25	0.00867		ZHX2	10360.75	0.00942
KDM2A	10099.25	0.00875		MROH9	10371.5	0.00943
RPL37	10103.5	0.00876		ZNF639	10392.25	0.00949
STOX1	10109.75	0.00877		NR5A2	10413.75	0.00952
PLAU	10121.5	0.00879		FEZF1	10422.5	0.00954
GADD45G	10137.5	0.00883		BTG4	10429	0.00956
SYF2	10152.75	0.00886		FN1	10461.25	0.00961
TAS2R4	10236.25	0.00899		CKMT2	10488	0.00966
XPO6	10241.25	0.00899		PARN	10541.75	0.00977
HOXB4	10264.75	0.00904		VDAC3	10548.25	0.00978
CCNT1	10327	0.00916		ZNF595	10582	0.00984
ITGA3	10410.25	0.00930		hsa-mir-150	10594.25	0.00985
ZNF689	10438	0.00934		WDR37	10596.25	0.00986
COL4A3BP	10498.5	0.00945		RBP5	10711.75	0.01004
ARGLU1	10498.75	0.00945		CKLF	10734.5	0.01010
NPM3	10539	0.00952		DHFR	10814.25	0.01025
PAH	10543.75	0.00952		HERC2	10886.75	0.01037
hsa-mir-4436b-2	10566	0.00956		TMEM216	10903	0.01040
QSOX1	10572.75	0.00958		CHERP	10936.75	0.01046
CCDC127	10607.25	0.00965		DPM1	10940	0.01047

SPATA3	10630.75	0.00969		PKDREJ	10948	0.01049
F11R	10657.5	0.00974		EN2	10958.5	0.01050
MUC15	10696.25	0.00981		ZNF776	10960	0.01051
hsa-mir-6884	10701.25	0.00982		SPRY1	10971	0.01053
DDRGK1	10718.25	0.00985		KCTD14	11012.5	0.01061
ST8SIA3	10731	0.00988		BCL3	11056	0.01068
AR	10738	0.00988		TNFSF12-TNFSF13	11104.75	0.01077
VPS37A	10811	0.01003		YIPF4	11110.25	0.01078
CFH	10813.25	0.01003		ZNF431	11112.75	0.01078
ZRANB2	10842.25	0.01008		NIP7	11210.5	0.01093
VSTM1	10858.25	0.01011		C3orf36	11239.75	0.01098
PSG3	10873.5	0.01013		KRT13	11240.25	0.01098
BEST3	10896.25	0.01017		NUDT13	11241.25	0.01098
BANK1	10912.75	0.01020		KIAA1211L	11259.5	0.01102
TAL1	10915.75	0.01021		KCNT2	11269.25	0.01103
PET117	10943.5	0.01026		FEV	11296.5	0.01109
COMMD7	10988	0.01034		TIMP1	11324.75	0.01115
PVR	11021	0.01039		DGKE	11376.75	0.01123
LOC284385	11040.25	0.01042		CHRNG	11430.5	0.01134
hsa-mir-6127	11047.25	0.01044		ACSM4	11439.5	0.01136
ATP6AP1	11097.75	0.01053		POLR1A	11486.75	0.01145
RPL30	11114.75	0.01058		C1orf172	11486.75	0.01145
GRIA2	11127.25	0.01060		CLCC1	11501.75	0.01149
SGCB	11152.25	0.01065		IQCF3	11507.75	0.01150
TMTC1	11199.5	0.01075		MBOAT4	11512.75	0.01151
SKA2	11218.25	0.01078		ATF5	11518.75	0.01152
RPLP2	11239.75	0.01083		FSTL4	11552.25	0.01158
BCAS1	11293.25	0.01094		TMX4	11624.5	0.01173
ACSM2A	11302.5	0.01096		ANKS4B	11731.25	0.01194
CENPF	11306.5	0.01097		TRIM52	11736.5	0.01194
ESD	11331.75	0.01103		GABRQ	11738.75	0.01194
THRAP3	11344	0.01105		HRH4	11755.5	0.01197
GARNL3	11375	0.01111		LOC100506422	11784	0.01203
EAF2	11511.75	0.01136		LMOD3	11801.5	0.01208
NDUFA8	11542.25	0.01141		COG3	11887.25	0.01225
CD180	11546.75	0.01141		PPP2R5D	11930	0.01233
KBTBD3	11560.5	0.01145		SAE1	11937.5	0.01234

CLCN7	11566.5	0.01146		CLDN10	11939.5	0.01235
PAX8	11585.75	0.01150		SF3B4	11948.75	0.01238
SLC16A9	11590	0.01152		CFHR5	11960.25	0.01241
hsa-mir-6863	11603.75	0.01155		NGB	12013.5	0.01251
UBE2V1	11612.25	0.01156		TK2	12047.25	0.01258
CRYBB3	11619.25	0.01157		TMEM69	12099.25	0.01271
DZIP1	11676.25	0.01168		PDE1B	12113.5	0.01273
NXPE3	11694.5	0.01171		STRN4	12242.75	0.01302
MINA	11719	0.01177		ADARB2	12270.25	0.01309
GDF10	11774.25	0.01191		KRTAP9-4	12343.75	0.01326
SPATA31A4	11804	0.01195		HDGF	12365.75	0.01332
DDX24	11812.5	0.01197		RAB11FIP1	12380.5	0.01335
TMEM251	11831	0.01201		NR2F6	12403	0.01341
hsa-mir-653	11900.75	0.01219		SCGB1D1	12410	0.01342
HKDC1	11949.25	0.01229		LOC158434	12432	0.01345
PPP2CA	11952.25	0.01229		CHST1	12441	0.01346
ATP1B4	11966.5	0.01233		GDF11	12442.75	0.01346
NEXN	11981.5	0.01237		HHLA3	12467.25	0.01351
CA7	12013.75	0.01242		SRP54	12468.25	0.01352
AAMP	12038.5	0.01248		CWC25	12570.75	0.01370
C12orf71	12204.75	0.01281		COX6C	12604.5	0.01377
CDC23	12222.25	0.01285		ARHGAP19	12607.25	0.01379
CTSO	12283.5	0.01300		HSD11B2	12617.75	0.01381
HGD	12288.25	0.01301		AFMID	12631.75	0.01383
hsa-mir-6516	12308.5	0.01306		ACTR1A	12672.25	0.01390
FITM1	12312.25	0.01307		IQCH	12701.25	0.01396
CRISP1	12326	0.01309		CSNK1G1	12743.75	0.01403
GCSAML	12333.25	0.01311		SLC12A2	12843.5	0.01429
PDDC1	12344.75	0.01312		DUT	12849.25	0.01431
VSIG8	12354.5	0.01314		hsa-mir-4780	12850.25	0.01431
GLTSCR1	12370.75	0.01317		hsa-mir-3907	12905.5	0.01446
DLG1	12372.25	0.01317		KPNA3	12907.75	0.01446
CCL24	12380.5	0.01319		TBX20	12916.75	0.01449
REN	12400.5	0.01322		CFH	12922.25	0.01450
hsa-mir-548a-1	12470.75	0.01337		CDK3	12949.75	0.01456
hsa-mir-4297	12478	0.01339		COL10A1	12974.25	0.01463

ADCY2	12520.25	0.01350		TMEM27	12997.25	0.01470
HRASLS2	12522.75	0.01350		OCIAD1	13001.25	0.01471
hsa-mir-3908	12532.5	0.01353		SERTAD1	13012.75	0.01473
MANSC1	12550.25	0.01355		INTS7	13023	0.01476
PDF	12551.5	0.01356		TOP3A	13109.75	0.01496
POM121C	12560.75	0.01359		KRT28	13123	0.01499
BTBD17	12584.5	0.01363		TMEM72	13151.25	0.01506
NUDT11	12616.25	0.01373		ANXA6	13218.75	0.01522
IL13RA1	12640.75	0.01377		UNC45B	13242	0.01527
CCDC74A	12680.5	0.01385		HLA-DRB1	13259.25	0.01531
GPATCH1	12723.5	0.01395		MSL1	13319.5	0.01547
PSMD6	12753.25	0.01405		ACTA2	13322.25	0.01548
MYOC	12758.75	0.01406		ANO7	13326.25	0.01549
MOB1A	12793.75	0.01413		CXCL10	13376.25	0.01560
PCDHGB3	12818.75	0.01419		TNFRSF9	13417.75	0.01571
ATP8A1	12842	0.01426		FIBIN	13423.5	0.01573
hsa-mir-600	12843.75	0.01426		CHIA	13435	0.01576
SCAF11	12852.25	0.01428		CRADD	13440.5	0.01578
ZFP90	12874.5	0.01433		KRT33A	13442.75	0.01578
MRPL35	12881.75	0.01435		DKC1	13462.5	0.01581
hsa-mir-4499	12931.5	0.01446		NonTargetingControlGuideForHuman_0147	13495.5	0.01588
ABCA8	12939.5	0.01449		CDHR5	13510.5	0.01592
SOX14	12949.25	0.01451		KCNAB2	13528.75	0.01598
FBXL15	12965.75	0.01456		HSF2	13539.25	0.01600
IFI27L2	13067	0.01480		CBX4	13586.5	0.01612
SRFBP1	13082.75	0.01484		hsa-mir-378c	13593.75	0.01614
FAM76B	13099.75	0.01487		KRTAP9-9	13602.75	0.01616
TMIE	13137	0.01496		DMRTB1	13615.75	0.01620
FKBP4	13192.75	0.01509		GK5	13643	0.01626
CSRP2BP	13199.5	0.01511		ODF2L	13668.75	0.01630
TNRC6C	13202	0.01512		EIF3B	13674.75	0.01631
RPL24	13319	0.01539		hsa-mir-23a	13677	0.01631
VASP	13340.75	0.01542		SNPH	13679.25	0.01632
RAI2	13345.25	0.01543		hsa-mir-8076	13692.75	0.01634
ARSD	13357.75	0.01546		HARS2	13694.25	0.01634
RPS8	13362.5	0.01547		POLI	13742.5	0.01645
hsa-mir-548s	13389.5	0.01553		C7orf73	13753	0.01646

PINLYP	13390.75	0.01553		YLPM1	13862.25	0.01673
FTMT	13394.25	0.01554		FGF23	13876.75	0.01676
KIAA1211L	13443.25	0.01564		TAS2R46	13877	0.01676
ATG4A	13488	0.01573		MFN2	13923.75	0.01689
SDAD1	13511.25	0.01579		TOX2	13955	0.01697
FAM131A	13607.75	0.01599		PJA2	13958.75	0.01698
COPS6	13624	0.01601		SART3	13976.25	0.01701
hsa-mir-1277	13646.5	0.01607		SOX21	13981.25	0.01703
LOC100996485	13674.5	0.01611		TCEB1	13992.75	0.01704
PPP2R5D	13705	0.01619		hsa-mir-4686	14031.75	0.01714
PSMB3	13829.25	0.01648		CCDC92	14062.25	0.01721
SNX1	13864.25	0.01655		TRIM27	14086.75	0.01727
TXNL4A	13873	0.01657		FTSJD1	14107.75	0.01732
ROPN1	13901.75	0.01665		OSBPL8	14135.75	0.01741
C14orf119	13958.25	0.01679		OR52I1	14144	0.01743
C15orf61	13996.75	0.01689		NUDC	14149.5	0.01745
ADAMTS5	14040.25	0.01699		DKK1	14185	0.01754
HIBADH	14051.5	0.01701		BLNK	14220.75	0.01763
SLITRK2	14061.5	0.01704		CCDC71L	14252.25	0.01771
CLDN5	14076.5	0.01707		FAM46C	14256.75	0.01772
C17orf97	14161.75	0.01726		TMCO5A	14263.25	0.01774
DNAJB3	14172.75	0.01728		RPS6KA2	14264.5	0.01774
AMER3	14246.25	0.01745		SLC26A1	14321.5	0.01789
PRPF4B	14255.5	0.01748		MYBL2	14353.5	0.01795
AK5	14265.5	0.01750		C7orf61	14423.5	0.01812
IDS	14287.5	0.01756		RPS2	14424	0.01812
MAOB	14307.25	0.01761		HPS3	14496.5	0.01832
ALKBH5	14326.5	0.01764		CYP17A1	14505.75	0.01834
STAT1	14345.75	0.01769		XAGE2	14605.25	0.01856
hsa-mir-6727	14362.25	0.01773		hsa-mir-198	14621	0.01859
IPMK	14366.5	0.01775		OR2T5	14634.25	0.01864
YBX3	14375.75	0.01777		RBM20	14647.5	0.01869
PLCL1	14419	0.01790		GULP1	14681.25	0.01876
hsa-mir-4280	14443	0.01796		SETX	14708.25	0.01881
CSNK2B	14446.5	0.01797		hsa-mir-18b	14708.75	0.01881
DHDH	14462	0.01799		CLGN	14768	0.01896
ATP10B	14467.75	0.01800		TBK1	14789.5	0.01901

MTX1	14483.25	0.01804		CACTIN	14830.25	0.01910
BPIFA2	14518.5	0.01812		ZNF280C	14876.25	0.01922
hsa-mir-8086	14546	0.01820		PRDX1	14937.5	0.01941
TEAD2	14561.25	0.01824		ARHGEF5	14966.75	0.01949
NKX2-1	14584.5	0.01831		TMC1	15052.5	0.01974
GPR110	14605.5	0.01837		POLM	15073.25	0.01979
GCGR	14606	0.01837		SH3BP1	15080.5	0.01981
hsa-mir-580	14618.5	0.01841		PHF20	15129	0.01994
CSTF2	14660.5	0.01850		DPM2	15139.75	0.01997
ADD3	14682.75	0.01857		SCGB1D2	15154	0.02000
OTUD4	14688.5	0.01858		FXN	15175.75	0.02007
ZNF365	14719	0.01869		WDR92	15196	0.02013
LPGAT1	14738	0.01872		KIAA0825	15242.5	0.02026
FOLR3	14776.5	0.01883		CD300A	15347.5	0.02050
CNKSR3	14785.5	0.01885		GBX1	15399	0.02063
AKT1S1	14846	0.01901		hsa-mir-621	15408.25	0.02065
GUCA2A	14859.25	0.01904		NCF2	15464.25	0.02078
CD5L	14946	0.01927		CDH11	15609	0.02118
DOCK5	14948.75	0.01928		TMEM52	15644.5	0.02130
NTF3	14982.25	0.01939		DPH2	15651.5	0.02131
NUDCD2	14989.5	0.01940		DIRAS2	15651.5	0.02131
ZNF202	15075	0.01965		THAP1	15660.25	0.02133
C9orf153	15078.25	0.01966		POLR2E	15702.75	0.02144
MC5R	15136.5	0.01980		C16orf97	15702.75	0.02144
OR10A3	15232	0.02006		SMCHD1	15704.75	0.02144
MRPL1	15247.75	0.02009		SLC4A8	15764.25	0.02160
CLEC4E	15261	0.02012		STX17	15817.75	0.02176
ATF3	15262	0.02013		HEATR5B	15858.75	0.02188
hsa-mir-5096	15378.25	0.02047		RPS23	15859	0.02188
MAB21L1	15415.75	0.02058		PTN	15879.75	0.02194
EPS8	15417.25	0.02058		NDUFAF6	15907	0.02201
CHSY1	15429.25	0.02061		MYLK4	15914.5	0.02203
CATSPERG	15454.5	0.02068		CDC42EP3	15944.25	0.02211
PYROXD2	15457	0.02069		TFCP2L1	15975.75	0.02220
MYADML2	15459	0.02069		NDUFC1	16023	0.02234
hsa-mir-6129	15514.5	0.02084		MEMO1	16064.5	0.02249
USP7	15520.75	0.02086		RBM48	16072	0.02250

OTC	15526.5	0.02088		BCCIP	16093.5	0.02255
NOC2L	15607.5	0.02111		EXOSC8	16110.75	0.02260
C17orf80	15619	0.02114		NonTargetingControlGuideForHuman_0717	16135	0.02266
TIMM21	15672.25	0.02130		OR8U1	16144.75	0.02268
IFNA8	15761.75	0.02158		EAF1	16212.75	0.02292
ALDH3B1	15820	0.02174		MOBP	16275.25	0.02307
OR7A10	15863.5	0.02187		GABRE	16283.25	0.02310
NT5E	15869.75	0.02188		TPM2	16300	0.02315
CNOT3	15913.75	0.02198		THRAP3	16373	0.02336
SIX5	15920.25	0.02200		TMF1	16388	0.02338
CALCR	15927	0.02201		MDH1	16480.25	0.02367
NAALAD2	15936	0.02204		FLYWCH1	16509.25	0.02374
ZNF430	16020.5	0.02226		KCNJ4	16571.5	0.02389
hsa-mir-626	16027.75	0.02229		TMPRSS11D	16625	0.02402
ZNF225	16055	0.02235		CCL18	16635.5	0.02407
CELA3A	16067.75	0.02239		DEDD2	16747	0.02436
C11orf35	16087.25	0.02243		PDK1	16774.25	0.02444
PRKAR1A	16119.5	0.02251		ZNF704	16806	0.02454
POLR2K	16126	0.02253		PIK3R6	16860.75	0.02470
ULK4	16134.25	0.02255		hsa-mir-633	16869	0.02472
C5orf47	16135.75	0.02255		ENDOD1	16873.25	0.02473
ZFP36	16140.75	0.02257		hsa-mir-4766	16890	0.02478
PROKR1	16151.75	0.02259		PXK	16920	0.02488
EMCN	16162	0.02261		FAM178A	16954.5	0.02500
MTRNR2L5	16171.75	0.02266		ABCC4	16970	0.02506
NFX1	16191.5	0.02272		NADK	16982	0.02509
OR10J1	16223.5	0.02280		CPEB3	16983	0.02509
CAPNS2	16326.5	0.02313		MAGEH1	16986.25	0.02510
EPHA6	16337	0.02316		ALG10B	16987.25	0.02510
OAF	16383.25	0.02330		ANAPC4	16996.25	0.02512
GSTM1	16389	0.02332		CTDSPL	17011.5	0.02516
ENDOD1	16411.25	0.02339		TNFSF12	17054.25	0.02528
hsa-mir-125a	16411.5	0.02339		NFIC	17123.75	0.02552
MTF1	16411.5	0.02339		OR6K2	17138.25	0.02556
SIAH2	16489.5	0.02362		GP6	17169.5	0.02565
MEST	16584	0.02392		FAM9A	17236.75	0.02583
KIAA0319L	16588	0.02394		hsa-mir-330	17253.25	0.02586

TSPAN5	16612.5	0.02401		UBE2D2	17286	0.02591
LGALS8	16630.75	0.02408		TMEM74	17297	0.02595
OR6C3	16657.25	0.02416		BTF3	17416.75	0.02635
hsa-mir-2467	16672.5	0.02421		TUBA1B	17455.25	0.02647
MTSS1L	16705.5	0.02432		TYK2	17483	0.02656
LRRC59	16755.5	0.02446		CLEC1A	17505.25	0.02662
FGF22	16907.5	0.02492		ZNF730	17539.75	0.02674
APOBEC3B	16950.25	0.02503		SLC5A2	17554	0.02677
EMR1	16951.25	0.02504		ENHO	17563.25	0.02680
ZSCAN25	16972.25	0.02509		HIST1H2BH	17598.25	0.02690
ZNF514	17025	0.02524		SCEL	17622.5	0.02696
MUCL1	17105	0.02549		HOXB8	17684.75	0.02717
RIMKLB	17145.25	0.02560		FGD3	17706.25	0.02723
FAM229B	17199.75	0.02576		WDR45	17709.25	0.02724
OR10H5	17238	0.02587		PSD3	17777.75	0.02745
OR4C45	17264.75	0.02597		BRD4	17785.5	0.02748
AK7	17264.75	0.02597		POU5F2	17859.5	0.02770
PLEKHG7	17268.75	0.02598		KRTAP4-6	17865.5	0.02771
DHCR7	17332	0.02617		SERPINB2	17961.75	0.02801
GNB2L1	17379	0.02631		KCTD11	18012.25	0.02812
ENO4	17440.5	0.02652		SGCE	18043.75	0.02823
hsa-mir-125b-1	17483.25	0.02665		ERH	18045.25	0.02823
IMPDH1	17502.75	0.02673		CAPN13	18051.25	0.02825
LIG4	17640.5	0.02715		KIF9	18121	0.02849
LIN54	17658.5	0.02721		PRPSAP1	18150.5	0.02858
hsa-mir-4512	17665.75	0.02724		POLG2	18196	0.02872
hsa-mir-1302-7	17676.25	0.02727		APCDD1L	18244.25	0.02886
hsa-mir-3196	17770.5	0.02758		HLA-DQA1	18259.5	0.02890
ASB4	17774.75	0.02760		NUB1	18331	0.02912
GINS2	17783	0.02763		CCDC80	18355.75	0.02921
GNAQ	17800.5	0.02768		NEK10	18376.25	0.02926
DIO3	17817	0.02774		TRA2B	18379	0.02927
SPATA7	17823.25	0.02777		PHC1	18394.25	0.02932
COX20	17886.25	0.02797		DOCK7	18405	0.02936
SOX5	17887	0.02797		RBBP8	18432.5	0.02945
SIGLEC7	17916.5	0.02804		LRSAM1	18492.25	0.02965
C5orf52	17928.75	0.02807		GRINA	18542.25	0.02983

ZCCHC14	17993.25	0.02831		hsa-mir-3193	18569.25	0.02994
KIAA0922	18008	0.02836		PACS1	18585.5	0.02999
FOXF2	18030.75	0.02845		SMC3	18675.75	0.03028
hsa-mir-6885	18124.75	0.02870		HIST1H2AE	18720.5	0.03040
FAM110A	18172.25	0.02887		WDR62	18791.25	0.03062
SF3A2	18176	0.02888		PLEKHM2	18857.5	0.03083
HMBOX1	18239.25	0.02906		TMBIM1	18952.25	0.03114
SIT1	18252.5	0.02908		PTBP2	19014.25	0.03134
OR2T8	18254.5	0.02909		GRSF1	19014.5	0.03134
CDH1	18260.5	0.02911		HDGFRP2	19122.75	0.03166
NonTargetingControlGuideForHuman_0820	18324.75	0.02934		CEP135	19151.5	0.03172
HERC1	18343	0.02940		ACVR2B	19232.25	0.03196
NEK8	18368.75	0.02951		MSANTD4	19251.25	0.03200
BIK	18453.75	0.02979		C9orf89	19442	0.03267
MIB2	18473	0.02984		HAUS7	19495	0.03282
C16orf55	18492	0.02989		SUPT20HL1	19504.75	0.03285
LTBP2	18513.25	0.02997		PDLIM1	19514.75	0.03289
GOLGA7	18533	0.03001		GCM1	19565	0.03306
MRPS18B	18550.5	0.03006		hsa-mir-3124	19678	0.03346
KDM5C	18559.25	0.03008		P2RX3	19680.75	0.03347
OTX1	18579	0.03015		hsa-mir-4682	19721	0.03361
SLX4	18596	0.03020		NARS2	19723.75	0.03362
GBP5	18634.5	0.03033		hsa-mir-4475	19727	0.03363
TM4SF1	18657.5	0.03041		OR2AE1	19768.5	0.03377
EIF4E1B	18690	0.03052		KRTAP12-3	19770.25	0.03377
C1orf173	18761	0.03072		PPIF	19796.5	0.03387
DYNC1LI2	18814.5	0.03088		POLR2J	19894.25	0.03417
CCDC61	18874.25	0.03109		NDUFA4	19926.75	0.03430
REPS1	18925.5	0.03126		HOXD11	19977.75	0.03449
KCTD12	18979.5	0.03142		SLC4A7	20002.75	0.03459
PRR25	18989.75	0.03144		CCL25	20147.25	0.03509
COX17	19076	0.03169		RNF182	20202.5	0.03525
PUSL1	19102	0.03178		SRA1	20222.75	0.03533
GDPD4	19158	0.03196		HDAC9	20236.25	0.03539
ZNF28	19232.5	0.03220		RECK	20267.75	0.03551
METRN	19246.25	0.03224		FAM177B	20328.25	0.03573
EIF3J	19249.5	0.03225		GNAZ	20342.75	0.03576

SERTAD4	19254.25	0.03227		TWF1	20350.75	0.03579
HECTD1	19263.25	0.03230		FGGY	20362.5	0.03584
NAIF1	19311.75	0.03244		SPRED3	20380.5	0.03591
HIF1A	19339	0.03253		CCL8	20406.75	0.03602
TMEM209	19381.75	0.03270		FUT8	20443.75	0.03615
hsa-mir-346	19488.5	0.03305		KCNIP4	20541.75	0.03648
FZD5	19557	0.03327		NonTargetingControlGuideForHuman_0418	20587.5	0.03662
ST7L	19604.25	0.03344		DSG4	20725.75	0.03711
XAB2	19630	0.03352		CDKN2C	20728.25	0.03712
PER2	19666	0.03367		hsa-mir-4660	20798	0.03734
PCDHGB4	19702.5	0.03378		FAM161B	20806.75	0.03739
RORB	19748	0.03395		hsa-mir-125b-1	20810.5	0.03739
ATRNL1	19786	0.03404		BET1	20890.5	0.03772
SLBP	19829.5	0.03420		MTRNR2L7	20933	0.03789
SATL1	19861.75	0.03431		C14orf28	20986.5	0.03809
MEF2D	19875	0.03434		BEND4	21000.5	0.03814
TOR1AIP1	19881.5	0.03437		UVRAG	21002	0.03815
CYB561A3	19982	0.03468		DDX4	21021	0.03823
hsa-mir-4283-2	19988.25	0.03470		KRT77	21208.75	0.03891
CCDC91	20079.25	0.03504		P2RY10	21225.25	0.03897
PKN2	20123.25	0.03520		MYRIP	21240.25	0.03905
hsa-mir-5688	20253.25	0.03571		MYH1	21271.5	0.03915
NOL7	20271.75	0.03578		C2CD4B	21283.75	0.03919
ZKSCAN5	20279.5	0.03582		TIMM10B	21328.5	0.03938
CCDC28A	20341	0.03601		TSPAN2	21371	0.03951
TNRC18	20415	0.03625		SMC6	21491.5	0.03999
AMOTL2	20457	0.03636		FAM129B	21511.5	0.04006
SNRNP35	20503	0.03652		SCUBE1	21604.25	0.04044
RAP1GDS1	20511.25	0.03656		RABEP1	21611.25	0.04046
hsa-mir-939	20548.25	0.03668		hsa-mir-3195	21620.75	0.04048
CYTH1	20569.75	0.03680		hsa-mir-606	21747.75	0.04099
AHSG	20594	0.03688		TAB3	21780.25	0.04113
CHCHD10	20673.5	0.03713		MATN3	21805.25	0.04119
CBLL1	20749.25	0.03738		C19orf59	21854.5	0.04137
KRTAP19-7	20780	0.03748		CAPN3	21887.5	0.04150
PRSS16	20823.25	0.03765		SEC61A1	21890	0.04152
GOLGA7B	20832.25	0.03768		MGST3	21900	0.04155

FAM32A	20853.25	0.03777		GCNT2	21951	0.04172
ARSD	20950.75	0.03813		STXBP1	22009.5	0.04193
hsa-mir-1299	20984.25	0.03827		CRIM1	22037	0.04204
PGM3	21001.25	0.03835		NonTargetingControlGuideForHuman_0820	22058.75	0.04213
APOBEC1	21027.75	0.03844		FYB	22138.25	0.04243
SFR1	21044.75	0.03853		TMEM130	22140	0.04244
ENO4	21216.25	0.03922		VPS28	22170.25	0.04258
SLC6A18	21248.25	0.03934		ANKFY1	22229.5	0.04281
CXADR	21280.5	0.03945		LARGE	22260.5	0.04294
ZFYVE28	21305	0.03953		EPB41L1	22260.75	0.04294
DNAJC16	21322.5	0.03959		UBP1	22327	0.04320
SPDYA	21374.25	0.03981		ZCCHC2	22348.25	0.04327
hsa-mir-4435-1	21389	0.03986		IER2	22350.5	0.04328
ARL2BP	21435.75	0.04007		SRPK2	22466	0.04369
HLCS	21550.5	0.04049		OR11A1	22511.5	0.04389
CCDC62	21574.5	0.04058		SLC39A7	22531	0.04398
RAD21	21602	0.04069		MORF4L2	22544	0.04402
hsa-mir-30d	21621.5	0.04077		FBLN5	22597.75	0.04425
CASKIN2	21659	0.04089		ZDHHC2	22612.75	0.04430
EMID1	21703.75	0.04106		BTF3L4	22643.25	0.04443
TWIST2	21747	0.04123		CSNK1A1L	22782.5	0.04491
SMC5	21985.5	0.04216		POLE2	22843.5	0.04517
ECM1	21987.75	0.04217		IMPACT	22942.5	0.04553
APPL1	21996.25	0.04220		CXorf61	23000.25	0.04577
COL11A1	22032.75	0.04234		LRRFIP1	23009.25	0.04581
MRPS24	22057.75	0.04244		AAED1	23017.25	0.04584
THEMIS2	22069.25	0.04248		XKRX	23111.25	0.04621
FOSL2	22149.5	0.04278		ASB16	23134.75	0.04630
PUS10	22188	0.04294		TMEM51	23146	0.04634
GPR12	22200	0.04298		KCNT1	23225.5	0.04668
SCAF11	22342	0.04349		INSL4	23258.5	0.04682
ISCU	22406	0.04376		ANGPTL3	23277.25	0.04686
EIF3I	22408	0.04377		RNF133	23305	0.04698
POLR2B	22472.75	0.04404		RAI2	23426.5	0.04752
ACSL1	22531.25	0.04429		PEX11A	23452.5	0.04760
ZNF232	22575	0.04448		RBM15	23495.5	0.04781
KAT5	22613.75	0.04463		FAM150B	23531.25	0.04796

ZGPAT	22639.75	0.04472		FTH1	23536.75	0.04799
ZBBX	22667	0.04484		FGB	23657	0.04853
RLN3	22675	0.04486		NCAPG2	23726	0.04880
PPCS	22745.75	0.04516		MAML2	23741.5	0.04886
TMIGD1	22894.5	0.04571		CCDC151	23765.5	0.04895
RPL6	22926.25	0.04584		ZNF592	23786.5	0.04904
ST8SIA6	22995.25	0.04613		ZNF804A	23851.5	0.04932
MRFAP1	22998.5	0.04615		GPR87	23872.75	0.04943
POLR3G	23053.5	0.04640		FAM117B	23911	0.04957
PRKCI	23093.5	0.04657		CARHSP1	23931.5	0.04966
BTBD2	23193.75	0.04696		GDNF	23938.25	0.04969
UCP3	23207.5	0.04702				
NPTX1	23211.5	0.04704				
LRSAM1	23371.75	0.04772				
hsa-mir-3684	23532.75	0.04836				
RHOXF2B	23593.75	0.04859				
E2F6	23621.5	0.04869				
TOR3A	23716.5	0.04906				
RNF113B	23819.75	0.04951				
CNTNAP2	23868.5	0.04971				
LHX1	23919.25	0.04995				

Table 2: Transcriptional dynamics of genes depleted in replicate 2CT genome-scale CRISPR screens

Gene name	Fold change mRNA 6hr coculture/0hr	pvalue (-log10)
RPAP2	3.83	1.386153
BIRC2	3.49	2.095161
ESD	2.78	1.655263
TWF1	2.15	1.127761
EGR2	2.13	1.422591
SCAF11	1.92	2.493371
TOR1AIP1	1.73	1.654647
LPGAT1	1.67	1.594682
TXLNB	1.65	0.736541
SERTAD2	1.62	1.964377
COG3	1.55	0.951055
ALG11	1.53	0.630745
RBL2	1.42	1.730386
BCL2	1.39	1.333402
ENDOD1	1.35	0.880535
AKIRIN1	1.31	0.846618
EAF2	1.3	0.313509
C14orf119	1.27	0.752152
PRPF3	1.22	0.822365
ENY2	1.21	0.719565
TRA2B	1.18	0.809857
SNX1	1.17	0.933405
THRAP3	1.17	1.068386
ISCU	1.09	0.277723
WDR45B	1.03	0.136798
EIF3I	1.02	0.092091
TMX4	-1.03	0.052917
ARSD	-1.05	0.069726
HHLA3	-1.05	0.042312
PPP2R5D	-1.06	0.239111
SART3	-1.06	0.201343
CINP	-1.13	0.501461
MANSC1	-1.13	0.079621
NUDC	-1.29	0.689154
SLC25A25	-1.31	1.128394
RPS16	-1.36	1.127576

FAM32A	-1.4	1.213536
DPM2	-1.62	2.076065
C15orf61	-1.72	1.713913
CYB5R3	-1.76	2.226299
NEK8	-1.81	2.116487
FBXL15	-2.15	2.270763

Table 3: Mapping top 2CT CRISPR depleted genes to protein-coding genes

Gene ID	Mapped ID	Gene name/Gene Symbol
HUMAN|HGNC=13921|UniProtKB=O95870	ABHD16A	Protein ABHD16A;ABHD16A;ortholog
HUMAN|HGNC=19195|UniProtKB=Q6H8Q1	ABLIM2	Actin-binding LIM protein 2;ABLIM2;ortholog
HUMAN|HGNC=18075|UniProtKB=Q9NZD4	AHSP	Alpha-hemoglobin-stabilizing protein;AHSP;ortholog
HUMAN|HGNC=25744|UniProtKB=Q9H9L7	AKIRIN1	Akirin-1;AKIRIN1;ortholog
HUMAN|HGNC=32456|UniProtKB=Q2TAA5	ALG11	GDP-Man:Man(3)GlcNAc(2)-PP-Dol alpha-1,2-mannosyltransferase;ALG11;ortholog
HUMAN|HGNC=28658|UniProtKB=Q6DCA0	AMMECR1L	AMMECR1-like protein;AMMECR1L;ortholog
HUMAN|HGNC=29135|UniProtKB=Q6UB98	ANKRD12	Ankyrin repeat domain-containing protein 12;ANKRD12;ortholog
HUMAN|HGNC=23725|UniProtKB=Q5T5U3	ARHGAP21	Rho GTPase-activating protein 21;ARHGAP21;ortholog
HUMAN|HGNC=25361|UniProtKB=Q8N264	ARHGAP24	Rho GTPase-activating protein 24;ARHGAP24;ortholog
HUMAN|HGNC=721|UniProtKB=P54793	ARSF	Arylsulfatase F;ARSF;ortholog
HUMAN|HGNC=588|UniProtKB=O94817	ATG12	Ubiquitin-like protein ATG12;ATG12;ortholog
HUMAN|HGNC=855|UniProtKB=P27449	ATP6V0C	V-type proton ATPase 16 kDa proteolipid subunit;ATP6V0C;ortholog
HUMAN|HGNC=24137|UniProtKB=Q6L9W6	B4GALNT3	Beta-1,4-N-acetylgalactosaminyltransferase 3;B4GALNT3;ortholog
HUMAN|HGNC=950|UniProtKB=Q92560	BAP1	Ubiquitin carboxyl-terminal hydrolase BAP1;BAP1;ortholog
HUMAN|HGNC=990|UniProtKB=P10415	BCL2	Apoptosis regulator Bcl-2;BCL2;ortholog
HUMAN|HGNC=590|UniProtKB=Q13490	BIRC2	Baculoviral IAP repeat-containing protein 2;BIRC2;ortholog
HUMAN|HGNC=15519|UniProtKB=Q14137	BOP1	Ribosome biogenesis protein BOP1;BOP1;ortholog
HUMAN|HGNC=27441|UniProtKB=Q3KP22	C11orf85	Membrane-anchored junction protein;C11orf85;ortholog
HUMAN|HGNC=32331|UniProtKB=Q5T5A4	C1orf194	Uncharacterized protein C1orf194;C1orf194;ortholog
HUMAN|HGNC=28250|UniProtKB=Q6P1W5	C1orf94	Uncharacterized protein C1orf94;C1orf94;ortholog
HUMAN|HGNC=28772|UniProtKB=Q9BVC5	C2orf49	Ashwin;C2orf49;ortholog
HUMAN|HGNC=26951|UniProtKB=Q86YL5	C8orf42	Testis development-related protein;TDRP;ortholog
HUMAN|HGNC=18200|UniProtKB=Q8WXE0	CASKIN2	Caskin-2;CASKIN2;ortholog
HUMAN|HGNC=1516|UniProtKB=P04040	CAT	Catalase;CAT;ortholog
HUMAN|HGNC=29588|UniProtKB=Q5BJE1	CCDC178	Coiled-coil domain-containing protein 178;CCDC178;ortholog
HUMAN|HGNC=30723|UniProtKB=Q6P9F0	CCDC62	Coiled-coil domain-containing protein 62;CCDC62;ortholog

HUMAN|HGNC=1578|UniProtKB=P20248	CCNA2	Cyclin-A2;CCNA2;ortholog
HUMAN|HGNC=1766|UniProtKB=Q9ULB5	CDH7	Cadherin-7;CDH7;ortholog
HUMAN|HGNC=1837|UniProtKB=P53567	CEBPG	CCAAT/enhancer-binding protein gamma;CEBPG;ortholog
HUMAN|HGNC=1876|UniProtKB=O15519	CFLAR	CASP8 and FADD-like apoptosis regulator;CFLAR;ortholog
HUMAN|HGNC=23789|UniProtKB=Q9BW66	CINP	Cyclin-dependent kinase 2-interacting protein;CINP;ortholog
HUMAN|HGNC=2080|UniProtKB=P54105	CLNS1A	Methylosome subunit pICln;CLNS1A;ortholog
HUMAN|HGNC=16999|UniProtKB=Q92989	CLP1	Polyribonucleotide 5'-hydroxyl-kinase Clp1;CLP1;ortholog
HUMAN|HGNC=18623|UniProtKB=Q96MW5	COG8	Conserved oligomeric Golgi complex subunit 8;COG8;ortholog
HUMAN|HGNC=17888|UniProtKB=O75575	CRCP	DNA-directed RNA polymerase III subunit RPC9;CRCP;ortholog
HUMAN|HGNC=2396|UniProtKB=P53673	CRYBA4	Beta-crystallin A4;CRYBA4;ortholog
HUMAN|HGNC=15982|UniProtKB=Q8IWT3	CUL9	Cullin-9;CUL9;ortholog
HUMAN|HGNC=10664|UniProtKB=Q6UX04	CWC27	Peptidyl-prolyl cis-trans isomerase CWC27 homolog;CWC27;ortholog
HUMAN|HGNC=2873|UniProtKB=P00387	CYB5R3	NADH-cytochrome b5 reductase 3;CYB5R3;ortholog
HUMAN|HGNC=21191|UniProtKB=P59103	DAOA	D-amino acid oxidase activator;DAOA;ortholog
HUMAN|HGNC=17347|UniProtKB=Q9BUQ8	DDX23	Probable ATP-dependent RNA helicase DDX23;DDX23;ortholog
HUMAN|HGNC=25360|UniProtKB=Q5T1V6	DDX59	Probable ATP-dependent RNA helicase DDX59;DDX59;ortholog
HUMAN|HGNC=15861|UniProtKB=Q9H5Z1	DHX35	Probable ATP-dependent RNA helicase DHX35;DHX35;ortholog
HUMAN|HGNC=2680|UniProtKB=Q9BTC0	DIDO1	Death-inducer obliterator 1;DIDO1;ortholog
HUMAN|HGNC=2902|UniProtKB=Q92796	DLG3	Disks large homolog 3;DLG3;ortholog
HUMAN|HGNC=29157|UniProtKB=Q9Y2G8	DNAJC16	DnaJ homolog subfamily C member 16;DNAJC16;ortholog
HUMAN|HGNC=2981|UniProtKB=Q9ULA0	DNPEP	Aspartyl aminopeptidase;DNPEP;ortholog
HUMAN|HGNC=23028|UniProtKB=Q9H4A9	DPEP2	Dipeptidase 2;DPEP2;ortholog
HUMAN|HGNC=3011|UniProtKB=Q07507	DPT	Dermatopontin;DPT;ortholog
HUMAN|HGNC=3208|UniProtKB=P24534	EEF1B2	Elongation factor 1-beta;EEF1B2;ortholog
HUMAN|HGNC=3226|UniProtKB=P98172	EFNB1	Ephrin-B1;EFNB1;ortholog
HUMAN|HGNC=3239|UniProtKB=P11161	EGR2	E3 SUMO-protein ligase EGR2;EGR2;ortholog
HUMAN|HGNC=3272|UniProtKB=Q13347	EIF3I	Eukaryotic translation initiation factor 3 subunit I;EIF3I;ortholog
HUMAN|HGNC=3296|UniProtKB=Q04637	EIF4G1	Eukaryotic translation initiation factor 4 gamma 1;EIF4G1;ortholog
HUMAN|HGNC=3297|UniProtKB=P78344	EIF4G2	Eukaryotic translation initiation factor 4 gamma 2;EIF4G2;ortholog
HUMAN|HGNC=28430|UniProtKB=Q9BV81	EMC6	ER membrane protein complex subunit 6;EMC6;ortholog
HUMAN|HGNC=1316|UniProtKB=Q9HC35	EML4	Echinoderm microtubule-associated protein-like 4;EML4;ortholog
HUMAN|HGNC=24449|UniProtKB=Q9NPA8	ENY2	Transcription and mRNA export factor ENY2;ENY2;ortholog
HUMAN|HGNC=3415|UniProtKB=P01588	EPO	Erythropoietin;EPO;ortholog
HUMAN|HGNC=3471|UniProtKB=P11474	ESRRA	Steroid hormone receptor ERR1;ESRRA;ortholog

HUMAN|HGNC=3522|UniProtKB=O95677	EYA4	Eyes absent homolog 4;EYA4;ortholog
HUMAN|HGNC=24563|UniProtKB=Q9Y421	FAM32A	Protein FAM32A;FAM32A;ortholog
HUMAN|HGNC=1253|UniProtKB=P58499	FAM3B	Protein FAM3B;FAM3B;ortholog
HUMAN|HGNC=18786|UniProtKB=Q14320	FAM50A	Protein FAM50A;FAM50A;ortholog
HUMAN|HGNC=17800|UniProtKB=Q9NSD9	FARSB	Phenylalanine--tRNA ligase beta subunit;FARSB;ortholog
HUMAN|HGNC=3595|UniProtKB=Q14517	FAT1	Protocadherin Fat 1;FAT1;ortholog
HUMAN|HGNC=3600|UniProtKB=P23142	FBLN1	Fibulin-1;FBLN1;ortholog
HUMAN|HGNC=16712|UniProtKB=Q969H0	FBXW7	F-box/WD repeat-containing protein 7;FBXW7;ortholog
HUMAN|HGNC=18522|UniProtKB=Q5VV16	FOXD4L5	Forkhead box protein D4-like 5;FOXD4L5;ortholog
HUMAN|HGNC=30968|UniProtKB=A6NGK3	GAGE10	G antigen 10;GAGE10;ortholog
HUMAN|HGNC=14264|UniProtKB=Q9NY12	GAR1	H/ACA ribonucleoprotein complex subunit 1;GAR1;ortholog
HUMAN|HGNC=11960|UniProtKB=Q6Y7W6	GIGYF2	PERQ amino acid-rich with GYF domain-containing protein 2;GIGYF2;ortholog
HUMAN|HGNC=28980|UniProtKB=Q14691	GINS1	DNA replication complex GINS protein PSF1;GINS1;ortholog
HUMAN|HGNC=4374|UniProtKB=O60234	GMFG	Glia maturation factor gamma;GMFG;ortholog
HUMAN|HGNC=18707|UniProtKB=Q7Z6J2	GRASP	General receptor for phosphoinositides 1-associated scaffold protein;GRASP;ortholog
HUMAN|HGNC=4579|UniProtKB=P39086	GRIK1	Glutamate receptor ionotropic, kainate 1;GRIK1;ortholog
HUMAN|HGNC=33383|UniProtKB=A0PJZ3	GXYLT2	Glucoside xylosyltransferase 2;GXYLT2;ortholog
HUMAN|HGNC=4801|UniProtKB=P40939	HADH	Trifunctional enzyme subunit alpha, mitochondrial;HADHA;ortholog
HUMAN|HGNC=4803|UniProtKB=P55084	HADHB	Trifunctional enzyme subunit beta, mitochondrial;HADHB;ortholog
HUMAN|HGNC=4848|UniProtKB=O43613	HCRTR1	Orexin receptor type 1;HCRTR1;ortholog
HUMAN|HGNC=28982|UniProtKB=Q12766	HMGXB3	HMG domain-containing protein 3;HMGXB3;ortholog
HUMAN|HGNC=25451|UniProtKB=Q1KMD3	HNRNPUL2	Heterogeneous nuclear ribonucleoprotein U-like protein 2;HNRNPUL2;ortholog
HUMAN|HGNC=25155|UniProtKB=Q86XE5	HOGA1	4-hydroxy-2-oxoglutarate aldolase, mitochondrial;HOGA1;ortholog
HUMAN|HGNC=5129|UniProtKB=P31273	HOXC8	Homeobox protein Hox-C8;HOXC8;ortholog
HUMAN|HGNC=5961|UniProtKB=Q9Y6K9	IKBKG	NF-kappa-B essential modulator;IKBKG;ortholog
HUMAN|HGNC=5993|UniProtKB=P14778	IL1R1	Interleukin-1 receptor type 1;IL1R1;ortholog
HUMAN|HGNC=15561|UniProtKB=Q9UBH0	IL36RN	Interleukin-36 receptor antagonist protein;IL36RN;ortholog
HUMAN|HGNC=6029|UniProtKB=P15248	IL9	Interleukin-9;IL9;ortholog
HUMAN|HGNC=29882|UniProtKB=Q9H1K1	ISCU	Iron-sulfur cluster assembly enzyme ISCU, mitochondrial;ISCU;ortholog
HUMAN|HGNC=28977|UniProtKB=P53990	IST1	IST1 homolog;IST1;ortholog
HUMAN|HGNC=6150|UniProtKB=P06756	ITGAV	Integrin alpha-V;ITGAV;ortholog
HUMAN|HGNC=6173|UniProtKB=O43736	ITM2A	Integral membrane protein 2A;ITM2A;ortholog
HUMAN|HGNC=21071|UniProtKB=Q6PHW0	IYD	Iodotyrosine deiodinase 1;IYD;ortholog
HUMAN|HGNC=6211|UniProtKB=P23352	KAL1	Anosmin-1;ANOS1;ortholog

HUMAN|HGNC=6217|UniProtKB=Q9BVA0	KATNB1	Katanin p80 WD40 repeat-containing subunit B1;KATNB1;ortholog
HUMAN|HGNC=6246|UniProtKB=Q9H3M0	KCNF1	Potassium voltage-gated channel subfamily F member 1;KCNF1;ortholog
HUMAN|HGNC=6249|UniProtKB=Q9UJ96	KCNG2	Potassium voltage-gated channel subfamily G member 2;KCNG2;ortholog
HUMAN|HGNC=6304|UniProtKB=P24390	KDELR1	ER lumen protein-retaining receptor 1;KDELR1;ortholog
HUMAN|HGNC=29266|UniProtKB=Q9P2G3	KLHL14	Kelch-like protein 14;KLHL14;ortholog
HUMAN|HGNC=16905|UniProtKB=O60662	KLHL41	Kelch-like protein 41;KLHL41;ortholog
HUMAN|HGNC=6356|UniProtKB=Q96PQ7	KLHL5	Kelch-like protein 5;KLHL5;ortholog
HUMAN|HGNC=6359|UniProtKB=Q9UBX7	KLK11	Kallikrein-11;KLK11;ortholog
HUMAN|HGNC=20523|UniProtKB=P60371	KRTAP10-6	Keratin-associated protein 10-6;KRTAP10-6;ortholog
HUMAN|HGNC=23598|UniProtKB=Q6L8H2	KRTAP5-3	Keratin-associated protein 5-3;KRTAP5-3;ortholog
HUMAN|HGNC=17095|UniProtKB=Q15031	LARS2	Probable leucine--tRNA ligase, mitochondrial;LARS2;ortholog
HUMAN|HGNC=29460|UniProtKB=Q5TA81	LCE2C	Late cornified envelope protein 2C;LCE2C;ortholog
HUMAN|HGNC=17787|UniProtKB=O14910	LIN7A	Protein lin-7 homolog A;LIN7A;ortholog
HUMAN|Gene=LPPR5|UniProtKB=Q32ZL2	LPPR5	Phospholipid phosphatase-related protein type 5;PLPPR5;ortholog
HUMAN|HGNC=6690|UniProtKB=Q12912	LRMP	Lymphoid-restricted membrane protein;LRMP;ortholog
HUMAN|HGNC=19742|UniProtKB=Q96L50	LRR1	Leucine-rich repeat protein 1;LRR1;ortholog
HUMAN|HGNC=19410|UniProtKB=Q86VH5	LRRTM3	Leucine-rich repeat transmembrane neuronal protein 3;LRRTM3;ortholog
HUMAN|HGNC=13940|UniProtKB=Q9Y333	LSM2	U6 snRNA-associated Sm-like protein LSm2;LSM2;ortholog
HUMAN|HGNC=1968|UniProtKB=Q99698	LYST	Lysosomal-trafficking regulator;LYST;ortholog
HUMAN|HGNC=25183|UniProtKB=Q8TC57	M1AP	Meiosis 1 arrest protein;M1AP;ortholog
HUMAN|HGNC=6780|UniProtKB=Q9ULX9	MAFF	Transcription factor MafF;MAFF;ortholog
HUMAN|HGNC=6823|UniProtKB=Q9UKM7	MAN1B1	Endoplasmic reticulum mannosyl-oligosaccharide 1,2-alpha-mannosidase;MAN1B1;ortholog
HUMAN|HGNC=13961|UniProtKB=P35410	MAS1L	Mas-related G-protein coupled receptor MRG;MAS1L;ortholog
HUMAN|HGNC=6904|UniProtKB=P31153	MAT2A	S-adenosylmethionine synthase isoform type-2;MAT2A;ortholog
HUMAN|HGNC=19866|UniProtKB=Q05BQ5	MBTD1	MBT domain-containing protein 1;MBTD1;ortholog
HUMAN|HGNC=7095|UniProtKB=O15344	MID1	E3 ubiquitin-protein ligase Midline-1;MID1;ortholog
HUMAN|HGNC=21460|UniProtKB=Q8TD10	MIPOL1	Mirror-image polydactyly gene 1 protein;MIPOL1;ortholog
HUMAN|HGNC=29636|UniProtKB=Q8NEH6	MNS1	Meiosis-specific nuclear structural protein 1;MNS1;ortholog
HUMAN|HGNC=17617|UniProtKB=Q96LA9	MRGPRX4	Mas-related G-protein coupled receptor member X4;MRGPRX4;ortholog
HUMAN|HGNC=16635|UniProtKB=P82673	MRPS35	28S ribosomal protein S35, mitochondrial;MRPS35;ortholog
HUMAN|HGNC=7394|UniProtKB=P07438	MT1B	Metallothionein-1B;MT1B;ortholog
HUMAN|HGNC=7411|UniProtKB=O94776	MTA2	Metastasis-associated protein MTA2;MTA2;ortholog
HUMAN|HGNC=7748|UniProtKB=Q6P3R8	NEK5	Serine/threonine-protein kinase Nek5;NEK5;ortholog
HUMAN|HGNC=29933|UniProtKB=Q86WI3	NLRC5	Protein NLRC5;NLRC5;ortholog

HUMAN|HGNC=17877|UniProtKB=Q9HAN9	NMNAT1	Nicotinamide/nicotinic acid mononucleotide adenylyltransferase 1;NMNAT1;ortholog
HUMAN|HGNC=32203|UniProtKB=Q5H8A3	NMS	Neuromedin-S;NMS;ortholog
HUMAN|HGNC=16821|UniProtKB=P78316	NOP14	Nucleolar protein 14;NOP14;ortholog
HUMAN|HGNC=7895|UniProtKB=Q99743	NPAS2	Neuronal PAS domain-containing protein 2;NPAS2;ortholog
HUMAN|HGNC=14124|UniProtKB=Q12980	NPRL3	Nitrogen permease regulator 3-like protein;NPRL3;ortholog
HUMAN|HGNC=8266|UniProtKB=Q8NH16	OR2L2	Olfactory receptor 2L2;OR2L2;ortholog
HUMAN|HGNC=8268|UniProtKB=Q96R28	OR2M2	Olfactory receptor 2M2;OR2M2;ortholog
HUMAN|HGNC=8510|UniProtKB=Q92882	OSTF1	Osteoclast-stimulating factor 1;OSTF1;ortholog
HUMAN|HGNC=20882|UniProtKB=Q9NWT1	PAK1IP1	p21-activated protein kinase-interacting protein 1;PAK1IP1;ortholog
HUMAN|HGNC=8621|UniProtKB=P23759	PAX7	Paired box protein Pax-7;PAX7;ortholog
HUMAN|HGNC=9719|UniProtKB=P50542	PEX5	Peroxisomal targeting signal 1 receptor;PEX5;ortholog
HUMAN|HGNC=8940|UniProtKB=O14832	PHYH	Phytanoyl-CoA dioxygenase, peroxisomal;PHYH;ortholog
HUMAN|HGNC=8971|UniProtKB=O00443	PIK3C2A	Phosphatidylinositol 4-phosphate 3-kinase C2 domain-containing subunit alpha;PIK3C2A;ortholog
HUMAN|HGNC=20764|UniProtKB=Q96S99	PLEKHF1	Pleckstrin homology domain-containing family F member 1;PLEKHF1;ortholog
HUMAN|HGNC=9200|UniProtKB=O00411	POLRMT	DNA-directed RNA polymerase, mitochondrial;POLRMT;ortholog
HUMAN|HGNC=23531|UniProtKB=Q5VZY2	PPAPDC1A	Phospholipid phosphatase 4;PLPP4;ortholog
HUMAN|HGNC=9358|UniProtKB=P48147	PREP	Prolyl endopeptidase;PREP;ortholog
HUMAN|HGNC=17348|UniProtKB=O43395	PRPF3	U4/U6 small nuclear ribonucleoprotein Prp3;PRPF3;ortholog
HUMAN|HGNC=16463|UniProtKB=O75400	PRPF40A	Pre-mRNA-processing factor 40 homolog A;PRPF40A;ortholog
HUMAN|HGNC=9480|UniProtKB=Q9NQE7	PRSS16	Thymus-specific serine protease;PRSS16;ortholog
HUMAN|HGNC=19096|UniProtKB=Q8NDX1	PSD4	PH and SEC7 domain-containing protein 4;PSD4;ortholog
HUMAN|HGNC=17822|UniProtKB=Q9H7Z7	PTGES2	Prostaglandin E synthase 2;PTGES2;ortholog
HUMAN|HGNC=9650|UniProtKB=P17706	PTPN2	Tyrosine-protein phosphatase non-receptor type 2;PTPN2;ortholog
HUMAN|HGNC=9692|UniProtKB=P26022	PTX3	Pentraxin-related protein PTX3;PTX3;ortholog
HUMAN|HGNC=26505|UniProtKB=Q3MIT2	PUS10	Putative tRNA pseudouridine synthase Pus10;PUS10;ortholog
HUMAN|HGNC=29982|UniProtKB=P83859	QRFP	Orexigenic neuropeptide QRFP;QRFP;ortholog
HUMAN|HGNC=9795|UniProtKB=Q92696	RABGGTA	Geranylgeranyl transferase type-2 subunit alpha;RABGGTA;ortholog
HUMAN|HGNC=9807|UniProtKB=O75943	RAD17	Cell cycle checkpoint protein RAD17;RAD17;ortholog
HUMAN|HGNC=9832|UniProtKB=P55895	RAG2	V(D)J recombination-activating protein 2;RAG2;ortholog
HUMAN|HGNC=9840|UniProtKB=P11234	RALB	Ras-related protein Ral-B;RALB;ortholog
HUMAN|HGNC=15864|UniProtKB=Q9BYM8	RBCK1	RanBP-type and C3HC4-type zinc finger-containing protein 1;RBCK1;ortholog
HUMAN|HGNC=9894|UniProtKB=Q08999	RBL2	Retinoblastoma-like protein 2;RBL2;ortholog
HUMAN|HGNC=16502|UniProtKB=P58872	RHBDL3	Rhomboid-related protein 3;RHBDL3;ortholog
HUMAN|HGNC=21158|UniProtKB=Q8IUD6	RNF135	E3 ubiquitin-protein ligase RNF135;RNF135;ortholog

HUMAN|HGNC=13432|UniProtKB=Q9NV58	RNF19A	E3 ubiquitin-protein ligase RNF19A;RNF19A;ortholog
HUMAN|HGNC=17985|UniProtKB=Q8WZ75	ROBO4	Roundabout homolog 4;ROBO4;ortholog
HUMAN|HGNC=25791|UniProtKB=Q8IXW5	RPAP2	Putative RNA polymerase II subunit B1 CTD phosphatase RPAP2;RPAP2;ortholog
HUMAN|HGNC=30350|UniProtKB=Q9H9Y2	RPF1	Ribosome production factor 1;RPF1;ortholog
HUMAN|HGNC=10302|UniProtKB=P30050	RPL12	60S ribosomal protein L12;RPL12;ortholog
HUMAN|HGNC=10371|UniProtKB=P05388	RPLP0	60S acidic ribosomal protein P0;RPLP0;ortholog
HUMAN|HGNC=10402|UniProtKB=P39019	RPS19	40S ribosomal protein S19;RPS19;ortholog
HUMAN|HGNC=6502|UniProtKB=P08865	RPSA	40S ribosomal protein SA;RPSA;ortholog
HUMAN|HGNC=10450|UniProtKB=O14718	RRH	Visual pigment-like receptor peropsin;RRH;ortholog
HUMAN|HGNC=13081|UniProtKB=Q9BY12	SCAPER	S phase cyclin A-associated protein in the endoplasmic reticulum;SCAPER;ortholog
HUMAN|HGNC=21088|UniProtKB=Q86SK9	SCD5	Stearoyl-CoA desaturase 5;SCD5;ortholog
HUMAN|HGNC=15950|UniProtKB=Q9BWW7	SCRT1	Transcriptional repressor scratch 1;SCRT1;ortholog
HUMAN|HGNC=8951|UniProtKB=P07093	SERPINE2	Glia-derived nexin;SERPINE2;ortholog
HUMAN|HGNC=30784|UniProtKB=Q14140	SERTAD2	SERTA domain-containing protein 2;SERTAD2;ortholog
HUMAN|HGNC=12950|UniProtKB=Q15637	SF1	Splicing factor 1;SF1;ortholog
HUMAN|HGNC=10809|UniProtKB=Q13326	SGCG	Gamma-sarcoglycan;SGCG;ortholog
HUMAN|HGNC=25321|UniProtKB=Q9H0F6	SHARPIN	Sharpin;SHARPIN;ortholog
HUMAN|HGNC=11014|UniProtKB=Q99726	SLC30A3	Zinc transporter 3;SLC30A3;ortholog
HUMAN|HGNC=11047|UniProtKB=Q9UN76	SLC6A14	Sodium- and chloride-dependent neutral and basic amino acid transporter B(0+);SLC6A14;ortholog
HUMAN|HGNC=23092|UniProtKB=Q8TCU3	SLC7A13	Solute carrier family 7 member 13;SLC7A13;ortholog
HUMAN|HGNC=14013|UniProtKB=Q9NTJ3	SMC4	Structural maintenance of chromosomes protein 4;SMC4;ortholog
HUMAN|HGNC=20465|UniProtKB=Q8IY18	SMC5	Structural maintenance of chromosomes protein 5;SMC5;ortholog
HUMAN|HGNC=18122|UniProtKB=Q9H6I2	SOX17	Transcription factor SOX-17;SOX17;ortholog
HUMAN|HGNC=32006|UniProtKB=Q5VVP1	SPATA31A6	Spermatogenesis-associated protein 31A6;SPATA31A6;ortholog
HUMAN|HGNC=24508|UniProtKB=B4DYI2	SPATA31C2	Spermatogenesis-associated protein 31C2;SPATA31C2;ortholog
HUMAN|HGNC=24031|UniProtKB=Q9HBM1	SPC25	Kinetochore protein Spc25;SPC25;ortholog
HUMAN|HGNC=11337|UniProtKB=Q99909	SSX3	Protein SSX3;SSX3;ortholog
HUMAN|HGNC=10863|UniProtKB=Q16842	ST3GAL2	CMP-N-acetylneuraminate-beta-galactosamide-alpha-2,3-sialyltransferase 2;ST3GAL2;ortholog
HUMAN|HGNC=23317|UniProtKB=P61647	ST8SIA6	Alpha-2,8-sialyltransferase 8F;ST8SIA6;ortholog
HUMAN|HGNC=11389|UniProtKB=Q15831	STK11	Serine/threonine-protein kinase STK11;STK11;ortholog
HUMAN|HGNC=30796|UniProtKB=Q9Y3F4	STRAP	Serine-threonine kinase receptor-associated protein;STRAP;ortholog
HUMAN|HGNC=11427|UniProtKB=Q9UNE7	STUB1	E3 ubiquitin-protein ligase CHIP;STUB1;ortholog
HUMAN|HGNC=19694|UniProtKB=Q6ZWJ1	STXBP4	Syntaxin-binding protein 4;STXBP4;ortholog
HUMAN|HGNC=27411|UniProtKB=Q6PIF2	SYCE2	Synaptonemal complex central element protein 2;SYCE2;ortholog

HUMAN|HGNC=11523|UniProtKB=O95359	TACC2	Transforming acidic coiled-coil-containing protein 2;TACC2;ortholog
HUMAN|HGNC=11585|UniProtKB=O60907	TBL1X	F-box-like/WD repeat-containing protein TBL1X;TBL1X;ortholog
HUMAN|HGNC=20854|UniProtKB=Q9H0W7	THAP2	THAP domain-containing protein 2;THAP2;ortholog
HUMAN|HGNC=11793|UniProtKB=P52888	THOP1	Thimet oligopeptidase;THOP1;ortholog
HUMAN|HGNC=11803|UniProtKB=O95411	TIAF1	TGFB1-induced anti-apoptotic factor 1;TIAF1;ortholog
HUMAN|HGNC=14523|UniProtKB=Q96MW7	TIGD1	Tigger transposable element-derived protein 1;TIGD1;ortholog
HUMAN|HGNC=33522|UniProtKB=A6NGC4	TLCD2	TLC domain-containing protein 2;TLCD2;ortholog
HUMAN|HGNC=24257|UniProtKB=Q9HC24	TMBIM4	Protein lifeguard 4;TMBIM4;ortholog
HUMAN|HGNC=16996|UniProtKB=Q15363	TMED2	Transmembrane emp24 domain-containing protein 2;TMED2;ortholog
HUMAN|HGNC=16823|UniProtKB=P17152	TMEM11	Transmembrane protein 11, mitochondrial;TMEM11;ortholog
HUMAN|HGNC=30366|UniProtKB=Q92545	TMEM131	Transmembrane protein 131;TMEM131;ortholog
HUMAN|HGNC=31723|UniProtKB=Q24JQ0	TMEM241	Transmembrane protein 241;TMEM241;ortholog
HUMAN|HGNC=32393|UniProtKB=Q6ZNR0	TMEM91	Transmembrane protein 91;TMEM91;ortholog
HUMAN|HGNC=32431|UniProtKB=Q6UXZ0	TMIGD1	Transmembrane and immunoglobulin domain-containing protein 1;TMIGD1;ortholog
HUMAN|HGNC=11905|UniProtKB=O14763	TNFRSF10B	Tumor necrosis factor receptor superfamily member 10B;TNFRSF10B;ortholog
HUMAN|HGNC=11983|UniProtKB=O75674	TOM1L1	TOM1-like protein 1;TOM1L1;ortholog
HUMAN|HGNC=12032|UniProtKB=Q12933	TRAF2	TNF receptor-associated factor 2;TRAF2;ortholog
HUMAN|HGNC=30832|UniProtKB=Q96Q05	TRAPPC9	Trafficking protein particle complex subunit 9;TRAPPC9;ortholog
HUMAN|HGNC=31454|UniProtKB=Q6A555	TXNDC8	Thioredoxin domain-containing protein 8;TXNDC8;ortholog
HUMAN|HGNC=12477|UniProtKB=P51965	UBE2E1	Ubiquitin-conjugating enzyme E2 E1;UBE2E1;ortholog
HUMAN|HGNC=12492|UniProtKB=P61088	UBE2N	Ubiquitin-conjugating enzyme E2 N;UBE2N;ortholog
HUMAN|HGNC=15664|UniProtKB=Q9NYU1	UGGT2	UDP-glucose:glycoprotein glucosyltransferase 2;UGGT2;ortholog
HUMAN|HGNC=20332|UniProtKB=Q9H1J1	UPF3A	Regulator of nonsense transcripts 3A;UPF3A;ortholog
HUMAN|HGNC=20485|UniProtKB=O75317	USP12	Ubiquitin carboxyl-terminal hydrolase 12;USP12;ortholog
HUMAN|HGNC=14340|UniProtKB=Q9UBQ0	VPS29	Vacuolar protein sorting-associated protein 29;VPS29;ortholog
HUMAN|HGNC=25072|UniProtKB=Q5MNZ6	WDR45B	WD repeat domain phosphoinositide-interacting protein 3;WDR45B;ortholog
HUMAN|HGNC=14540|UniProtKB=Q9H4A3	WNK1	Serine/threonine-protein kinase WNK1;WNK1;ortholog
HUMAN|HGNC=12786|UniProtKB=O00755	WNT7A	Protein Wnt-7a;WNT7A;ortholog
HUMAN|HGNC=28304|UniProtKB=Q96EC8	YIPF6	Protein YIPF6;YIPF6;ortholog
HUMAN|HGNC=31675|UniProtKB=Q9Y5A9	YTHDF2	YTH domain-containing family protein 2;YTHDF2;ortholog
HUMAN|HGNC=17908|UniProtKB=O43298	ZBTB43	Zinc finger and BTB domain-containing protein 43;ZBTB43;ortholog
HUMAN|HGNC=29362|UniProtKB=Q9C0D7	ZC3H12C	Probable ribonuclease ZC3H12C;ZC3H12C;ortholog
HUMAN|HGNC=20368|UniProtKB=Q5T200	ZC3H13	Zinc finger CCCH domain-containing protein 13;ZC3H13;ortholog
HUMAN|HGNC=14881|UniProtKB=O60315	ZEB2	Zinc finger E-box-binding homeobox 2;ZEB2;ortholog

HUMAN|HGNC=12863|UniProtKB=Q9Y6Q3	ZFP37	Zinc finger protein 37 homolog;ZFP37;ortholog
HUMAN|HGNC=20997|UniProtKB=Q9H091	ZMYND15	Zinc finger MYND domain-containing protein 15;ZMYND15;ortholog
HUMAN|HGNC=12907|UniProtKB=Q15973	ZNF124	Zinc finger protein 124;ZNF124;ortholog
HUMAN|HGNC=12920|UniProtKB=P52737	ZNF136	Zinc finger protein 136;ZNF136;ortholog
HUMAN|HGNC=23708|UniProtKB=Q6ZR52	ZNF493	Zinc finger protein 493;ZNF493;ortholog
HUMAN|HGNC=13168|UniProtKB=Q03936	ZNF92	Zinc finger protein 92;ZNF92;ortholog
HUMAN|HGNC=25820|UniProtKB=Q9C0D3	ZYG11B	Protein zyg-11 homolog B;ZYG11B;ortholog

Table 4: Preliminary Identification of tumor targets for combination immunotherapy

Druggable Gene Category	Matching Gene Count	Matching Gene(s)
DRUGGABLE GENOME	68	ABHD16A, ARSF, BAP1, BCL2, BIRC2, CAT, CCNA2, CFLAR, CWC27, CYB5R3, DNAJC16, DNPEP, DPEP2, DPT, EFNB1, EPO, ESRRA, FAM3B, FAT1, FBLN1, GRIK1, HCRTR1, HNRNPUL2, IKBKG, IL1R1, IL36RN, IL9, ITGAV, ANOS1, KCNF1, KCNG2, KLHL5, KLK11, LARS2, LRRTM3, MAN1B1, MAS1L, MID1, MRGPRX4, NEK5, NMS, OR2L2, OR2M2, PIK3C2A, PREP, PRSS16, PTPN2, PTX3, QRFP, RABGGTA, RBCK1, RHBDL3, RNF135, RRH, SCD5, SERPINE2, SHARPIN, SLC6A14, SLC7A13, ST3GAL2, STK11, THOP1, TNFRSF10B, TXNDC8, UBE2N, USP12, WNK1, WNT7A
KINASE	22	CCNA2, CLP1, DLG3, EPO, FBXW7, GMFG, HMGXB3, IKBKG, LRRTM3, NEK5, NLRC5, PIK3C2A, PTPN2, RALB, RBL2, STK11, TNFRSF10B, TOM1L1, TRAF2, UBE2N, WNK1, ZEB2
TUMOR SUPPRESSOR	18	BAP1, BCL2, BIRC2, BOP1, CCNA2, CUL9, EIF4G1, EIF4G2, FBXW7, GIGYF2, PRPF40A, RAD17, RBL2, SMC5, STK11, STXBP4, TOM1L1, UBE2E1
PROTEASE	17	BAP1, BIRC2, CFLAR, DNPEP, DPEP2, FBLN1, ANOS1, KLK11, NEK5, PREP, PRSS16, RHBDL3, SERPINE2, THOP1, TNFRSF10B, TRAF2, USP12
TRANSPORTER	15	ATP6V0C, BCL2, DLG3, EPO, GRIK1, ITGAV, KCNF1, KCNG2, SLC30A3, SLC6A14, SLC7A13, TMEM241, UPF3A, VPS29, WNK1
SERINE THREONINE KINASE	10	CCNA2, IKBKG, NEK5, RALB, STK11, TNFRSF10B, TRAF2, UBE2N, WNK1, ZEB2
HISTONE MODIFICATION	9	BAP1, CCNA2, ENY2, EYA4, MTA2, PAX7, TBL1X, UBE2E1, UBE2N
DNA REPAIR	8	CEBPG, CINP, EYA4, NPAS2, RAD17, SMC5, STUB1, UBE2N
G PROTEIN COUPLED RECEPTOR	7	CRCP, HCRTR1, MAS1L, MRGPRX4, OR2L2, OR2M2, RRH
ION CHANNEL	7	DLG3, EPO, GRIK1, ITGAV, KCNF1, KCNG2, WNK1
TRANSCRIPTION FACTOR BINDING	7	BCL2, CEBPG, EGR2, MTA2, RNF19A, SOX17, TBL1X
CELL SURFACE	6	EPO, IL1R1, ITGAV, SERPINE2, TNFRSF10B, WNT7A
CLINICALLY ACTIONABLE	6	BAP1, BCL2, FAT1, FBXW7, SOX17, STK11
TYROSINE KINASE	5	FBXW7, GMFG, LRRTM3, PTPN2, WNK1
TRANSCRIPTION FACTOR COMPLEX	4	MTA2, NPAS2, RBL2, SOX17

B30_2 SPRY DOMAIN	3	HNRNPUL2, MID1, RNF135
DRUG RESISTANCE	3	BCL2, CAT, HADH
NEUTRAL ZINC METALLOPEPTIDASE	3	DNPEP, DPEP2, THOP1
PROTEASE INHIBITOR	3	BIRC2, ANOS1, SERPINE2
PROTEIN PHOSPHATASE	3	EYA4, PTPN2, RPAP2
EXTERNAL SIDE OF PLASMA MEMBRANE	2	ITGAV, SERPINE2
GROWTH FACTOR	2	GMFG, IL9
HORMONE ACTIVITY	2	EPO, QRFP
NUCLEAR HORMONE RECEPTOR	2	ESRRA, SF1
THIOREDOXIN	2	DNAJC16, TXNDC8
ABC TRANSPORTER	1	ATP6V0C
LIPID KINASE	1	RBL2
PHOSPHATIDYLINOSITOL 3 KINASE	1	PIK3C2A

Table 5: Inhibitors utilized in study

Inhibitor	Alternative nomenclature	Target	Source
Venetoclax	ABT-199	BCL2	Selleckchem
Navitoclax	ABT-263	BCL2	Selleckchem
LCL161		BIRC2	Selleckchem
Birinapant		BIRC2	Selleckchem
Fomepizole		CAT	Selleckchem
Tosedostat	CHR2797	DNPEP	Tocris
XCT790		ESRRA	Sigma Aldrich
Compound 29		ESRRA	Synthesized by collaborator
Topiramate		GRIK1	Selleckchem
ACET		GRIK1	Tocris
Almorexant	ACT-078573	HCRTR1	Selleckchem
SB334867		HCRTR1	R&D systems
Blocking antibody	AF269	IL1R1	R&D systems
Blocking antibody	AF209	IL9	R&D systems
Blocking antibody	ab16821	ITGAV	Abcam
Cilengitide		ITGAV	Selleckchem
Guanidine HCL		KCNF1	Sigma Aldrich
Dalfampridine	4-aminopyridine	KCNF1	Sigma Aldrich
Guanidine HCL		KCNG2	Sigma Aldrich
Dalfampridine	4-aminopyridine	KCNG2	Sigma Aldrich
Dactolisib	BEZ235	PIK3C2A	Selleckchem

Apitolisib	GDC-0980	PIK3C2A	Selleckchem
S17092		PREP	Sigma Aldrich
WNK463		WNK1	Selleckchem

Table 6: sgRNA sequences

sgRNA Name	sgRNA sequence
RPAP2 sgRNA1	GGCCCAGCGAAGTCCGCCAT
RPAP2 sgRNA2	AAATTCTCGTAACTTGGCAG
RPAP2 sgRNA3	CGCTGCTCTCGAAAAGCCGC
BIRC2 sgRNA1	TGGAGACGTATTCTTAGAGG
BIRC2 sgRNA2	ACATATTCAACTTTCCCCGC
BIRC2 sgRNA3	ATATTCAACTTTCCCCGCCG
ESD sgRNA1	CGTTGTTTTTCGATTGCAAG
ESD sgRNA2	TAGACCACAAACACTTACGA
ESD sgRNA3	CACTTACGAGGGCTGGTATC
EGR2 sgRNA1	GCAAGACGCCGGTGCACGAG
EGR2 sgRNA2	TCAAGGTGTCCGGGTCCGAG
EGR2 sgRNA3	CTCGTGCACCGGCGTCTTGC
SCAF11 sgRNA1	TGTCTTCGAGCTATCTGCGC
SCAF11 sgRNA2	TCTGGTTGGGTATCTAACCG
SCAF11 sgRNA3	CTGTACCGATCATTTCCTCG
TOR1AIP1 sgRNA1	CATAAACTTACGTCGGCTGG
TOR1AIP1 sgRNA2	TCAACAACTATGGCGGGCGA
TOR1AIP1 sgRNA3	GCGCGTACTACCTTCGGTCT
LPGAT1 sgRNA1	AAGCGGTTCTGGTATATCGA
LPGAT1 sgRNA2	CTTCATGGTCGTCAACAACC
LPGAT1 sgRNA3	CTTACTGTCCAGCACTCGAA
SERTAD2 sgRNA1	CCAGGGGCGTAGTGCTTCCG
SERTAD2 sgRNA2	CGTAGTGCTTCCGAGGTCGC
SERTAD2 sgRNA3	GTAGTGCTTCCGAGGTCGCA
RBL2 sgRNA1	CCGCCTCAACATGGACGAGG
RBL2 sgRNA2	CGACGGCATAGCGCACCCCT
RBL2 sgRNA3	CTATGCGTAGCTGTAGAAAC
BCL2 sgRNA1	AAGCGTCCCCGCGCGGTGAA
BCL2 sgRNA2	ACCTGACGCCCTTCACCGCG
BCL2 sgRNA3	GGGGCCGTACAGTTCCACAA

Methods

Human specimens

Peripheral blood mononuclear cells (PBMCs) were isolated from healthy donors and tumor samples were isolated from patients with melanoma and GI cancers. All human specimens were collected with informed consent and procedures approved by the institutional review board (IRB) of the National Cancer Institute (NCI).

Mice

All animal experiments were approved by the Institutional Animal Care and Use Committees of the NCI and were performed in accordance with NIH guidelines. C57BL/6NCR mice were obtained from Charles River Laboratories at NCI Frederick. B6.Cg-*Thy1*^{a}/Cy Tg(TcraTcrb)8Rest/J (PMEL1) mice were purchased from Jackson Laboratory. All mice were maintained under specific pathogen-free conditions. Female mice aged 6-8 weeks were used for *in vivo* experiments.

Cell culture

Melanoma cell lines Mel624.38 were isolated from surgically resected metastases as previously described (Robbins et al., 2008) and were cultured in RPMI 1640 (Invitrogen) medium supplemented with 10% fetal bovine serum (FBS, Hyclone, Logan, UT), 2 mM L-glutamine and 1% penicillin-streptomycin. A375 melanoma cells were obtained from the American Type Culture Collection (Manassas, VA) and cultured in RPMI 1640 medium supplemented with 10% FBS, 2 mM L-glutamine and 1% penicillin-streptomycin. Transduced T lymphocytes were cultured in RPMI 1640 supplemented with 10% FBS, 2 mM L-glutamine and 1% penicillin-streptomycin.

Retroviral transduction of human T cells with TCRs

Retroviral vectors for TCRs recognizing the HLA-A*02-restricted melanoma antigens NY-ESO-1 (NY-ESO-1:157-165 epitope) and MART-1 (MART-1:27-35 epitope, DMF5) were generated as previously described (Johnson et al., 2006; Robbins et al., 2008). Neo-antigen-reactive TCRs were identified and expressed in primary human T cells as previously described (Lo et al., 2019; Malekzadeh et al., 2019). For transduction of human T cells, $CD8^{+}$ T cells seeded at 2 x 10^{6} cells per well in a 24-well plate were stimulated with anti-CD3 antibody OKT3 (5 ug/mL coated) and anti-CD28 antibody (5 ug/mL soluble) along with IL-2 (200 IU/mL) on day 0. Non-tissue culture treated 24-well plates were coated with 0.5 mL per well of 10 µg/mL RetroNectin (Takara) on day 1 and stored overnight at 4°C. Vector supernatant (1 mL per well) was added to plates on day 2 followed by centrifugation at 2000g for 2h at 32°C. 800 µL was aspirated and T cells were added at 1 x 10^{6} cells/mL, centrifuged for 10 min at 1500 rpm and incubated overnight. A second transduction was performed the following day as described above. Cells were subsequently maintained in culture at 1 x 10^{6} cells/mL and expanded until day 10, after which they were used or cryo-preserved for future use.

Lentiviral production and purification

Lentiviral particles were produced and purified as described previously (Patel et al., 2017). In brief, HEK293FT cells (Invitrogen) were cultured in DMEM supplemented with 10% FBS, 2 mM L-glutamine and 1% penicillin-streptomycin. One day prior to transfection, HEK293FT cells were seeded in T-225 flasks at 60% confluency. One hour prior to transfection, media was aspirated and replaced with 13 mL OptiMEM media (Invitrogen). Each flask of cells were transfected with 100 µL Lipofectamine 200 and 200 µL Plus reagent (Invitrogen) along with 20 µg of lentiCRISPRv2 plasmid or pooled plasmid human GeCKOv.2 (Genome-scale CRISPR knockout) library, 15 µg psPAX2 and 10 µg pMD2.G. 6-8 hr after transfection, media was replaced with 20 mL of DMEM supplemented with 10% FBS and 1% BSA. Media containing viral particles was collected 48 hr post-transfection and titer was assayed with Lenti-X GoStix (Clontech). Viral supernatant was centrifuged at 3,000 r.c.f. at 4°C for 10 min followed by filtration through 0.45 µm low-protein binding membrane. For pooled library plasmids, viral supernatants were concentrated by centrifugation at 4,000 r.c.f at 4°C for 35 min in Amicon Ultra-15 filters (Millipore Ultracel-100K). Concentrated viral supernatants were stored in aliquots at -80°C.

2CT T cell and tumor cell co-culture

Two days prior to co-culture, T cells were thawed in T cell media containing 3 U/mL DNase (Genentech Inc.) overnight. Tumor cells were seeded at desired density on this day in T cell media. After 24 hr, T cells were cultured in T cell media supplemented with 300 IU/mL IL-2 for 24 hr. T cells were co-cultured with tumor cells at various effector:target (E:T) ratios for specified durations. After co-culture, T cells were removed by washing tumor cells with PBS and tumor cells were detached using trypsin. Cells were stained with fixable Live/Dead dye (Invitrogen) followed by human anti-CD3 antibody (clone SK7, BD) in FACS staining buffer (PBS + 0.2% BSA). Cell counts were normalized with CountBright Absolute Counting Beads (Invitrogen) by FACS.

2CT GeCKOv.2 screens, genomic DNA extractions and screen analysis

2CT genome-wide CRISPR screens were performed as previously described (Patel et al., 2017), with some modifications. In brief, Mel624 cells were transduced independently with both A and B GeCKOv.2 libraries. For each screen, cells were split into two groups of $5x10^7$ transduced Mel624 cells. One group was co-cultured with ESO T cells at an E:T ratio of 1:3 for each library. A second group of transduced Mel624 cells were cultured under the same density and conditions, but without ESO T cells. The co-culture phase was maintained for 6 hr, after which the T cells were removed as described above. The recovery phase was maintained for another 48 hr and surviving cells were frozen to evaluate sgRNA depletion. gDNA was extracted from frozen tumor cells using previously optimized (Chen et al., 2015) ammonium acetate and alcohol precipitation procedure to isolate gDNA with AL buffer (Qiagen) substituted for the initial cell lysis step. sgRNA abundance was detected as previously described (Patel et al., 2017).

Arrayed validation of targets with CRISPR/Cas9

Selected targets that were identified from the genome-scale CRISPR screen and DTA analysis were further studied using additional sgRNA targeting sequences. We utilized 3 newly designed sgRNA guide sequences for each gene as listed in **Table 6**. We cloned these sgRNAs into the lentiGuide-Puro vector as previously described (Sanjana et al., 2014). A375 cells were

transduced with lentiCas9-Blast (Addgene) and selected with 5 μg/mL blasticidin for 10 days, after which cells were transduced with lentiGuide-Puro sgRNA constructs. Cells were then selected with 1 μg/mL puromycin for 7 days. In some experiments (**Figures 6-7)**, sgRNA guide sequences were cloned into the lentiCRISPRv2 vector for mechanistic studies as previously described (Patel et al., 2017).

RNA sequencing and analysis

mRNA-seq was performed on Mel624 melanoma cells and NY-ESO-1 TCR transduced primary human T cells that were co-cultured and separated into purified populations by FACS. Separate sequencing was performed on A375 melanoma cells that were transduced with Cas9 and non-targeting sgRNA or Cas9 and BIRC2-targeting sgRNA. Libraries were prepared using TruSeq RNA sample prep kit (FC-122-1001, Illumina). Approximately 40 million reads were sequenced and aligned to the human genome (hg19 for Mel624/NY-ESO-1 T cell experiment, hg38 for A375 experiments) with TopHat 2.0.11. Uniquely retained mapped reads were used to calculate differentially expressed genes using edgeR or Cuffdiff. Fisher's exact test or t-tests were used to calculate significance with indicated *P* values and fold-change thresholds. To filter for RNA contamination derived from incomplete FACS-based purification of ESO T cells and Mel624 melanoma cells, we filtered out genes that had 100-fold enrichments in expression in the opposing cell type under basal conditions. RNA-sequencing raw data files are deposited at GEO-GSE137824.

ChIP-sequencing

Chromatin Immunoprecipitations were performed following manufacturer's instructions (ChIP-IT Express Shearing Kit, Active Motif). In brief, A375 cells transduced with Cas9 and non-targeting sgRNA or with Cas9 and BIRC2-targeting sgRNA were fixed with formaldehyde for 7 min on a rocking platform and quenched with glycine solution. Cells were pelleted with PMSF and protease inhibitor cocktail and stored at -80°C prior to lysis. Cells were suspended in ice cold lysis buffer to extract nuclear material, which was then sheared by incubating with enzymatic cocktail for 10 min at 37°C. 40 μg of sheared chromatin/sample was incubated with protein G magnetic beads with α-RelB (10544, Cell Signaling) or α-NF-κB2 antibodies (37359 Cell Signaling) overnight. Magnetic beads were washed with buffers to remove unbound immune complexes and chromatin was eluted with 150 μL of elution buffer. Reverse crosslinking was performed on eluted DNA, followed by phenol chloroform extraction. Samples were sequenced on a HiSeq4000 in paired-end mode with approximately 40 million reads/sample. Sequenced reads were trimmed for adapters and aligned to the human genome (hg38) with Bowtie v2 and uniquely mapped reads were retained. The output of Bowtie was converted to BAM files, normalized using RPKM and converted to coverage tracks in big wig format using Deeptools (Command #BamCoverage -b Bam_File –normalizeUsingRPKM – binSize 10 –smoothLength 30 -bl hg38.blacklist.bed –centerReads –minMappingQuality 30 -o Output_File.bw). Tracks generated were viewed using the IGV (Integrative Genomics Viewer).

Tumor Cell Chemokine and Cytokine Secretion

A375 cell production of chemokine proteins was quantified using a CBA Human Chemokine Kit (BD Biosciences Cat #552990) and GM-CSF production was measured using Human GM-CSF ELISA Kit (Abcam Cat #ab174448). In brief, A375 cells transduced with Cas9 and non-targeting sgRNA or BIRC2-targeting sgRNAs were plated at 4 x 10^5 in a 6-well dish and cultured for 24 hr. Media supernatant was collected and spun at 1500rpm for 10 min to pellet cells and debris. Supernatant was collected for analysis. In some cases, media was diluted 1:5 using assay diluent to ensure detected values were within standard calibration curves.

Tumor Pathway Activation Screen

Tumor pathway activation was performed as previously described (Martz et al., 2014), with minor modifications. In brief, lentiviral particles were generated for each pathway activation construct and A375 melanoma cells were transduced by spinfection at an MOI of 0.3. Transduced cells were incubated for 24 hr, followed by puromycin selection. After selection, cells were plated and 2CT assay was conducted with ESO T cells at a 1:3 ratio for 16hr.

Lentiviral transduction of tumor cells

Lentiviral transduction of tumor cells was performed as previously described (Patel et al., 2017). In brief, tumor cell culture media was replaced with RPMI 1640 media supplemented with 10% FBS and 8μg/mL polybrene. Lentiviral particles were added at an MOI of 0.3, followed by spinfection at 1500 rpm for 30 min. Following this, cells were incubated for 24 hr, after which the culture media was aspirated and replaced with RPMI 1640 media supplemented with 10% FBS and selection antibiotic. For puromycin-resistant constructs, puromycin was added at 1μg/mL. For blasticidin-resistant constructs, blasticidin was added at 5μg/mL. Cells were maintained under antibiotic selection until non-transduced control cells were eliminated by drugs.

High throughput inhibitor screen

A375 melanoma cells were plated at 1x10^4 cells/well in 150μL of complete RPMI in a 96-well flat bottom plate and incubated for 24 hr. Inhibitors were then added in 50μL of complete RPMI (concentrated to reach desired concentration after addition), followed by addition of ESO T cells at a 1:3 E:T ratio in complete RPMI to a total of 250μL. Cells were incubated for 16 hr, after which cells were washed twice with PBS, and WST1 reagent (Sigma Aldrich) was added in complete RPMI and cell viability was assessed.

Inhibitor sources

Inhibitors were purchased from commercial suppliers as listed below, or were provided (Compound 29, (Patch et al., 2011)) by the Donald McDonnell Laboratory (Duke University). ABT199 (Selleckchem #S8048), ABT263 (Selleckchem #S1001), LCL161 (Selleckchem #S7009), Birinapant (Selleckchem #S7015), Fomepizole (Selleckchem #S1717), CHR2797 (Tocris #3595), XCT790 (Sigma Aldrich #X4753), Topiramate (Selleckchem #S1438), ACET (Tocris #2728), Almorexant (Selleckchem #S2160), SB334867 (R&D Systems, #1960), anti-IL1R1 (R&D Systems, #AF269), anti-IL9 (R&D Systems, #AF209), anti-ITGAV (Abcam, #ab16821), Cilengitide (Selleckchem, #S7077), Guanidine HCl (Sigma Aldrich, #G3272), Dalfampridine (Sigma Aldrich,

#275875), BEZ235 (Selleckchem, #S1009), Apitolisib (Selleckchem, #S2696), S17092 (Sigma Aldrich, #SML0181), WNK463 (Selleckchem, #S8358).

FACS-based 2CT inhibitor validations

Tumor cells were plated at $3x10^4$ cells/well in 250μL of complete RPMI in a 48-well flat bottom plate and incubated for 24 hr. Inhibitors were then added in 50μL of complete RPMI, followed by addition of TCR-transduced T cells at a 1:3 E:T ratio in complete RPMI to a total of 400μL. Cells were incubated for 16hr, and analyzed as described for 2CT assay.

Murine ACT models

For *in vivo* immunotherapy experiments, we utilized previously described (Hanada et al., 2019) B16 melanoma cells expressing a chimeric mouse-human gp100 antigen (B16mhGP100). We generated gene-deleted B16mhGP100 cells using lentiviruses encoding sgRNAs targeting *Birc2* as described above. C57BL/6 mice were subcutaneously implanted with $5x10^5$ B16mhGP100 cells and tumors were allowed to grow for 10 days. Mice were then irradiated (6 Gy) and injected intravenously with $5x10^6$ Pmel $CD8^+$ T cells. Mice received intraperitoneal injections of IL-2 in PBS ($6x10^4$ IU in 0.5mL) once daily for 3 consecutive days. In certain experiments, mice received intraperitoneal injections of LCL-161 or birinapant in Captisol (30% in H_2O acidified to pH 4 with citric acid). Injections of inhibitors was performed every other day for 5 total injections. Tumor measurements were performed in a blinded fashion by an independent investigator approximately every two days after T cell transfer. Tumor area was calculated as length x width of the tumor. Mice with tumors in excess of 400 mm^2 were euthanized.

Pathway Enrichment Analysis

For gene pathway analysis, enriched or depleted genes were examined for gene category over-representation using Ingenuity Pathway Analysis (QIAGEN). For analysis of CRISPR depleted genes, the top 250 significant genes by RIGER analysis were selected. For analysis of RNA-sequencing experiments, all differentially expressed genes were analyzed. Fisher's exact test ($P < 0.05$) was used to compute significance for over-representation of genes in a pathway.

cBioportal analysis of human melanoma patient datasets

Analysis of human melanoma patient gene expression was performed using the Skin Cutaneous Melanoma geneset (TCGA, PanCancer Atlas). Samples were selected for which mRNA data was available and gene expression correlation analysis was performed.

Identification of druggable targets for screening

Validated tumor resistance genes (**Figure 3B)** along with the top 250 depleted genes from CRISPR screens as calculated by rank-sum of replicate screens was analyzed by PANTHER (Mi et al., 2019) to map gene list to protein coding genes. 237 identified protein coding genes were analyzed using DGIDB (Griffith et al., 2013) to identify genes that are druggable. Genes were analyzed as 'druggable gene category results' and filtered on categories 'inhibitor, allosteric modulator, antagonist, blocker, channel blocker, desensitize the target, gating inhibitor, incorporation into and destabilization, inhibitor, competitive inhibitor, inhibitory allosteric modulator, inhibitory immune response, intercalation, inverse agonist, negative modulator,

neutralizer, partial antagonist, reducer, suppressor'. Results were manually curated for commercial availability of inhibitors.

T cell migration

Tumor cells were plated at $1x10^4$ cells in complete RPMI in a 96-well receiver plate (Corning #3382) and incubated for 24h. Following this, ESO T cells were added to a 96-well transwell plate (Corning #3387) at $1x10^5$ cells/well in 100μL complete RPMI and the T cell plate was added to the tumor cell plate and incubated for 5 hr. Media supernatant from tumor cell wells was collected, wells were washed with PBS which was also collected, then tumor cells were detached with trypsin and collected. Total contents of each well were stained with fixable viability dye and αCD3e, and migrated T cells were enumerated by FACS counting.

Flow cytometry

Tumor cells or T cells suspended in FACS staining buffer were stained with fluorochrome-conjugated antibodies against CD3e (SK7, BD) and murine TCRβ (12-5961-82, ThermoFisher). Cell viability was determined using propidium iodide exclusion or fixable Live/Dead kit (Invitrogen). Intracellular staining assay on ESO T cells was conducted after 5-6 hr co-culture with non-targeting sgRNA or BIRC2-targeting sgRNA modified A375 cells in the presence of monensin (BD, 512092KZ) and brefeldin A (BD, 512301KZ). Staining was performed using manufacturer's instructions using antibodies against IFNγ (25723.11, BD) or TNFα (12-7349-41, ThermoFisher). Flow cytometric data were acquired using either a FACSCanto II or LSRII Fortessa cytometer (BD), and data were analyzed using FlowJo version 10.5.3 software (FlowJo LLC).

Immunoblotting

Immunoblotting was performed as described previously (Jacobs et al., 2008). Primary antibodies were followed by mouse- or rabbit-conjugated horseradish peroxidase (HRP) secondary antibodies. HRP-conjugated antibodies (anti-mouse or anti-rabbit IgG HRP conjugate, Promega) were detected by enhanced chemiluminescence detections (Thermofisher) using a Biorad ChemiDoc MP. This included the following antibodies: BIRC2 (108361, Abcam), BIRC3 (3130, Cell Signaling), HLA Class I (70328, Abcam), ICAM1 (4915, Cell Signaling), IRF1 (8478 Cell Signaling), phospho-JAK1 (3331, Cell Signaling), Lamin A/C (4777, Cell Signaling), phospho-NF-κB p65 (3033, Cell Signaling), NF-κB2 p100/p52 (4882, Cell Signaling), RelB (10544, Cell Signaling), XIAP (2042, Cell Signaling). Alternatively, primary antibodies were followed by fluorescently labeled anti-mouse or rabbit antibodies and imaged using a Biorad ChemiDoc MP. This included the following antibodies: β-actin (A5441, Sigma).

Nuclear and cytoplasmic extraction and fractionation

Cells were collected and cytoplasmic and nuclear protein extraction and fractionation protocol was performed as specified in manufacturer protocol (Thermofisher, Cat #78835). Extracted proteins were analyzed by immunoblot. 45 μg protein per lane was loaded for cytoplasmic fractions and 17.5 μg protein per lane was loaded for nuclear fractions.

Statistical Analysis

Sample sizes were determined by prior experience and estimated power calculations. Statistical analysis was performed with Prism (GraphPad Software Inc.). Data were compared using either a two-tailed Student's *t* test or one-way ANOVA with multiple comparisons corrected with Dunnett adjustment. *P* values < 0.05 were considered significant. For adoptive transfer experiments, mice were randomized prior to cell transfer and treatments. Tumor treatment graphs were compared by using the Wilcoxon rank sum test and analysis of animal survival was analyzed by a log-rank test.

Supplemental Figure Titles and Legends

Figure S1, related to Figure 1. **Tumor encounter drives T cell anabolic growth. (A)** Sorting strategy for isolation of NY-ESO-1 TCR-expressing T cells and Mel624 melanoma cells following co-culture. **(B)** Ingenuity Pathway Analysis of T cell genes that were differentially expressed following co-culture with Mel624 melanoma cells. Data is pooled from three independent experiments **(B)**.

Figure S2, related to Figure 4. **Combining inhibitors with tumor-specific T cells increases tumor cell elimination**. **(A)** A375 melanoma cells were co-cultured with ESO T cells along with inhibitors at 500 nM except for α-ITGAV at 0.25 μg/mL and tumor cell elimination was measured by flow cytometry. **(B)** A375 melanoma cells were co-cultured with or without ESO T cells along with inhibitors at (left panel) 5μM except for α-ITGAV at 2.5 μg/mL (left panel) or at 500 nM except for α-ITGAV at 0.25 μg/mL (right panel). Tumor cell elimination was measured by flow cytometry. **(C)** Genomic DNA from SB4238 (NCKAP1 mutant) and SB4235 tumor lines (NCKAP1 wild type) was collected and Sanger Sequencing was performed at the NCKAP1 locus to confirm the presence of a mutation. **(D)** Primary human T cells were transduced with GFP or a NCKAP1 reactive TCR and co-cultured with SB4238 tumor cells for 16h. ELISA was performed to determine IFNγ secretion. **(E)** Primary human T cells were transduced with a NCKAP1 reactive TCR and co-cultured with SB4247 or SB4238 tumor cells for 16h. ELISA was performed to determine IFNγ secretion. **(F)** Subcutaneous tumor growth in mice receiving ACT of PMEL1 T cells along with vehicle or Birinapant (50 mg drug/kg body weight). Mice were treated with Birinapant via IP injection every 48hr beginning 24hr after PMEL1 T cell infusion for a total of 5 doses. Data are representative of four **(A-B)** or two experiments **(D-F).** * $P < 0.05$, ** $P < 0.01$. *P* values for *in vitro* assays **(A-C)** calculated by one-way ANOVA with multiple comparisons corrected with Dunnett adjustment. *P* values for *in vivo* assays **(F)** calculated by Wilcoxon rank sum test**.**

Figure S3, related to Figure 6. **BIRC2 inhibits non-canonical NF-κB activity. (A)** A375 melanoma cells were transduced with Cas9 and non-targeting (NT) sgRNA or BIRC2-targeting sgRNAs and nuclear and cytoplasmic protein fractions were isolated and western blot analysis was performed. **(B)** Correlation of BIRC2 and NFKB2 expression in human melanoma tumors was assessed using cBioportal (Cerami et al., 2012; Gao et al., 2013). Data are representative of two **(A)** independent experiments.

Figure S4, related to Figure 6. **Expression of NFKB2 and IRF1 predicts response to immunotherapy**. **(A)** Various biomarkers for response to immunotherapy (y axis), including expression of *NFKB2* + *IRF1* expression, were compared using previously published genesets with TIDE online platform (Jiang et al., 2018).

Figure S5, related to Figure 7. **Non-canonical NF-κB signaling is associated with expression of inflammation-related genes. (A-C)** Correlation of NFKB2 expression with **(A)** CCL5, **(B)** CXCL10 and **(C)** CSF2 expression in human melanoma tumors was assessed using cBioportal. **(D-E)**

ChIPseq was performed on A375 cells transduced with Cas9 and non-targeting (NT) sgRNA or BIRC2-targeting sgRNA. **(D)** Association of RelB with HLA-C locus and **(E)** association of NFKB2 with MMP9 locus were assessed. **(F)** Western blot analysis of B16-mhGP100 melanoma cells transduced with Cas9 and non-targeting sgRNA or Cas9 and BIRC2-targeting sgRNA. Data are representative of two independent experiments **(D-F)**.

References

Borrello, I.M., Levitsky, H.I., Stock, W., Sher, D., Qin, L., DeAngelo, D.J., Alyea, E.P., Stone, R.M., Damon, L.E., Linker, C.A., et al. (2009). Granulocyte-macrophage colony-stimulating factor (GM-CSF)-secreting cellular immunotherapy in combination with autologous stem cell transplantation (ASCT) as postremission therapy for acute myeloid leukemia (AML). Blood *114*, 1736-1745.

Brahmer, J.R., Tykodi, S.S., Chow, L.Q., Hwu, W.J., Topalian, S.L., Hwu, P., Drake, C.G., Camacho, L.H., Kauh, J., Odunsi, K., et al. (2012). Safety and activity of anti-PD-L1 antibody in patients with advanced cancer. N Engl J Med *366*, 2455-2465.

Cerami, E., Gao, J., Dogrusoz, U., Gross, B.E., Sumer, S.O., Aksoy, B.A., Jacobsen, A., Byrne, C.J., Heuer, M.L., Larsson, E., et al. (2012). The cBio cancer genomics portal: an open platform for exploring multidimensional cancer genomics data. Cancer Discov *2*, 401-404.

Chen, S., Sanjana, N.E., Zheng, K., Shalem, O., Lee, K., Shi, X., Scott, D.A., Song, J., Pan, J.Q., Weissleder, R., et al. (2015). Genome-wide CRISPR screen in a mouse model of tumor growth and metastasis. Cell *160*, 1246-1260.

Dangaj, D., Bruand, M., Grimm, A.J., Ronet, C., Barras, D., Duttagupta, P.A., Lanitis, E., Duraiswamy, J., Tanyi, J.L., Benencia, F., et al. (2019). Cooperation between Constitutive and Inducible Chemokines Enables T Cell Engraftment and Immune Attack in Solid Tumors. Cancer Cell *35*, 885-900 e810.

Dubrez-Daloz, L., Dupoux, A., and Cartier, J. (2008). IAPs: more than just inhibitors of apoptosis proteins. Cell Cycle *7*, 1036-1046.

Dutta, J., Fan, Y., Gupta, N., Fan, G., and Gelinas, C. (2006). Current insights into the regulation of programmed cell death by NF-kappaB. Oncogene *25*, 6800-6816.

Eckelman, B.P., and Salvesen, G.S. (2006). The human anti-apoptotic proteins cIAP1 and cIAP2 bind but do not inhibit caspases. J Biol Chem *281*, 3254-3260.

Eil, R., Vodnala, S.K., Clever, D., Klebanoff, C.A., Sukumar, M., Pan, J.H., Palmer, D.C., Gros, A., Yamamoto, T.N., Patel, S.J., et al. (2016). Ionic immune suppression within the tumour microenvironment limits T cell effector function. Nature *537*, 539-543.

Facciabene, A., Motz, G.T., and Coukos, G. (2012). T-regulatory cells: key players in tumor immune escape and angiogenesis. Cancer Res *72*, 2162-2171.

Gao, J., Aksoy, B.A., Dogrusoz, U., Dresdner, G., Gross, B., Sumer, S.O., Sun, Y., Jacobsen, A., Sinha, R., Larsson, E., et al. (2013). Integrative analysis of complex cancer genomics and clinical profiles using the cBioPortal. Sci Signal *6*, pl1.

Gattinoni, L., Klebanoff, C.A., and Restifo, N.P. (2012). Paths to stemness: building the ultimate antitumour T cell. Nat Rev Cancer *12*, 671-684.

Griffith, M., Griffith, O.L., Coffman, A.C., Weible, J.V., McMichael, J.F., Spies, N.C., Koval, J., Das, I., Callaway, M.B., Eldred, J.M., et al. (2013). DGIdb: mining the druggable genome. Nat Methods *10*, 1209-1210.

Hanada, K.I., Yu, Z., Chappell, G.R., Park, A.S., and Restifo, N.P. (2019). An effective mouse model for adoptive cancer immunotherapy targeting neoantigens. JCI Insight *4*.

Harlin, H., Meng, Y., Peterson, A.C., Zha, Y., Tretiakova, M., Slingluff, C., McKee, M., and Gajewski, T.F. (2009). Chemokine expression in melanoma metastases associated with CD8+ T-cell recruitment. Cancer Res *69*, 3077-3085.

Jacobs, S.R., Herman, C.E., Maciver, N.J., Wofford, J.A., Wieman, H.L., Hammen, J.J., and Rathmell, J.C. (2008). Glucose uptake is limiting in T cell activation and requires CD28-mediated Akt-dependent and independent pathways. J Immunol *180*, 4476-4486.
Jiang, P., Gu, S., Pan, D., Fu, J., Sahu, A., Hu, X., Li, Z., Traugh, N., Bu, X., Li, B., et al. (2018). Signatures of T cell dysfunction and exclusion predict cancer immunotherapy response. Nat Med *24*, 1550-1558.
Johnson, L.A., Heemskerk, B., Powell, D.J., Jr., Cohen, C.J., Morgan, R.A., Dudley, M.E., Robbins, P.F., and Rosenberg, S.A. (2006). Gene transfer of tumor-reactive TCR confers both high avidity and tumor reactivity to nonreactive peripheral blood mononuclear cells and tumor-infiltrating lymphocytes. J Immunol *177*, 6548-6559.
Jung, S.A., Park, Y.M., Hong, S.W., Moon, J.H., Shin, J.S., Lee, H.R., Ha, S.H., Lee, D.H., Kim, J.H., Kim, S.M., et al. (2015). Cellular inhibitor of apoptosis protein 1 (cIAP1) stability contributes to YM155 resistance in human gastric cancer cells. J Biol Chem *290*, 9974-9985.
Kishton, R.J., Sukumar, M., and Restifo, N.P. (2017). Metabolic Regulation of T Cell Longevity and Function in Tumor Immunotherapy. Cell Metab *26*, 94-109.
Liu, B., Guo, H., Xu, J., Qin, T., Guo, Q., Gu, N., Zhang, D., Qian, W., Dai, J., Hou, S., et al. (2018). Elimination of tumor by CD47/PD-L1 dual-targeting fusion protein that engages innate and adaptive immune responses. MAbs *10*, 315-324.
Lo, W., Parkhurst, M., Robbins, P.F., Tran, E., Lu, Y.C., Jia, L., Gartner, J.J., Pasetto, A., Deniger, D., Malekzadeh, P., et al. (2019). Immunologic Recognition of a Shared p53 Mutated Neoantigen in a Patient with Metastatic Colorectal Cancer. Cancer immunology research *7*, 534-543.
Malekzadeh, P., Pasetto, A., Robbins, P.F., Parkhurst, M.R., Paria, B.C., Jia, L., Gartner, J.J., Hill, V., Yu, Z., Restifo, N.P., et al. (2019). Neoantigen screening identifies broad TP53 mutant immunogenicity in patients with epithelial cancers. J Clin Invest *129*, 1109-1114.
Manguso, R.T., Pope, H.W., Zimmer, M.D., Brown, F.D., Yates, K.B., Miller, B.C., Collins, N.B., Bi, K., LaFleur, M.W., Juneja, V.R., et al. (2017). In vivo CRISPR screening identifies Ptpn2 as a cancer immunotherapy target. Nature *547*, 413-418.
Martz, C.A., Ottina, K.A., Singleton, K.R., Jasper, J.S., Wardell, S.E., Peraza-Penton, A., Anderson, G.R., Winter, P.S., Wang, T., Alley, H.M., et al. (2014). Systematic identification of signaling pathways with potential to confer anticancer drug resistance. Sci Signal *7*, ra121.
Maude, S.L., Frey, N., Shaw, P.A., Aplenc, R., Barrett, D.M., Bunin, N.J., Chew, A., Gonzalez, V.E., Zheng, Z., Lacey, S.F., et al. (2014). Chimeric antigen receptor T cells for sustained remissions in leukemia. N Engl J Med *371*, 1507-1517.
Mi, H., Muruganujan, A., Huang, X., Ebert, D., Mills, C., Guo, X., and Thomas, P.D. (2019). Protocol Update for large-scale genome and gene function analysis with the PANTHER classification system (v.14.0). Nat Protoc *14*, 703-721.
Pan, D., Kobayashi, A., Jiang, P., Ferrari de Andrade, L., Tay, R.E., Luoma, A.M., Tsoucas, D., Qiu, X., Lim, K., Rao, P., et al. (2018). A major chromatin regulator determines resistance of tumor cells to T cell-mediated killing. Science *359*, 770-775.
Park, J.H., Riviere, I., Gonen, M., Wang, X., Senechal, B., Curran, K.J., Sauter, C., Wang, Y., Santomasso, B., Mead, E., et al. (2018). Long-Term Follow-up of CD19 CAR Therapy in Acute Lymphoblastic Leukemia. N Engl J Med *378*, 449-459.

Patch, R.J., Searle, L.L., Kim, A.J., De, D., Zhu, X., Askari, H.B., O'Neill, J.C., Abad, M.C., Rentzeperis, D., Liu, J., et al. (2011). Identification of diaryl ether-based ligands for estrogen-related receptor alpha as potential antidiabetic agents. J Med Chem *54*, 788-808.
Patel, S.J., Sanjana, N.E., Kishton, R.J., Eidizadeh, A., Vodnala, S.K., Cam, M., Gartner, J.J., Jia, L., Steinberg, S.M., Yamamoto, T.N., et al. (2017). Identification of essential genes for cancer immunotherapy. Nature *548*, 537-542.
Peng, D., Kryczek, I., Nagarsheth, N., Zhao, L., Wei, S., Wang, W., Sun, Y., Zhao, E., Vatan, L., Szeliga, W., et al. (2015). Epigenetic silencing of TH1-type chemokines shapes tumour immunity and immunotherapy. Nature *527*, 249-253.
Restifo, N.P., Marincola, F.M., Kawakami, Y., Taubenberger, J., Yannelli, J.R., and Rosenberg, S.A. (1996). Loss of functional beta 2-microglobulin in metastatic melanomas from five patients receiving immunotherapy. Journal of the National Cancer Institute *88*, 100-108.
Ribas, A., Lawrence, D., Atkinson, V., Agarwal, S., Miller, W.H., Jr., Carlino, M.S., Fisher, R., Long, G.V., Hodi, F.S., Tsoi, J., et al. (2019). Combined BRAF and MEK inhibition with PD-1 blockade immunotherapy in BRAF-mutant melanoma. Nat Med *25*, 936-940.
Robbins, P.F., Li, Y.F., El-Gamil, M., Zhao, Y., Wargo, J.A., Zheng, Z., Xu, H., Morgan, R.A., Feldman, S.A., Johnson, L.A., et al. (2008). Single and dual amino acid substitutions in TCR CDRs can enhance antigen-specific T cell functions. J Immunol *180*, 6116-6131.
Robert, L., Ribas, A., and Hu-Lieskovan, S. (2016). Combining targeted therapy with immunotherapy. Can 1+1 equal more than 2? Semin Immunol *28*, 73-80.
Rosenberg, S.A., and Restifo, N.P. (2015). Adoptive cell transfer as personalized immunotherapy for human cancer. Science *348*, 62-68.
Rosenberg, S.A., Yang, J.C., Sherry, R.M., Kammula, U.S., Hughes, M.S., Phan, G.Q., Citrin, D.E., Restifo, N.P., Robbins, P.F., Wunderlich, J.R., et al. (2011). Durable complete responses in heavily pretreated patients with metastatic melanoma using T-cell transfer immunotherapy. Clinical cancer research : an official journal of the American Association for Cancer Research *17*, 4550-4557.
Sanjana, N.E., Shalem, O., and Zhang, F. (2014). Improved vectors and genome-wide libraries for CRISPR screening. Nat Methods *11*, 783-784.
Sartorius, U.A., and Krammer, P.H. (2002). Upregulation of Bcl-2 is involved in the mediation of chemotherapy resistance in human small cell lung cancer cell lines. Int J Cancer *97*, 584-592.
Sharma, P., Hu-Lieskovan, S., Wargo, J.A., and Ribas, A. (2017). Primary, Adaptive, and Acquired Resistance to Cancer Immunotherapy. Cell *168*, 707-723.
Shifrut, E., Carnevale, J., Tobin, V., Roth, T.L., Woo, J.M., Bui, C.T., Li, P.J., Diolaiti, M.E., Ashworth, A., and Marson, A. (2018). Genome-wide CRISPR Screens in Primary Human T Cells Reveal Key Regulators of Immune Function. Cell *175*, 1958-1971 e1915.
Singleton, K.R., Crawford, L., Tsui, E., Manchester, H.E., Maertens, O., Liu, X., Liberti, M.V., Magpusao, A.N., Stein, E.M., Tingley, J.P., et al. (2017). Melanoma Therapeutic Strategies that Select against Resistance by Exploiting MYC-Driven Evolutionary Convergence. Cell Rep *21*, 2796-2812.
Topalian, S.L., Drake, C.G., and Pardoll, D.M. (2015). Immune checkpoint blockade: a common denominator approach to cancer therapy. Cancer Cell *27*, 450-461.

Topalian, S.L., Hodi, F.S., Brahmer, J.R., Gettinger, S.N., Smith, D.C., McDermott, D.F., Powderly, J.D., Carvajal, R.D., Sosman, J.A., Atkins, M.B., et al. (2012). Safety, activity, and immune correlates of anti-PD-1 antibody in cancer. N Engl J Med *366*, 2443-2454.

Van Allen, E.M., Miao, D., Schilling, B., Shukla, S.A., Blank, C., Zimmer, L., Sucker, A., Hillen, U., Foppen, M.H.G., Goldinger, S.M., et al. (2015). Genomic correlates of response to CTLA-4 blockade in metastatic melanoma. Science *350*, 207-211.

Vodnala, S.K., Eil, R., Kishton, R.J., Sukumar, M., Yamamoto, T.N., Ha, N.H., Lee, P.H., Shin, M., Patel, S.J., Yu, Z., et al. (2019). T cell stemness and dysfunction in tumors are triggered by a common mechanism. Science *363*.

Vredevoogd, D.W., Kuilman, T., Ligtenberg, M.A., Boshuizen, J., Stecker, K.E., de Bruijn, B., Krijgsman, O., Huang, X., Kenski, J.C.N., Lacroix, R., et al. (2019). Augmenting Immunotherapy Impact by Lowering Tumor TNF Cytotoxicity Threshold. Cell *178*, 585-599 e515.

Wang, B., Tian, T., Kalland, K.H., Ke, X., and Qu, Y. (2018). Targeting Wnt/beta-Catenin Signaling for Cancer Immunotherapy. Trends Pharmacol Sci *39*, 648-658.

Yamamoto, T.N., Kishton, R.J., and Restifo, N.P. (2019). Developing neoantigen-targeted T cell-based treatments for solid tumors. Nat Med.

Yang, Y., Kelly, P., Shaffer, A.L., 3rd, Schmitz, R., Yoo, H.M., Liu, X., Huang, D.W., Webster, D., Young, R.M., Nakagawa, M., et al. (2016). Targeting Non-proteolytic Protein Ubiquitination for the Treatment of Diffuse Large B Cell Lymphoma. Cancer Cell *29*, 494-507.

Zaretsky, J.M., Garcia-Diaz, A., Shin, D.S., Escuin-Ordinas, H., Hugo, W., Hu-Lieskovan, S., Torrejon, D.Y., Abril-Rodriguez, G., Sandoval, S., Barthly, L., et al. (2016). Mutations Associated with Acquired Resistance to PD-1 Blockade in Melanoma. N Engl J Med *375*, 819-829.

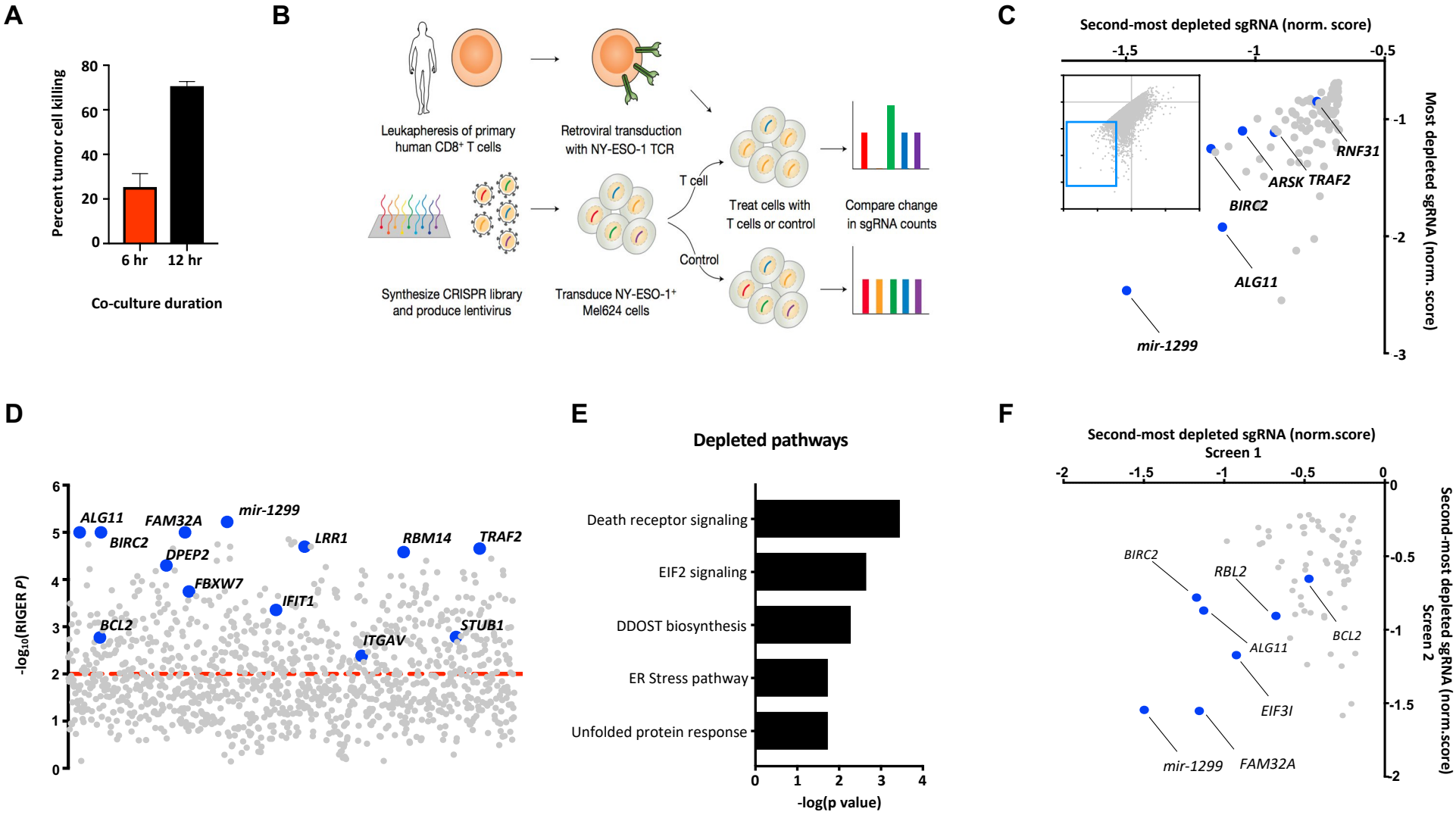
A
Percent tumor cell killing
80
60
40
20
0
6 hr
12 hr
Co-culture duration
B
Leukapheresis of primary human CD8+ T cells
Retroviral transduction with NY-ESO-1 TCR
Synthesize CRISPR library and produce lentivirus
Transduce NY-ESO-1+ Mel624 cells
T cell
Control
Treat cells with T cells or control
Compare change in sgRNA counts
C
Second-most depleted sgRNA (norm. score)
-1.5
-1
-0.5
Most depleted sgRNA (norm. score)
-1
-2
-3
RNF31
ARSK
TRAF2
BIRC2
ALG11
mir-1299
D
-log10(RIGER P)
6
5
4
3
2
1
0
ALG11
FAM32A
mir-1299
BIRC2
LRR1
RBM14
TRAF2
DPEP2
FBXW7
IFIT1
BCL2
ITGAV
STUB1
E
Depleted pathways
Death receptor signaling
EIF2 signaling
DDOST biosynthesis
ER Stress pathway
Unfolded protein response
0
1
2
3
4
-log(p value)
F
Second-most depleted sgRNA (norm.score) Screen 1
-2
-1.5
-1
-0.5
0
Second-most depleted sgRNA (norm.score) Screen 2
0
-0.5
-1
-1.5
-2
BIRC2
RBL2
BCL2
ALG11
EIF3I
mir-1299
FAM32A

Figure 1

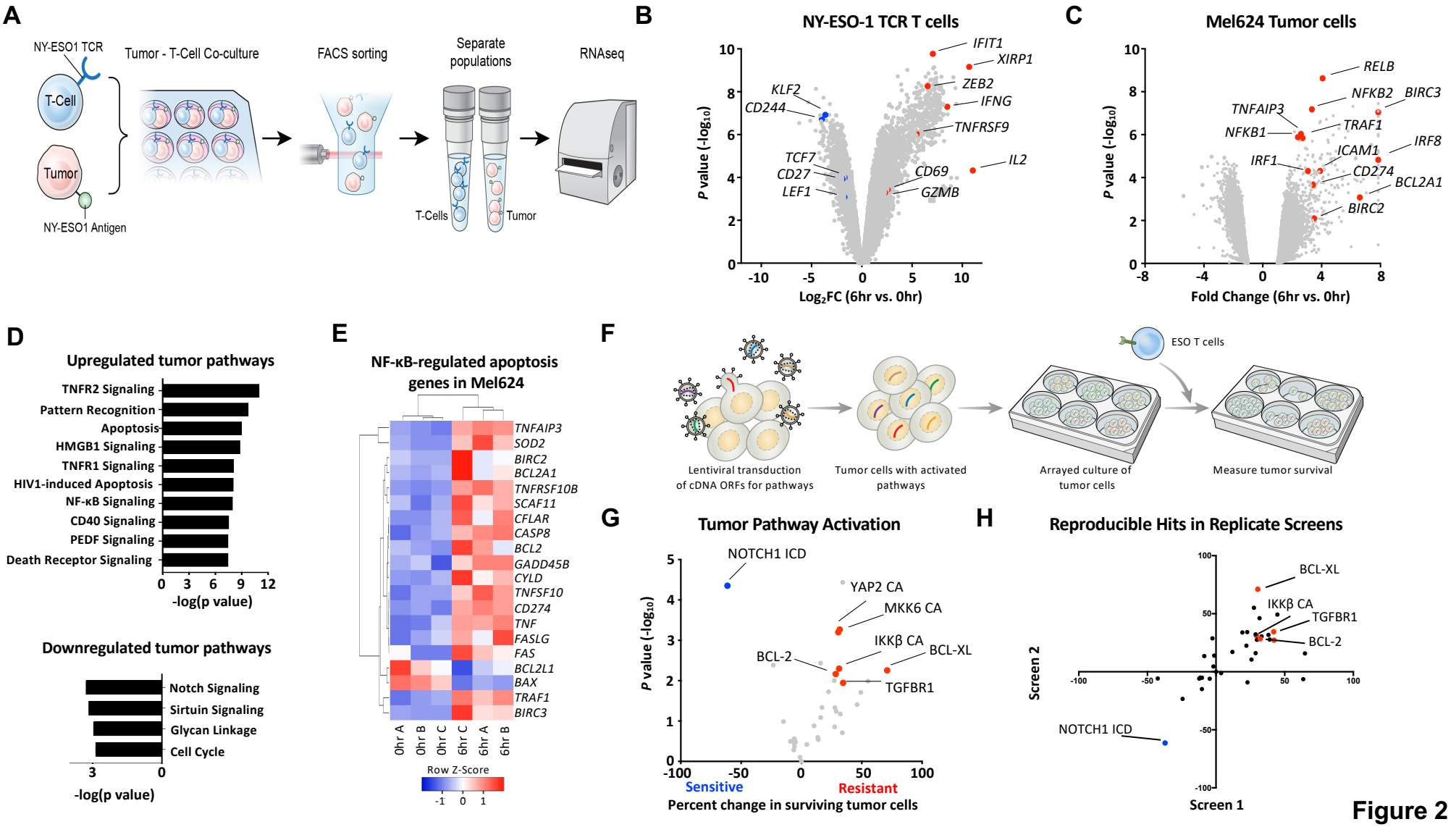
A
NY-ESO1 TCR
T-Cell
Tumor
NY-ESO1 Antigen
Tumor - T-Cell Co-culture
FACS sorting
Separate populations
T-Cells
Tumor
RNAseq
B
NY-ESO-1 TCR T cells
P value (-log10)
Log2FC (6hr vs. 0hr)
IFIT1
XIRP1
ZEB2
IFNG
TNFRSF9
IL2
CD69
GZMB
KLF2
CD244
TCF7
CD27
LEF1
C
Mel624 Tumor cells
P value (-log10)
Fold Change (6hr vs. 0hr)
RELB
NFKB2
BIRC3
TNFAIP3
TRAF1
NFKB1
IRF8
ICAM1
IRF1
CD274
BCL2A1
BIRC2
D
Upregulated tumor pathways
TNFR2 Signaling
Pattern Recognition
Apoptosis
HMGB1 Signaling
TNFR1 Signaling
HIV1-induced Apoptosis
NF-κB Signaling
CD40 Signaling
PEDF Signaling
Death Receptor Signaling
-log(p value)
Downregulated tumor pathways
Notch Signaling
Sirtuin Signaling
Glycan Linkage
Cell Cycle
-log(p value)
E
NF-κB-regulated apoptosis genes in Mel624
TNFAIP3
SOD2
BIRC2
BCL2A1
TNFRSF10B
SCAF11
CFLAR
CASP8
BCL2
GADD45B
CYLD
TNFSF10
CD274
TNF
FASLG
FAS
BCL2L1
BAX
TRAF1
BIRC3
0hr A
0hr B
0hr C
6hr C
6hr A
6hr B
Row Z-Score
F
ESO T cells
Lentiviral transduction of cDNA ORFs for pathways
Tumor cells with activated pathways
Arrayed culture of tumor cells
Measure tumor survival
G
Tumor Pathway Activation
P value (-log10)
NOTCH1 ICD
YAP2 CA
MKK6 CA
IKKβ CA
BCL-2
BCL-XL
TGFBR1
Sensitive
Resistant
Percent change in surviving tumor cells
H
Reproducible Hits in Replicate Screens
Screen 2
Screen 1
BCL-XL
IKKβ CA
TGFBR1
BCL-2
NOTCH1 ICD

Figure 2

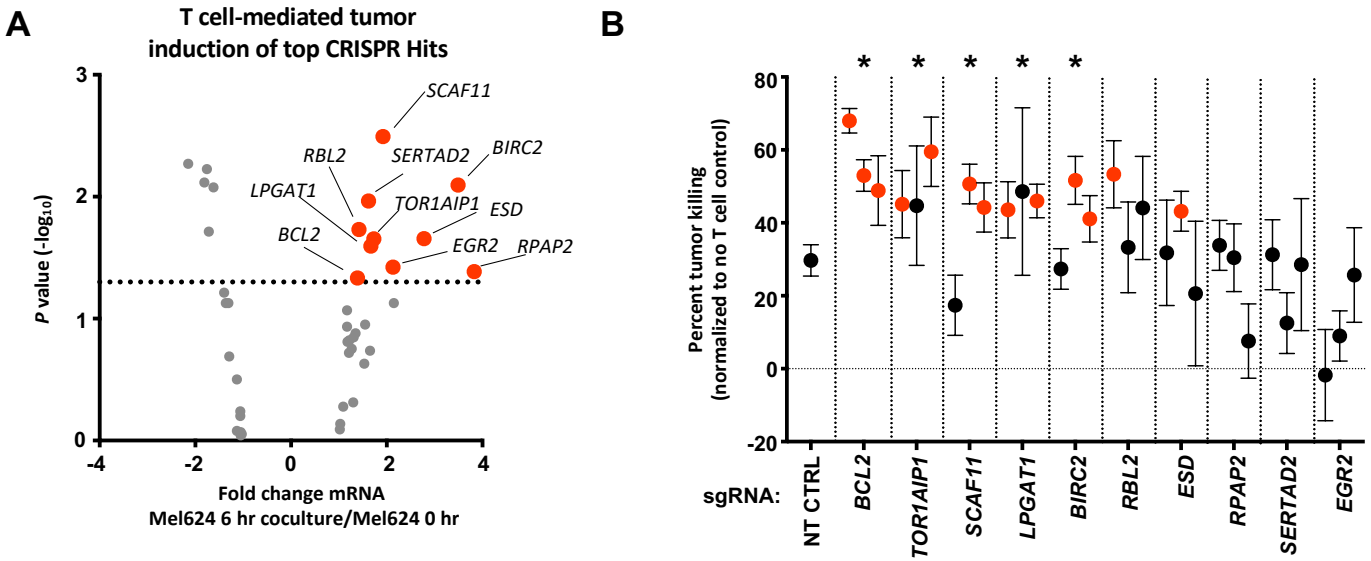
A
T cell-mediated tumor induction of top CRISPR Hits
SCAF11
RBL2
SERTAD2
BIRC2
LPGAT1
TOR1AIP1
ESD
BCL2
EGR2
RPAP2
P value (-log10)
Fold change mRNA
Mel624 6 hr coculture/Mel624 0 hr
B
Percent tumor killing
(normalized to no T cell control)
sgRNA:
NT CTRL
BCL2
TOR1AIP1
SCAF11
LPGAT1
BIRC2
RBL2
ESD
RPAP2
SERTAD2
EGR2

Figure 3

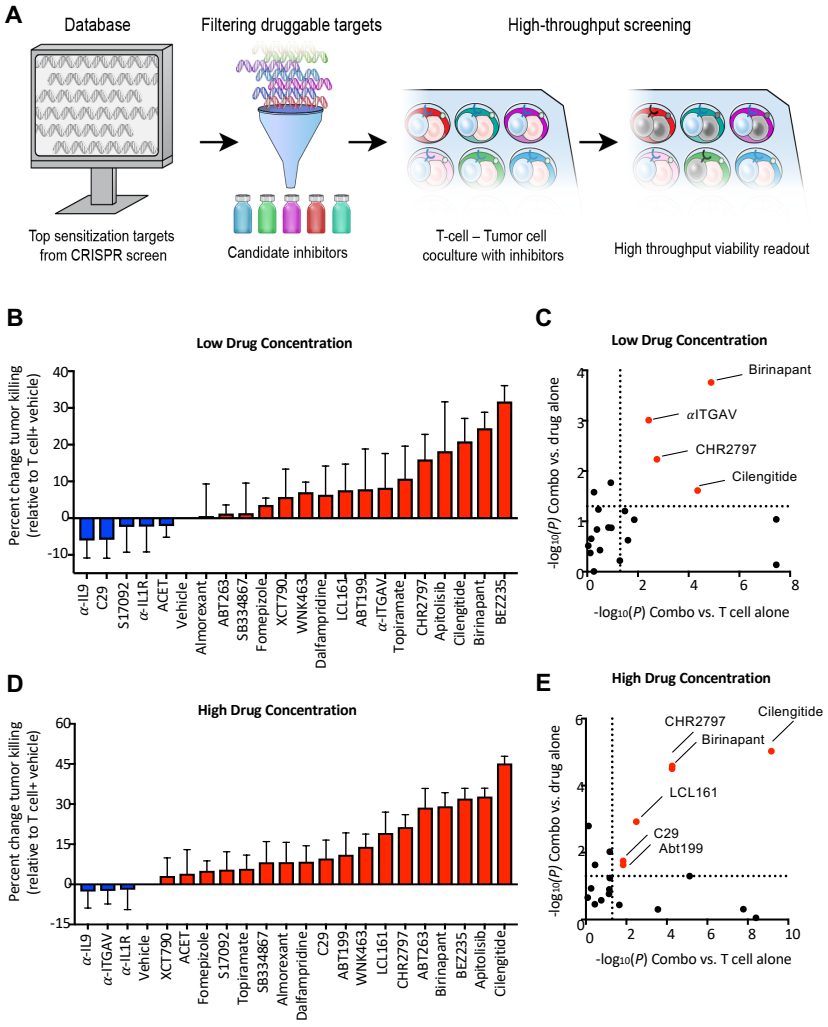
A
Database
Filtering druggable targets
High-throughput screening
Top sensitization targets from CRISPR screen
Candidate inhibitors
T-cell – Tumor cell coculture with inhibitors
High throughput viability readout
B
Low Drug Concentration
Percent change tumor killing (relative to T cell+ vehicle)
α-IL9
C29
S17092
α-IL1R
ACET
Vehicle
Almorexant
ABT263
SB334867
Fomepizole
XCT790
WNK463
Dalfampridine
LCL161
ABT199
α-ITGAV
Topiramate
CHR2797
Apitolisib
Cilengitide
Birinapant
BEZ235
C
Low Drug Concentration
Birinapant
αITGAV
CHR2797
Cilengitide
-log10(P) Combo vs. drug alone
-log10(P) Combo vs. T cell alone
D
High Drug Concentration
Percent change tumor killing (relative to T cell+ vehicle)
α-IL9
α-ITGAV
α-IL1R
Vehicle
XCT790
ACET
Fomepizole
S17092
Topiramate
SB334867
Almorexant
Dalfampridine
C29
ABT199
WNK463
LCL161
CHR2797
ABT263
Birinapant
BEZ235
Apitolisib
Cilengitide
E
High Drug Concentration
CHR2797
Cilengitide
Birinapant
LCL161
C29
Abt199
-log10(P) Combo vs. drug alone
-log10(P) Combo vs. T cell alone

Figure 4

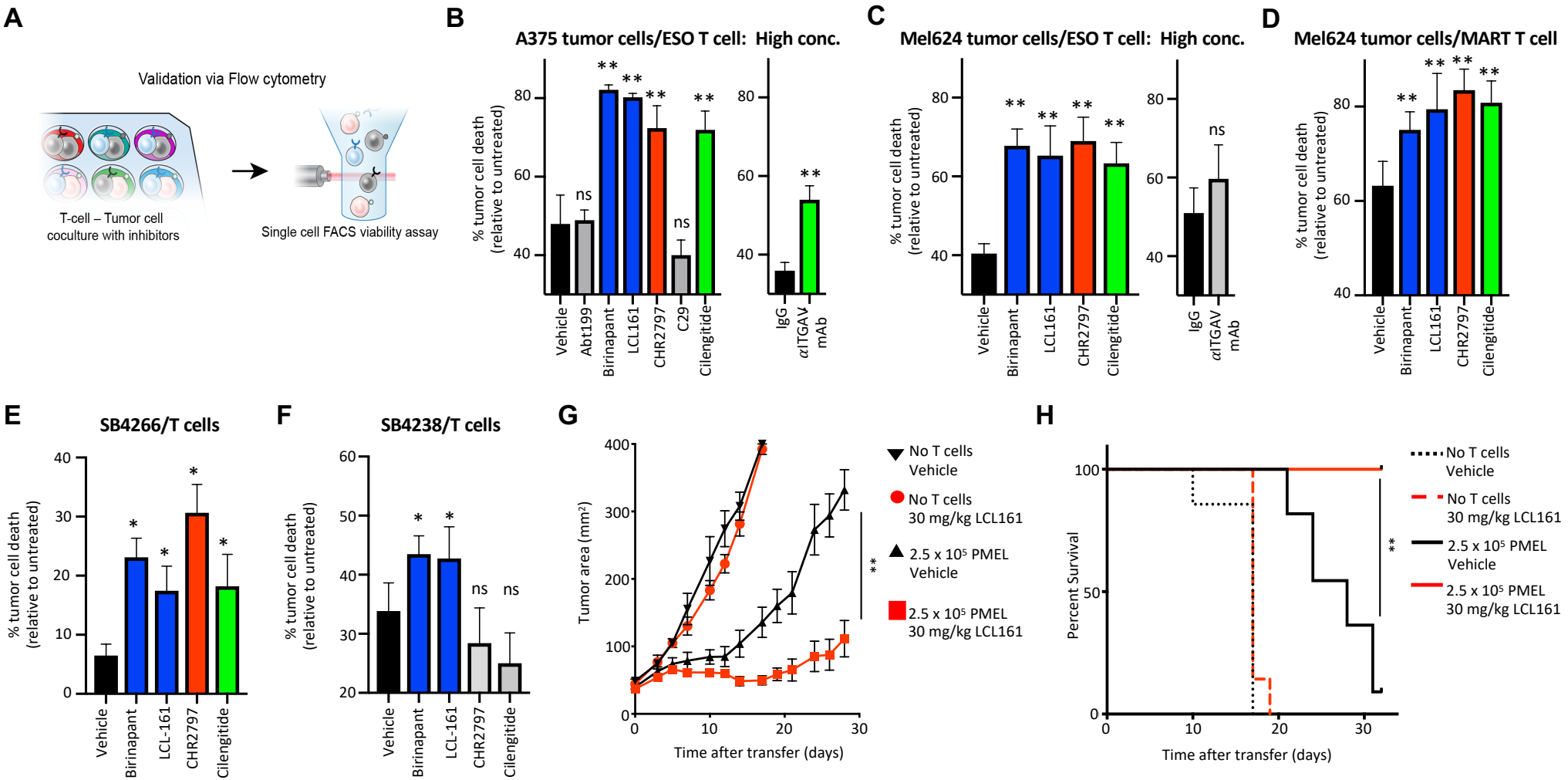
A
Validation via Flow cytometry
T-cell – Tumor cell coculture with inhibitors
Single cell FACS viability assay
B
A375 tumor cells/ESO T cell: High conc.
% tumor cell death (relative to untreated)
Vehicle
Abt199
Birinapant
LCL161
CHR2797
C29
Cilengitide
IgG
αITGAV mAb
C
Mel624 tumor cells/ESO T cell: High conc.
D
Mel624 tumor cells/MART T cell
E
SB4266/T cells
F
SB4238/T cells
G
Tumor area (mm²)
Time after transfer (days)
No T cells Vehicle
No T cells 30 mg/kg LCL161
2.5 x 10⁵ PMEL Vehicle
2.5 x 10⁵ PMEL 30 mg/kg LCL161
H
Percent Survival

Figure 5

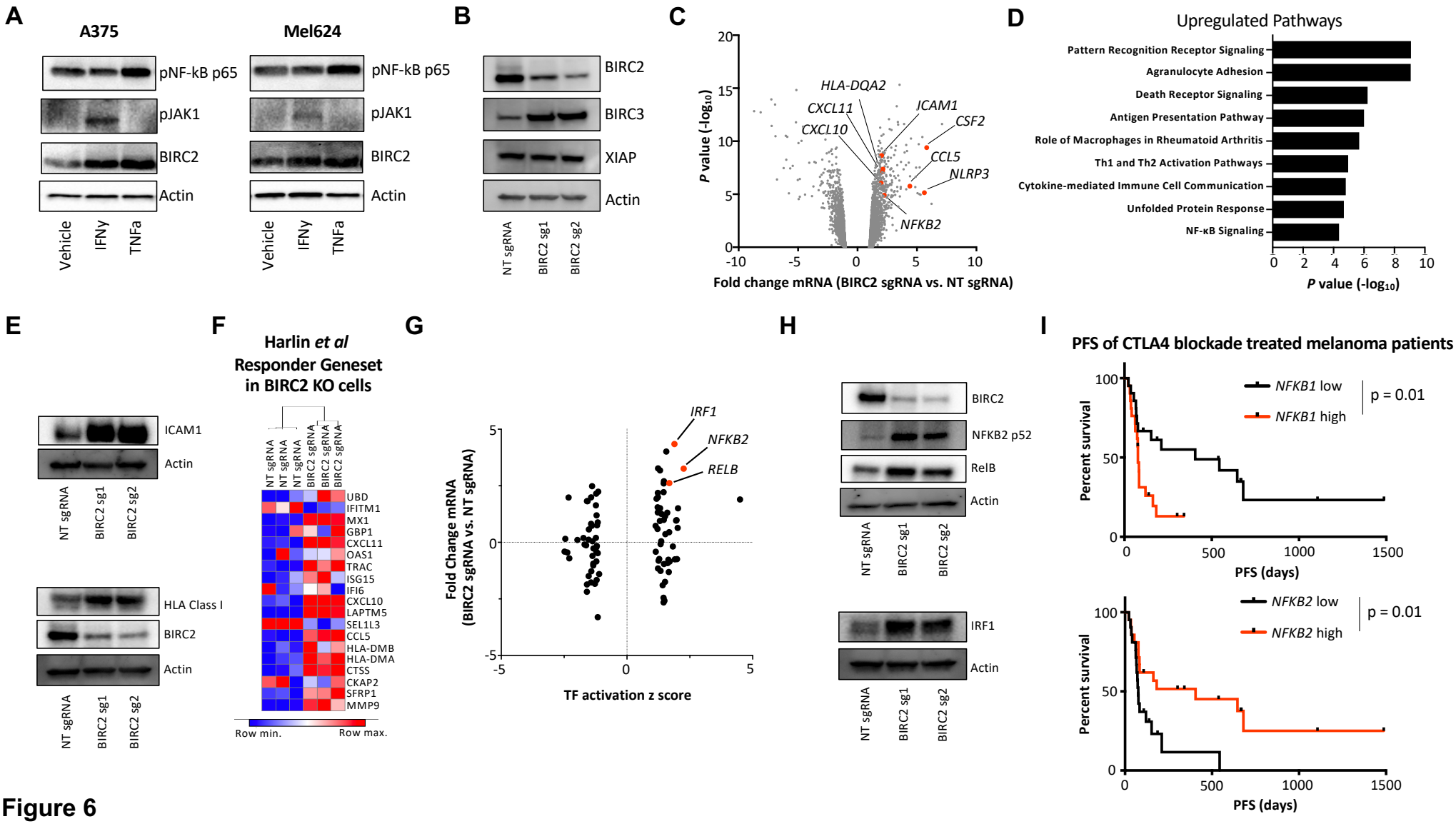
A
A375
Mel624
pNF-kB p65
pJAK1
BIRC2
Actin
Vehicle
IFNγ
TNFa
B
BIRC2
BIRC3
XIAP
Actin
NT sgRNA
BIRC2 sg1
BIRC2 sg2
C
P value (-log10)
Fold change mRNA (BIRC2 sgRNA vs. NT sgRNA)
HLA-DQA2
CXCL11
CXCL10
ICAM1
CSF2
CCL5
NLRP3
NFKB2
D
Upregulated Pathways
Pattern Recognition Receptor Signaling
Agranulocyte Adhesion
Death Receptor Signaling
Antigen Presentation Pathway
Role of Macrophages in Rheumatoid Arthritis
Th1 and Th2 Activation Pathways
Cytokine-mediated Immune Cell Communication
Unfolded Protein Response
NF-κB Signaling
P value (-log10)
E
ICAM1
Actin
HLA Class I
BIRC2
F
Harlin et al
Responder Geneset
in BIRC2 KO cells
UBD
IFITM1
MX1
GBP1
CXCL11
OAS1
TRAC
ISG15
IFI6
CXCL10
LAPTM5
SEL1L3
CCL5
HLA-DMB
HLA-DMA
CTSS
CKAP2
SFRP1
MMP9
Row min.
Row max.
G
Fold Change mRNA
(BIRC2 sgRNA vs. NT sgRNA)
TF activation z score
IRF1
NFKB2
RELB
H
BIRC2
NFKB2 p52
RelB
Actin
IRF1
I
PFS of CTLA4 blockade treated melanoma patients
NFKB1 low
NFKB1 high
p = 0.01
Percent survival
PFS (days)
NFKB2 low
NFKB2 high
p = 0.01

Figure 6

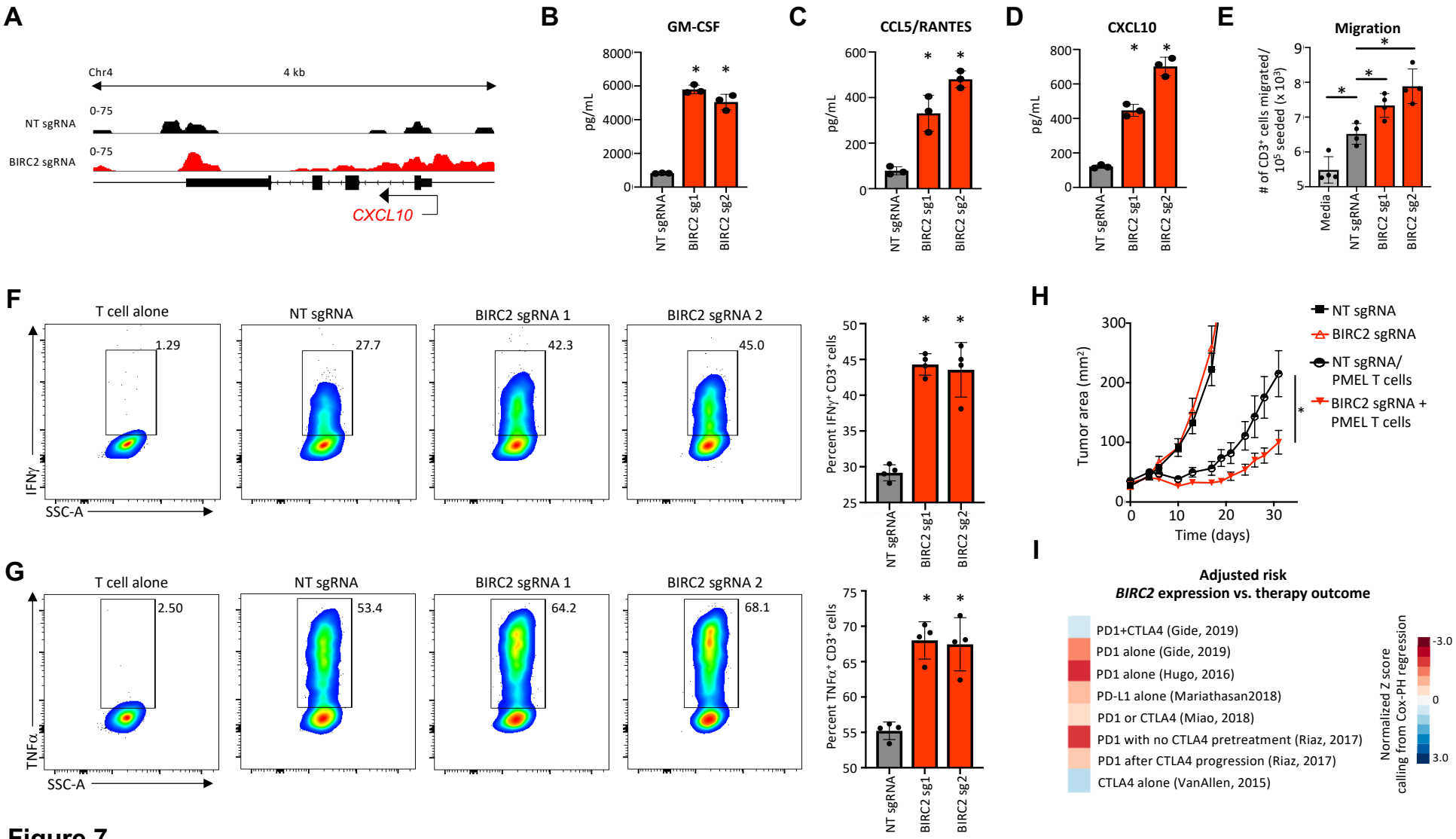
A
Chr4
4 kb
NT sgRNA
0-75
BIRC2 sgRNA
0-75
CXCL10
B
GM-CSF
pg/mL
NT sgRNA
BIRC2 sg1
BIRC2 sg2
C
CCL5/RANTES
pg/mL
D
CXCL10
pg/mL
E
Migration
# of CD3+ cells migrated/ 10^5 seeded (x 10^3)
Media
F
T cell alone
NT sgRNA
BIRC2 sgRNA 1
BIRC2 sgRNA 2
1.29
27.7
42.3
45.0
IFNγ
SSC-A
Percent IFNγ+ CD3+ cells
G
2.50
53.4
64.2
68.1
TNFα
Percent TNFα+ CD3+ cells
H
Tumor area (mm²)
Time (days)
NT sgRNA
BIRC2 sgRNA
NT sgRNA/ PMEL T cells
BIRC2 sgRNA + PMEL T cells
I
Adjusted risk
BIRC2 expression vs. therapy outcome
PD1+CTLA4 (Gide, 2019)
PD1 alone (Gide, 2019)
PD1 alone (Hugo, 2016)
PD-L1 alone (Mariathasan2018)
PD1 or CTLA4 (Miao, 2018)
PD1 with no CTLA4 pretreatment (Riaz, 2017)
PD1 after CTLA4 progression (Riaz, 2017)
CTLA4 alone (VanAllen, 2015)
Normalized Z score calling from Cox-PH regression
-3.0
0
3.0

Figure 7

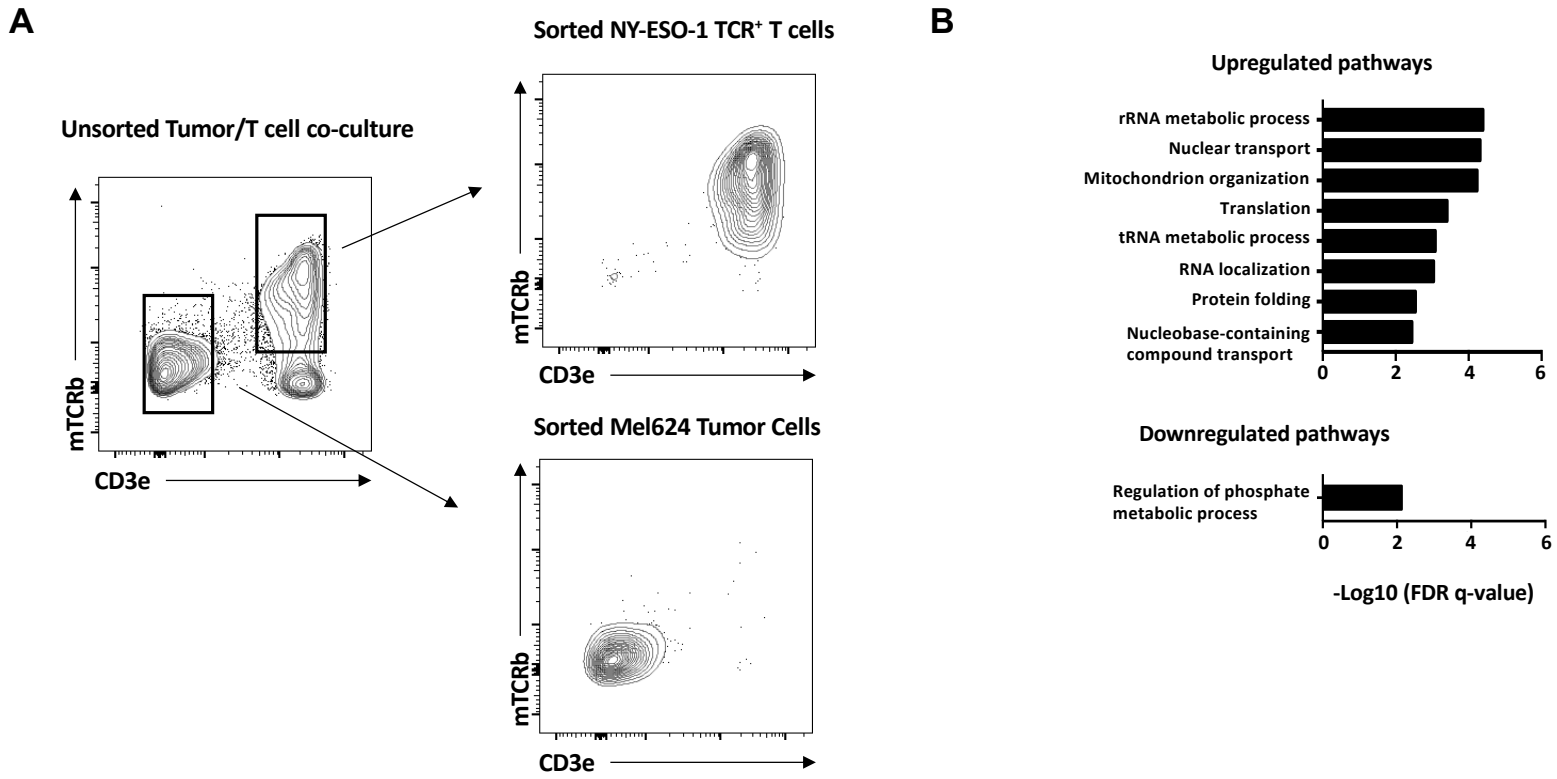

Supplemental Figure 1

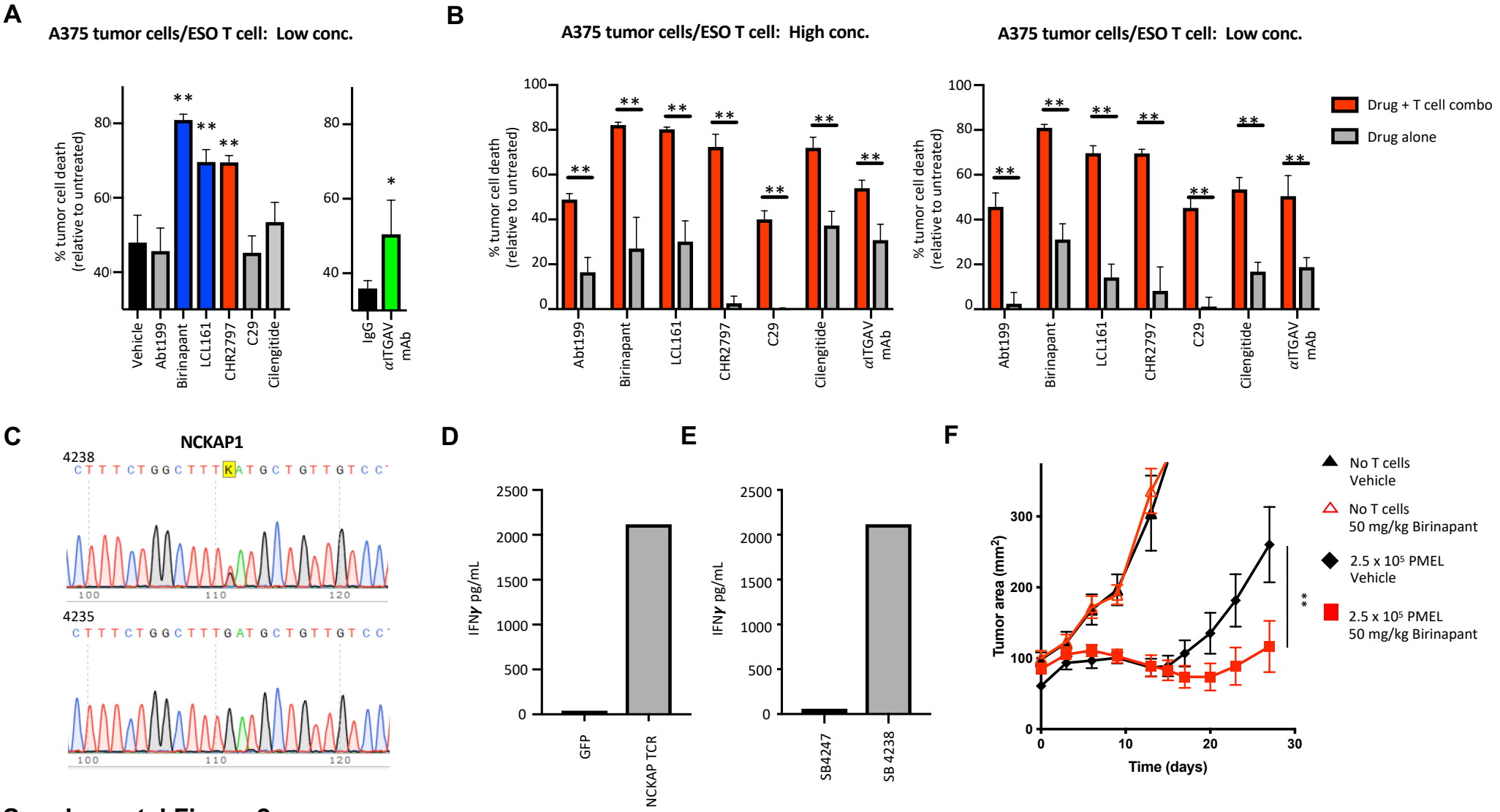

Supplemental Figure 2

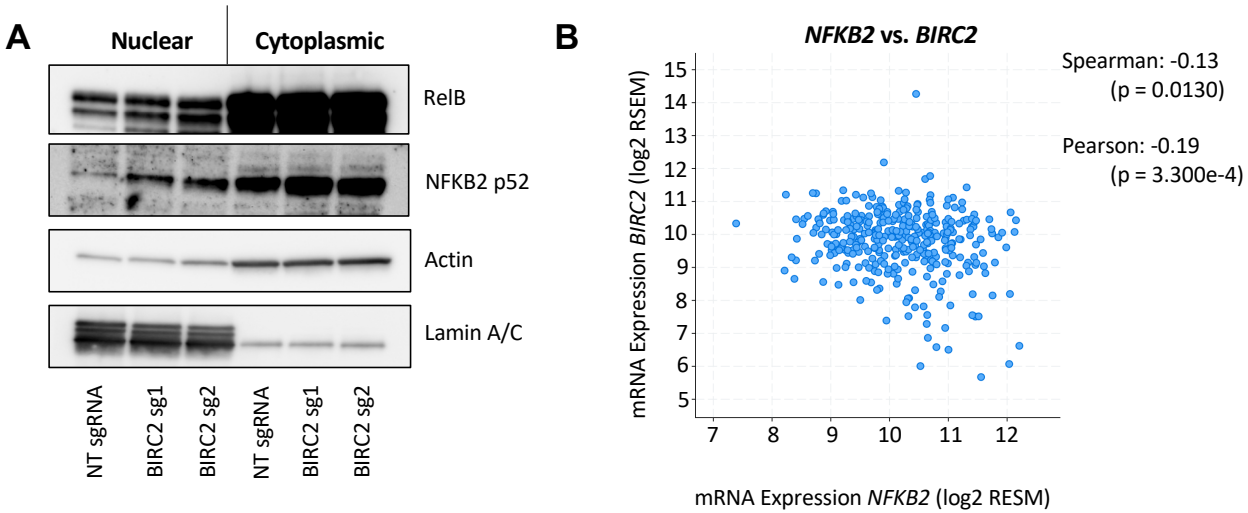

Supplemental Figure 3

A

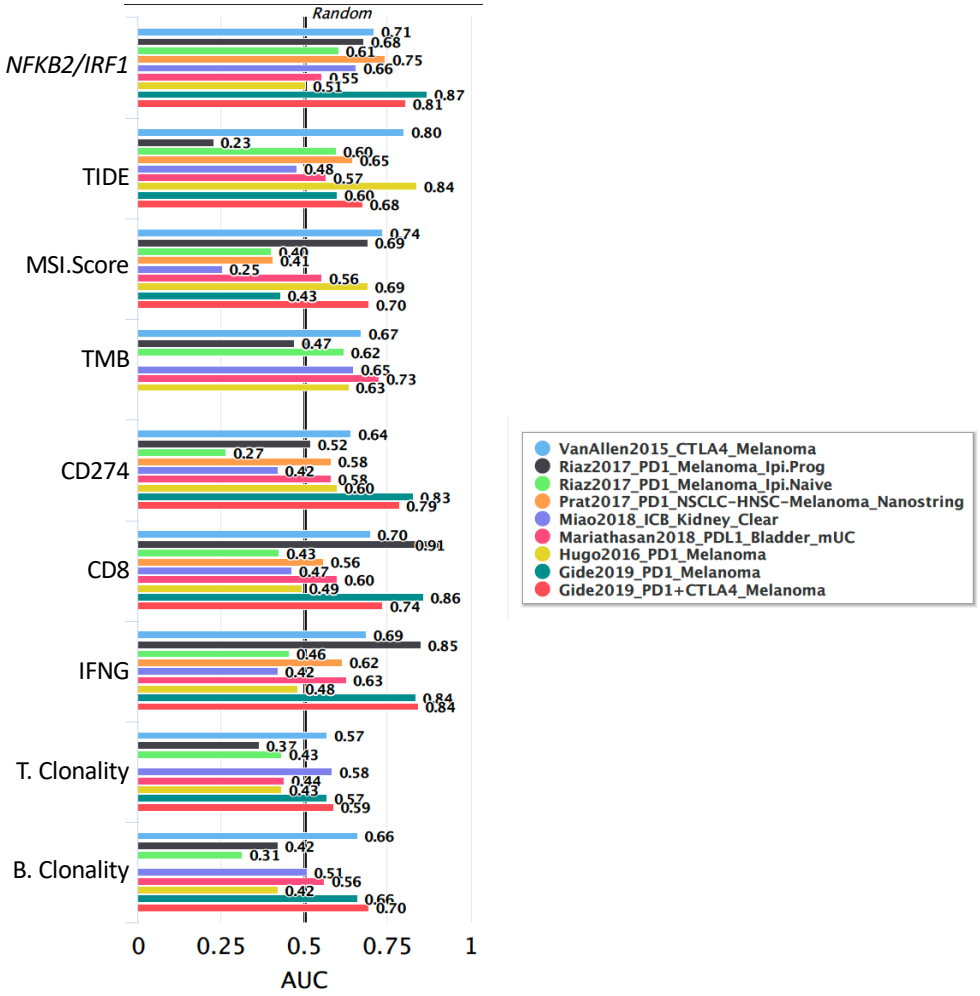

Supplemental Figure 4

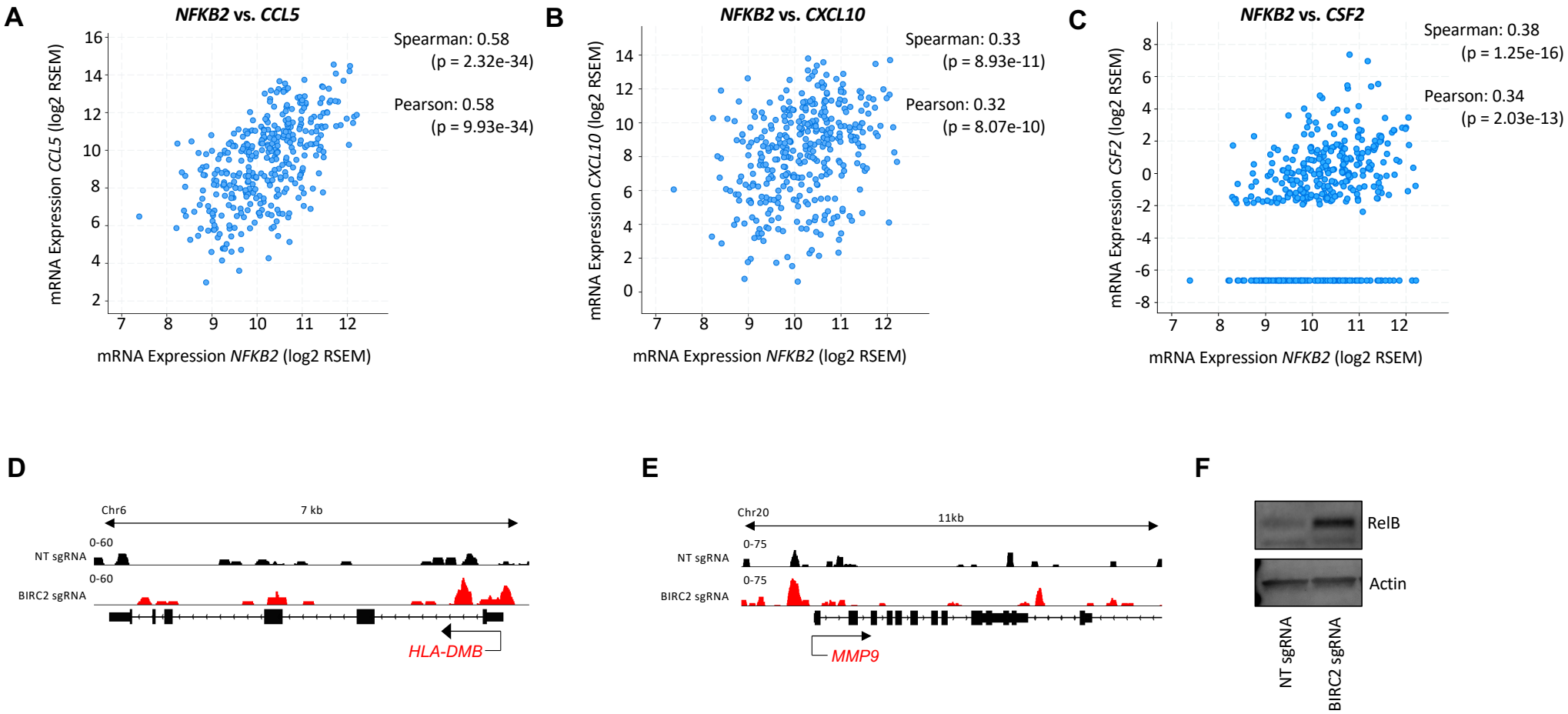

Supplemental Figure 5